Title

Streamlined Synthesis of Sulfated Cellulose Nanofibrils using Chlorosulfonic Acid and Their Applications in Conducting Materials

Author

Pingrey, Benjamin Earl

Publication Date

2023

Peer reviewed|Thesis/dissertation

Streamlined Synthesis of Sulfated Cellulose Nanofibrils using Chlorosulfonic Acid and Their Applications in Conducting Materials

By

BENJAMIN EARL PINGREY

DISSERTATION

Submitted in partial satisfaction of the requirements for the degree of

DOCTOR OF PHILOSOPHY

in

Chemical Engineering

in the

OFFICE OF GRADUATE STUDIES

of the

UNIVERSITY OF CALIFORNIA

DAVIS

Approved:

You-Lo Hsieh, Chair

Marjorie Longo

Tonya Kuhl

Committee in Charge

2023

ACKNOWLEDGEMENTS

I would like to express my deepest appreciation to my advisor, Dr. You-Lo Hsieh. Your guidance throughout the course of my graduate work has helped to illuminate my way when navigating both academia and the world of science in general.

I am extremely grateful to Dr. Marjorie Longo and Dr. Tonya Kuhl for serving on both my qualifying and dissertation committees. Your insights have helped set the direction for my work and ensure its technical rigor and scientific merit.

I would like to extend my thanks to the American Association of Textile Chemists and Colorists for providing funding a portion of my research.

Special thanks to the United States Department of Defense's SMART Scholarship for Service Program and the Naval Undersea Warfare Center, Division Keyport for sponsoring me for the past four years. Your support has been instrumental to my success.

Lastly, words cannot express my gratitude to my family and friends for all the support they have given me. This endeavor would not have been possible without you.

ABSTRACT

Cellulose nanofibrils (CNF) are one-dimensional semicrystalline nanomaterials liberated from native cellulose through chemical or mechanical processes, or some combination thereof. Individually, they possess high mechanical strength, with estimated tensile strength and Young's modulus as high as 7.5 GPa and 150 GPa, respectively. They also serve as a diverse platform for further chemical modification due to their abundant surface hydroxyl groups, which can be functionalized through a wide array of chemical reactions. Isolating CNF from cellulose can be an energy intensive process and chemical pretreatments are often utilized to reduce the required energy expenditure.

Herein a streamlined scheme for producing sulfated cellulose nanofibrils (SCNF) is proposed and optimized, utilizing chlorosulfonic acid to simultaneously functionalize cellulose while also acting as a pretreatment to facilitate defibrillation into nanofibrils. Through careful manipulation of reaction conditions, SCNF are produced with a wide range of sulfation levels without destroying the underlying cellulose 1β crystalline structure.

Utilizing wet-spinning, SCNF was spun into fibers with a tensile strength and Young's modulus of 675 MPa and 26 GPa, respectively. It was also demonstrated that SCNF could serve as host polyelectrolytes for the conducting polymer poly(3,4-ethylenedioxythiophene) (PEDOT) to create dispersible polyelectrolyte complexes, with shear-mediated alignment of nanofibrils allowing for the creation of fibers with a conductivity of more than 6000 S/cm. Additionally, SCNF were able to aid in aqueous exfoliation of graphite flakes and dispersion of graphene, producing exclusively monolayers and bilayers.

TABLE OF CONTENTS

INTRODUCTION

Nanocellulose is a term that encompasses a variety of nanomaterials that can be isolated from cellulose produced by various plants, animals, and bacteria. Cellulose nanofibrils (CNF) are a type of nanocellulose that is obtained by liberating the elementary fibrils in native cellulose through chemical and/or mechanical means. CNF are of interest due to their high inherent tensile strength and modulus and the ease with which their surface hydroxyls may be transformed to a wide variety of moieties. However, interest in CNF and nanocelluloses in general is still largely relegated to academia, and the production of CNF economically and at scale is an ongoing challenge. This dissertation details a streamlined process by which sulfated cellulose nanofibrils (SCNF) may be produced from plant cellulose through a combined chemical/mechanical treatment, and demonstrates several uses and applications thereof.

Chapter 1 consists of a review of the scientific literature surrounding relevant topics, including cellulose, nanocelluloses, polymer wet-spinning, intrinsically conducting polymers, poly(3,4-ethylenedioxythiophene) (PEDOT) and its polyelectrolyte complexes with poly(styrene sulfonate) (PSS), and graphene.

Chapter 2 discusses the simultaneous functionalization and pretreatment of cellulose with chlorosulfonic acid in anhydrous N,N-dimethylformamide (DMF), followed by mechanical blending to produce SCNF in yields exceeding 90 wt%. Varying reaction times (30-60 minutes) and quantities of acid used (0.75-1.5 moles per mole of anhydroglucose) allowed for the creation of SCNF with variable charges in the range of 1.0 – 2.2 mmol/g. Aqueous SCNF suspensions exhibited thixotropy, as well as shear thinning behavior that closely followed power law models.

SCNF dispersions were wet-spun into organic or mixed organic/ionic coagulants, producing continuous fibers possessing a tensile strength and Young's modulus of up to 675 ± 120 MPa and 26 ± 5 GPa, respectively.

Chapter 3 demonstrates the use of SCNF alongside poly(styrene sulfonate) (PSS) as a host polyelectrolyte for the intrinsically conducting polymer poly(3,4-ethylenedioxythiophene) (PEDOT), allowing for the creation of stable aqueous PEDOT dispersions. PEDOT is polymerized in the presence of varying ratios of PSS and SCNF. PEDOT synthesized in conjunction with a polyanion containing 30 wt% SCNF and 70 wt% PSS exhibited a conductivity of 0.14 S/cm, nearly a threefold increase over that synthesized with no SCNF. Utilizing ethylene glycol (EG) as a secondary dopant, PEDOT synthesized with a 10% SCNF polyanion exhibited a conductivity of 37.5 S/cm, 58% higher than that synthesized with PSS alone. PEDOT:PSS/SCNF complexes with up to 50 wt% PEDOT fractions were aqueous dispersible at any composition of PSS and SCNF in the polyanion, though no substantial increase in conductivity was observed when the PEDOT contents were elevated beyond the commonly reported 29 wt%. Fibers wet-spun from PEDOT:PSS/SCNF dispersions containing 30% SCNF in the polyanion boasted impressive conductivities of 40 ± 4 S/cm, which increased to 6150 ± 1000 S/cm after treatment with EG vapor.

Chapter 4 showcases the use of SCNF for both exfoliating and dispersing graphene from graphite through blending in aqueous media. This process converted up to 3.9 wt% graphite to graphene: a relatively low yield. However, the graphene produced consisted exclusively of mono- and bilayers, with 42% being desirable monolayers. Produced graphene sheets had widths ranging from 76 to 353 nm, with the majority being between 150-200 nm. The graphene/SCNF

dispersions, containing 19.5 wt% graphene, could be formed into free-standing films through vacuum filtration, possessing a conductivity of 0.60 ± 0.05 S/cm.

CHAPTER 1. Background and Review of Literature

Cellulose

Cellulose is the most abundant biopolymer on the planet, with an approximate 10^{11} tons produced annually from plants, bacteria, algae, and even animals such as tunicates.[1] It has been utilized extensively in the papermaking and textiles industries, first in native form and later as cellulose derivatives.[2] Chemically, cellulose consists of β(1,4) linked anhydro *d*-glucose units, with each repeat unit—cellobiose—consisting of two anhydroglucose units (AGU) in alternating chair configurations (**Figure 1.1**).[1] Its chain lengths can vary considerably based on source, with wood pulp having degrees of polymerization (DPs) typically between 300 and 1700 while cotton and other plant fibers can have DPs anywhere from 800 to 10,000.[2] Cellulose is a semicrystalline polymer, and it is known to structure itself into a variety of crystalline polymorphs depending on the source and processing. The crystalline domains in native cellulose from plants and animals possess a structure referred to as cellulose I, which itself consists of two crystalline phases: Iα and Iβ. Cellulose Iα is predominantly bacterial in origin, and consists of a triclinic unit cell with one chain. Iβ is the form found predominantly in plants, and consists of a monoclinic unit cell with two parallel chains.[3] When cellulose is dissolved and regenerated from solution, it forms a structure known as cellulose II, with an antiparallel chain configuration.[2]

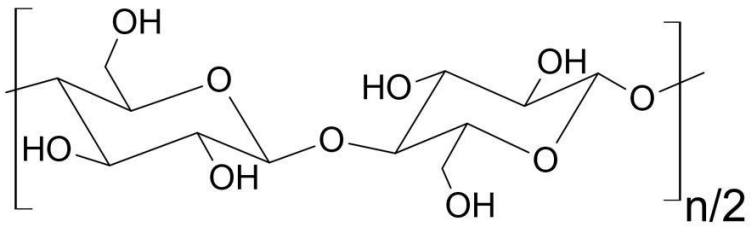

Figure 1.1 Cellulose chain structure

A number of solvent systems have been utilized to dissolve cellulose, either for regeneration or for derivatization. It is known to dissolve in solutions of N,N-dimethyl acetamide (DMAc) containing small amounts (ca. 5 wt%) of lithium chloride.[4] N-methylmorpholine-N-oxide (NMMO) is also utilized industrially in the Lyocell process.[2] Other more niche solvent systems include concentrated phosphoric acid, ammonium thiocyanate in liquid ammonia, and tetrabutylammonium fluoride trihydrate in dimethyl sulfoxide (DMSO).[2]

Cellulose has been extensively derivatized to suit specific applications. Often, derivatization renders the product soluble in one or more common solvents, aiding in processing. Cellulose esters and ethers[2], phosphates[5], aldehydes[6], and carboxylates[7] have all been produced. Of particular interest to this work are cellulose sulfates. Sulfation of cellulose has been carried out through the use of a two-step process involving the cleavage of the cellulose ring between C2 and C3 through the use of sodium metaperiodate to produce a dialdehyde, followed by treatment with sodium bisulfite to produce cellulose decorated with C2 and C3 sulfonate groups.[8,9] On cotton, this treatment was able to introduce up to 0.947 mmol/g charged sulfonate groups.[10] Complexes between SO_3 and pyridine have been used to directly sulfate cellulose dissolved in DMAc and LiCl.[11] Sulfoethyl cellulose ethers with degrees of substitution (DS) of up to 0.65 sulfoethyl groups per AGU have been synthesized by using sodium vinylsulfonate in a mixture of isopropanol (IPA) and sodium hydroxide (NaOH).[12] Deep eutectic solvents consisting of sulfamic acid and urea have been shown to add up to 3 mmol/g of sulfate groups to cellulose, though a carbamation side reaction is believed to occur during this process as well.[13] Chlorosulfonic acid has also been utilized in the creation of cellulose decorated with sulfate half-ester groups through bimolecular substitution (S_N2)[14], most commonly using N,N-

dimethylformamide as a solvent.[15,16] NMR studies have shown that this reaction can heavily favor substitution of cellulose's primary C6 hydroxyl, following expected reaction rate trends for bimolecular substitution.[17] Treatment with concentrated sulfuric acid can add a small number of sulfate half-ester groups to cellulose, though this process leads to significant hydrolysis of amorphous regions and is not typically utilized for the purposes of sulfation.

Sulfation processes have a number of documented ramifications for the properties of resulting cellulose sulfates. Sulfate half-ester groups can undergo self-catalyzed de-esterification at temperatures above 50 °C.[18] This occurs only when the sulfated cellulose is kept in free acid form and can be avoided by neutralization to form the corresponding cellulose sulfate salts. The presence of sulfate groups consistently diminishes the thermal stability of cellulose sulfate compared to native forms, with initial decomposition temperatures measured by thermogravimetric analysis (TGA) at around 150 °C.[15] Additionally, the hydrophilicity of sulfate groups leads cellulose sulfates to both absorb more moisture than native cellulose and have mechanical properties that can vary strongly with moisture level.[9]

Nanocellulose

In native lignocellulosic materials, cellulose chains are arranged in crystalline bundles known as elementary fibrils.[2] These relatively pristine and crystalline groups of cellulose chains exhibit impressive mechanical performance, with a Young's modulus of approximately 140 GPa.[19] Dissolution of cellulose destroys the cellulose I structure, with regeneration into cellulose II significantly reducing the tensile modulus to 88 GPa.[19] Several strategies have been developed in order to liberate the elementary fibrils present in native cellulose without compromising their crystalline structure. These processes produce various types of cellulose nanomaterials, or

nanocelluloses, which leverage the inherent strength of elementary fibrils to possess impressive mechanical strength and modulus.[20]

Treatment of cellulose with concentrated acid causes hydrolysis of the β(1,4) glycosidic linkages, leading to depolymerization. This process preferentially attacks amorphous regions, leaving behind pristine cellulose nanocrystals (CNC). Sulfuric acid is the most commonly utilized reagent, although others such as hydrochloric acid and phosphoric acid have also been demonstrated.[21,22] Sulfuric and phosphoric acid hydrolysis lead to CNCs decorated with small quantities of sulfate and phosphate groups, respectively. While CNCs are often produced in low yields, they are highly crystalline and their mechanical strength and modulus approach the theoretical level predicted for pristine cellulose crystals.[23] CNC generally appear as nanorods, with dimensions that vary based on and correspond to the elementary fibril size for a particular cellulose source.[24,25] Typical sizes range from between 50-1000 nm long and 3-50 nm wide.[21] It is extremely well documented that dispersions of CNC in water and nonpolar solvents can exhibit chiral nematic liquid crystalline behavior[26–34] and can be aligned under magnetic fields.[35] This chirality is likely a result of the right-handed chirality of cellulose itself.[36] CNC dispersions can also exhibit thixotropy and shear thinning behavior as a result of the high aspect ratio of the nanocrystals.[26] This has been leveraged in order to align CNCs through the use of mechanical shearing, as in the case of blade coating.[37] Including CNC into composite materials has been shown to increase their tensile strength and Young's modulus with CNC loadings as low as 1 wt%.[38,39]

As an alternative to harsh and low-yielding acid hydrolysis, a combination of chemical and/or mechanical treatments can be used to separate inter-crystalline chains, yielding cellulose

nanofibrils (CNF). When produced through entirely mechanical means, such as homogenization[40] or aqueous counter-collision[41], nanofibrils of unfunctionalized cellulose can be produced. These fibrils can have typical lateral dimensions on the order of 4-20 nm and lengths of 500-2000 nm. In order to reduce the amount of energy needed to liberate nanofibrils, mechanical disintegration is often preceded by chemical pretreatment. The most common of these treatments is carboxylation mediated by the aminoxyl radical 2,2,6,6-tetramethyl piperidine-1-oxyl (TEMPO).[42] A hallmark of TEMPO-mediated oxidation is the specificity to primary alcohols, ensuring that carboxylation occurs exclusively at the cellulose C6 hydroxyl group.[43] Easy conversion of carboxylated cellulose into nanofibrils was found to require carboxylate contents of at least 0.8 mmol/g.[42] TEMPO CNF, like most anionic CNF produced through a combined chemical-mechanical process, tend to have finer dimensions than those produced through exclusively mechanical means. Nominally, TEMPO CNF can have lateral dimensions of 1.5-2 nm and lengths of up to a micron.[44] It is important to note that a loss of crystallinity often accompanies chemical treatment; TEMPO CNF can see a ca. 25% reduction in crystallinity compared to the cellulose source.[42] Despite this reduction in crystalline ordering, the nanofibrils can still retain impressive mechanical strength, with Young's Modulus as high as 150 GPa being observed.[5]

While TEMPO oxidation is the most commonly variant, other reactions and schemes have been employed to produce CNF functionalized with a wide variety of groups, including carboxymethyl[45], aldehyde[10], and phosphate[46] moieties. Sulfated and sulfonated cellulose nanofibrils (SCNF) have also been created, relying on several different reaction systems. Most expansively, the periodate-bisulfite scheme described previously has been applied to create cellulose nanofibrils with between 0.18-0.51 mmol/g anionic sulfonate[47]; this charge is

significantly lower than the range typically observed for TEMPO-oxidized CNF.[42] However, only a portion of aldehyde groups (15-30%) are successfully sulfonated by this scheme, and residual aldehydes weaken the resulting materials by exposing the cellulose chains to depolymerization reactions through β-alkoxy fragmentation.[47] The sulfamic acid/urea deep eutectic solvent system has also been used to create SCNF, producing high sulfate group concentrations ranging from 1.44-3.00 mmol/g, while also bearing 1.61-4.46 mmol/g of carbamate groups due to side reaction with urea.[13] Chlorosulfonic acid has been utilized to add additional sulfate groups to both CNC[15] and to unfunctionalized CNF produced through mechanical refining.[16] Prior to the current work, chlorosulfonic acid has not been explored as a pretreatment to simultaneously functionalize and pretreat cellulose to facilitate defibrillation into SCNF.

Polymer Spinning of CNF

Translating the impressive mechanical properties of nanocellulose into useful macroscopic structures remains a challenge. It is important to note that the majority of the mechanical strength of cellulose 1β, and in turn CNF and CNC, lies in the direction parallel to the polymer chain. [19] Therefore, an effective means of drawing out this potential is to align the nanomaterials during processing into bulk form. The simplest way of carrying out alignment is through the application of shear force to nanocellulose dispersions. Leveraging this effect, nanocellulose dispersions may be spun into macroscopic fibers of high strength and modulus.[48] A number of different spinning techniques may be applied. Dry-spinning involves extruding the dispersion, or spin dope, directly into air and evaporating the solvent, forming a continuous filament. Dry-spinning can be applied to viscous CNF dispersions without any other polymers present, and has been utilized to produce fibers with a tensile strength of up to 220 MPa and

Young's modulus of 12.6 GPa.[49] However, the fact that water is the predominant solvent for CNF makes dry-spinning tedious to perform on the laboratory scale, as drying requires significant heat or time. Far more common are wet-spinning techniques, where the CNF dope is instead extruded into an antisolvent that causes nanofibrils to rapidly coagulate, forming a filament.[48] A wide variety of organic solvents have been utilized for CNF wet-spinning including ethanol[50], dioxane[50], tetrahydrofuran[50] (THF), and acetone.[51] Aside from organic solvents, another coagulation strategy that has been employed for spinning anionic CNF is to utilize an aqueous solution of salts with multivalent cations, wherein coagulation occurs due to both the screening of electrostatic double-layer repulsion between charged fibrils and ionic crosslinking of the fibrils with the cations.[52] Employing this strategy, TEMPO CNF has been spun into 5 wt% aqueous $CaCl_2$, producing fibers with a tensile strength and Young's modulus 543.1 MPa and 37.5 GPa, respectively. Additionally, the calcium coagulated fibers were found to be less susceptible to moisture than ones coagulated through the organic solvent route. This addresses a key flaw in many materials fabricated solely from nanocellulose: the primary means by which cellulose nanofibrils interact is through hydrogen bonding, and the addition of moisture disrupts this hydrogen bonding, causing a significant drop in strength.[53]

Conducting polymers

The vast majority of polymers are electrical insulators, but a subset of polymers can conduct electricity as semiconductors or, under certain conditions, metallic conductors. These are referred to as intrinsically conducting polymers (ICPs). The differentiating factor between semiconductors and metallic conductors lies in how conductivity fluctuates with a change in temperature. In semiconductors, conductivity increases as temperature is raised; in metallic

conductors, the opposite is true. Semiconductors with very low electrical conductivity are termed insulators, but it should be noted that this classification is one of convenience, and is not indicative of any other significant differences between the two groups.[54] The conductivity of a polymer can be understood by looking at its chain structure and molecular orbitals. While the various ICPs may vary in chain structure, molecular weight, or the incorporation of heteroatoms, they all contain a conjugated π systems along the backbone. The chain structure of common ICPs is shown in **Figure 1.2**.

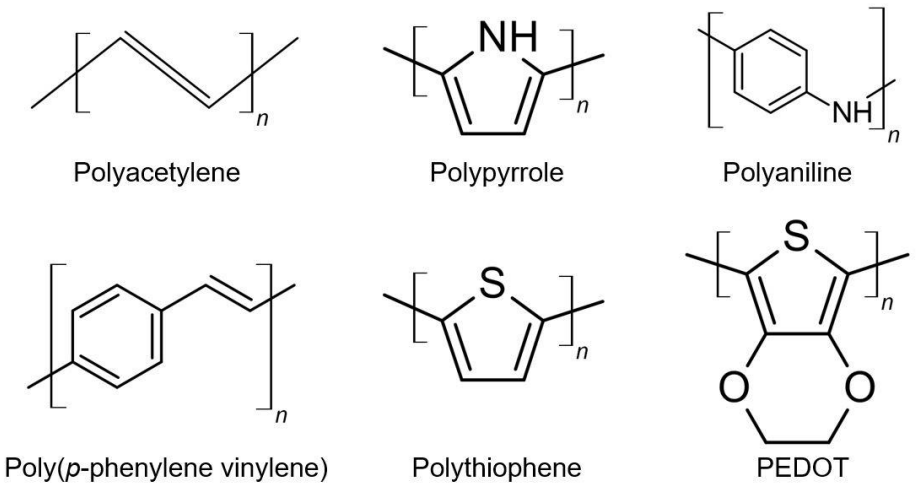

Figure 1.2 Structure of common conducting polymers

It is the band gap—the energy difference between the highest occupied molecular orbital (HOMO) and lowest unoccupied molecular orbital (LUMO)—that determines conductivity.[55] As an example, consider the simplest polymer, polyethylene, with a backbone consisting entirely of single bonded, SP_3 hybridized carbons. Due to the single, σ bonds between carbons on the backbone, the molecular orbitals for the polymer are spread into bands. The HOMO in polyethylene would be at the top of the band formed by σ bonding orbitals—referred to as the valence band—whereas the LUMO is at the bottom of the band formed by σ antibonding (σ*)

orbitals—called the conduction band. In this case, the band gap is large and gives rise to insulating behavior.

Next, consider polyacetylene, the simplest intrinsically conducting polymer (ICP), which has a backbone that instead consists of SP_2 hybridized carbons with alternating double bonds and a conjugated system of π electrons delocalized throughout the length of the chain. The valence band for this polymer consists of π bonding orbitals, which have a higher energy level than the σ orbitals. The conduction band consists of π antibonding (π*) orbitals, which are at a lower energy level than σ* orbitals. This makes the band gap for polyacetylene significantly smaller than for polyethylene, giving rise to intrinsic conductivity.[54]

The conductivity of ICPs in their pristine molecular state, while many orders of magnitude above that of insulating polymers, is often still too low to be useful. This issue can be resolved through modification with various dopants. This process can be analogous to *p*- and *n*-type doping in inorganic semiconductors, creating additional energy levels within the bandgap.[55] The exact process of doping for ICPs varies with the particular polymer, but they in general involve redox reactions of the polymer chain. Oxidation of the chain leads to the abstraction of electrons, and is analogous to *p*-type doping, whereas reduction is similar to *n*-type doping. In either case, the polymeric chain is no longer a neutral polymer but a polymeric ion. For ICPs, doping via oxidation is far more common, with the "*n*-type" doping being relatively rare. The abstraction of an electron from an ICP leads to the formation of a radical cation, or polaron (charge +1, spin ½). As a second electron is abstracted during further oxidation, abstraction can occur either at a different point, forming another polaron, or at the same site, forming a bipolaron (charge +2, spin 0). Bipolarons are favored in the case that the energy gained by interaction with the lattice

is greater than the Coulomb repulsion between two charges being confined together.[56] The presence of polarons or bipolarons is specific to each ICP and can be explored by measuring and comparing both charge and spin for a polymer.[55] Doping has a profound effect on the conductivity of ICPs, increasing it by many orders of magnitude. As an example, in *trans*-polyacetylene, doping can be carried out through reaction with halogen vapors, with iodine being the most effective, increasing conductivity by as much as seven orders of magnitude.[57] In this case, charge-transfer π complexes were formed between the polyacetylene and halogens, leaving the chain cationic (*p*-type).

PEDOT

Central to the present work is the ICP Poly(3,4-ethylenedioxythiophene) (PEDOT). PEDOT is a polythiophene derivative developed by Bayer AG in the 1980s.[58] Its monomer, 3,4-ethylenedioxythiophene (EDOT), consists of polythiophene that is disubstituted with an ethylene glycol unit at the C3 and C4 positions, forming a second six-membered ring. This particular substitution provides a number of advantages. Firstly, it prevents undesirable linkages at the C3 and C4 sites, meaning that polymerization proceeds uniformly between the C2 and C5 sites. Having the C3 and C4 substitutions linked together to form a bicyclic structure leads to more uniform packing of chains compared to thiophene derivatives with individual C3 and C4 substitutions. Finally, The presence of electronegative oxygen atoms adjacent to the thiophene ring stabilizes protonated EDOT and PEDOT species that form during polymerization and doping, rendering EDOT and PEDOT less liable to degradation and undesirable side reactions, particularly in the presence of oxygen and moisture.[55,59]

The mechanism by which EDOT is polymerized into PEDOT does not adhere strictly to the conventions of step and chain polymerization, but instead proceeds by way of acid catalyzed formation of EDOT dimers and trimers with subsequent oxidation into PEDOT. EDOT dimer and trimer formation proceeds initially by protonation in the α position in the presence of strong acids (**Figure 1.3**).[55] These dimers and trimers exist in equilibrium with the monomeric form and

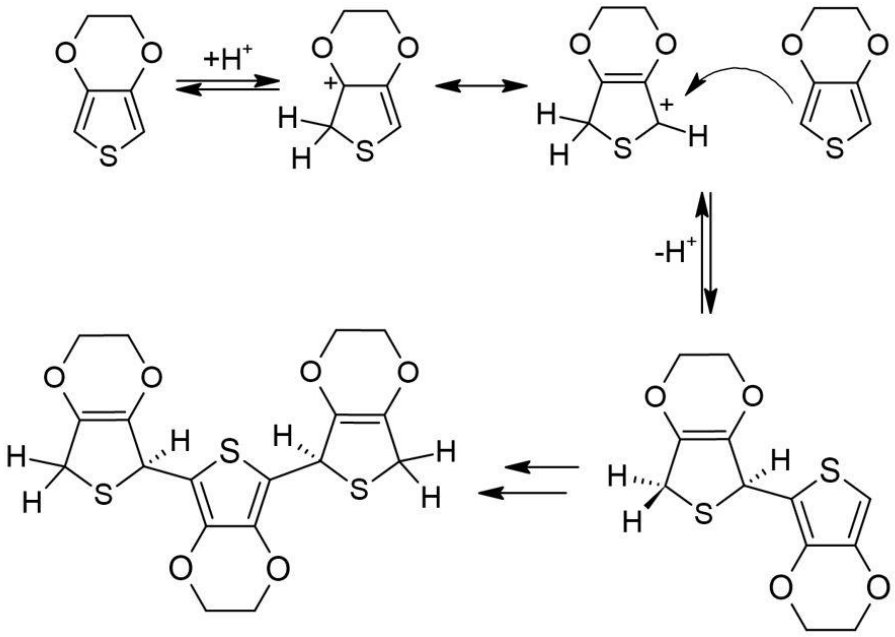

Figure 1.3 Acid catalyzed dimer- and trimerization of EDOT

play an important role in poylermization, as they are more succeptible to oxidation than EDOT itself. Oxidation is carried out either chemically[60] or electrochemically[61], with common chemical oxidants being Iron salts like Iron(III)-tosylate[62] or persulfate salts[55], often activated catalytic amounts of iron or other metals.[63] During PEDOT polymerization, doping occurs as a result of excess oxidants in the system, which lead to the abstraction of electrons from the neutral PEDOT chain. Typical doping levels for PEDOT peak at one positive charge per three thiophene units; as PEDOT favors the formation of bipolarons, this is equivalent to one bipolaron delocalized across six thiophene units.[64]

PEDOT possesses a number of characteristics that have led to its relevance in industry. Pristine crystals of PEDOT can boast conductivities of up to 8797 S/cm[65] only falling behind polyacetylene in terms of electrical performance. However, unlike polyacetylene, PEDOT is stable when exposed to air for extended periods of time. Additionally, it can withstand elevated temperatures of up to 250 °C, allowing it to be integrated into parts that utilize high-temperature lead-free solders.[55] A major commercial uze of PEDOT is as an electrode in solid electrolyte capacitors. PEDOT is coated on top of an oxide dielectric layer, often tantalum or aluminum, to form a self-healing electrode.[66] Defects in the dielectric that would lead to a short cause an influx of current that locally destroys the PEDOT around the defect, cutting off the short circuit and allowing the capacitor to function. Additionally, thin films of PEDOT exhibit high optrical transparency (>75%[67]) in the visible region. This has led to them being investigated as replacements to transparent conductive oxides like indium-tin-oxide (ITO) for photovoltaics, organic LEDs, or other similar applications.[68] PEDOT is also more flexible than traditional inorganic semiconductors, and has been utilized in applications requiring flexible circuits, such as in triboelectric generators.[69] Finally, PEDOT possesses a high Seebeck coefficient, making it a promising thermoelectric material. [70]

PEDOT, particularly in its doped form, is not soluble in any known solvents. This means that fabrication with PEDOT can be a tedious process, often involving polymerizing the polymer directly onto the desired substrate through techniques like chemical vapor deposition.[71] A workaround to this was found when it was noted that cationic, doped PEDOT can form polyelectrolyte complexes that are dispersible in aqueous media.[72] Because PEDOT precipitates rapidly during polymerization, these complexes must be formed in-situ during EDOT

polymerization by adding the anionic host polyelectrolyte (HPE) to the reaction mixture. The first polyanion used for complexation with PEDOT was poly(styrene sulfonate) (PSS), and it has also remained the most popular choice in commercial PEDOT dispersions[55], referred to as PEDOT:PSS and sold under a variety of trade names including Baytron™, Clevios™, and Orgacon™. A wide variety of other polyanions have been used to create dispersible PEDOT complexes, including but not limited to pectin, hyaluronate, dextran sulfate, poly(4-styrenesulfonyl trifluoromethsulfulfonyl)imide, poly(4-styrenesulfonyl methylsulfonyl)imide, and poly(4-styrenesulfonyl phenylsulfonyl)imide, poly(methacrylsulfonyl trifluoromethylsulfonyl)imide.[73] Complexes have also been formed between PEDOT and the anionic conducting polymer poly[2-(3-thienyl)-ethoxy-4-butylsulfonate].[74] While most of these alternative host polyelectrolytes have failed provide significant advantages over PEDOT:PSS, those formed between PEDOT and cellulose sulfate showed promise, producing a nearly four-fold increase in conductivity over PEDOT:PSS.[75] This may be attributed in part to the similarity in charge spacing between doped PEDOT and the cellulose sulfate used, which is known to contribute to an increased degree of ordering in polyelectrolyte complexes.[76]

Secondary Doping of PEDOT:PSS

One factor that has led to the success of PEDOT:PSS is the discovery that certain compounds can be added to the conducting dispersions to yield dramatically increased conductivity. These compounds are broadly referred to in the literature as *conductivity enhancers* or, more commonly, *secondary dopants*.[77] It is important to note that the term secondary dopant, while widespread, is somewhat of a misnomer, representing an entirely different set of phenomena than the doping of conducting polymers described in previously (i.e. redox reactions

on an ICP chain leading to a change in electronic structure). Secondary dopants can be a wide range of low molecular weight compounds added to dispersions either prior to or after processing. The most commonly reported secondary dopants are ethylene glycol (EG)[78,79] and dimethyl sulfoxide (DMSO)[78,80], both of which can yield conductivity increases of more than three orders of magnitude when added to PEDOT:PSS dispersions. Other solvents that can act as secondary dopants include N-methyl-2-pyrrolidone (NMP)[81,82], diethylene glycol[83], N,N-dimethylformamide (DMF)[80], tetrahydrofuran (THF) [80], 2-nitroethanol[79], and glycerol.[84] What is notable about these compounds is that they are generally evaporated by oven-drying the PEDOT dispersion after processing, meaning their conductivity enhancement occurs without their actual presence in the final material. Other compounds that do remain embedded in the PEDOT:PSS matrix have been shown to bring about increased conductivity as well, including sorbitol[81,84,85], meso-erythritol[79], imidazolium-based ionic liquids[86,87], copper(II) chloride[88], and various anionic surfactants[89]. Treatment of PEDOT:PSS with strong acids has also yielded significant increases in conductivity.[90,91] The mechanism behind the increase in conductivity upon addition of these various additives has been debated in the literature, with a number of explanations being proposed. It has been proposed additives act by screening electrostatic interactions binding PEDOT to PSS, allowing PEDOT to aggregate into larger more cohesive domains that transfer charge more effectively.[89] Others have suggested that solvent-based secondary dopants induce phase separation between PEDOT and PSS, reducing the prevalence and thickness of insulating PSS layers between PEDOT-rich regions.[92] Another school of thought is that treatment with secondary dopants simply washes away insulating PSS.[90] Regardless of the specific mechanisms,

the use of secondary doping has brought PEDOT:PSS dispersions into the spotlight, bridging the gap between their conductivity and that of PEDOT itself.

Templating PEDOT using cellulose nanomaterials

It should be evident from the previous examples that the conductivity of PEDOT and PEDOT dispersions is a complex function of many experimental and process variables. The inherent heterogeneity of PEDOT:PSS systems means that their conductivity is as much dependent on supramolecular structure and ordering as it is on molecular factors such as degree of polymerization or chain oxidation level. One strategy that has been utilized to induce organization of PEDOT on a molecular scale is to template it with 1D nanomaterials, including nanocelluloses.

It has been observed that straight mixing of TEMPO CNF with commercial PEDOT:PSS led to a twofold increase in the conductivity of cast films with CNF loadings of up to 50 wt%, from 18.8 to 40.8 S/m. This increase occurred despite the inclusion of additional insulating material into the matrix. In this case it was noted that PEDOT in the composite material showed changes in its x-ray diffraction (XRD) pattern that suggest that more PEDOT chains were adopting a quinoid form, with increasing double-bond character on the links between thiophene units.[93] It has been demonstrated that the nanoscale dimensions of CNF appear to play an important role in its interactions with PEDOT and PEDOT:PSS. When carboxymethylated CNF was mixed with a commercial PEDOT:PSS blend, PEDOT:PSS was observed to organize itself into bead-like structures along the nanofibril surface, with a high degree of π-stacking between PEDOT chains measured through wide-angle XRD (WAXD). However, dissolved carboxymethylcellulose (CMC) produced no such organization, and instead led to films with a high degree of phase separation

between the different components. It is particularly telling that the films incorporating carboxymethyl CNF had conductivities nearly three times higher than those made with CMC.[94] Several other works have reported on the mixing of commercial PEDOT:PSS blends with unfunctionalized nanocellulose[95,96] and cellulose nanocrystals[97] to similar effect.

Apart from mixing nanocellulose into commercial PEDOT:PSS blends, an alternative strategy that has been employed is the polymerization of EDOT in the presence of nanocelluloses. Polymerizing EDOT with hydrogels of unfunctionalized bacterial nanocellulose with either ferric chloride[98] or ferric tosylate[99] has produced PEDOT coated hydrogels that have explored for their capacitive properties and as biocompatible electrodes. Others have created similar hydrogels incorporating PSS into the reaction mixture as well.[100] Analogously, EDOT has been chemically[101] and electrochemically[61,101] polymerized onto CNCs to produce films with high specific surface area, suggested for use in supercapacitors and catalytic applications.

It has also been demonstrated that stable PEDOT dispersions can be created by polymerizing EDOT in the presence of sulfated cellulose nanofibrils, with the anionic nanofibrils acting as host polyelectrolyte for PEDOT chains.[102] For this work, sulfated CNF were produced through treatment with sulfamic acid in urea, followed by homogenization. The degree of substitution of sulfate groups was measured at 0.497, although the previously described carbamation side reaction involved with this reaction scheme[13] means that other functionality was likely present. It was observed that the PEDOT/nanocellulose dispersion could be made with a higher fraction of PEDOT than commercial dispersions, possibly owing to the hydroxyl groups on cellulose aiding in aqueous dispersions. However, the use of secondary dopants was not

examined in this work and the properties, behavior, and utility of PEDOT dispersions with nanofibrillar host polyelectrolytes is still not well examined or understood.

Graphene

Graphene consists of planar sheets of SP^2 hybridized carbons. It is lauded for an impressive array of impressive in-plane physical, thermal, and electrical properties, including an electron carrier mobility of up to 200,000 $cm^2 \cdot V^{-1} \cdot s^{-1}$, thermal conductivity of 3000 $W \cdot m^{-1} \cdot K^{-1}$, and a tensile modulus of 1 TPa; among the highest ever measured.[103] Producing large quantities of high-quality graphene remains a challenge.

The production of graphene can proceed through either top-down or bottom-up approaches. Top-down approaches generally involve exfoliating graphene from graphite. The simplest method of doing so is by applying cellophane tape to graphite and lifting it off, a process which removes a sheet of graphene but is neither scalable nor efficient.[103] For larger scale production, the focus has been on exfoliating graphene in solution through the use of chemical modification, such as oxidation to form graphene oxide followed by ultrasonication in DMF and reduction into graphene with hydrazine.[104] Other strategies include mechanical treatment (often sonication) in organic liquids with surface energies close to that of graphite (ca. 70-80 mJ/m^2)[105] such as DMF[106], N-methyl-2-pyrrolidone (NMP)[107], and 1,2-dichloroethane.[108] Bottom up strategies for fabricating graphene can involve growing it directly from organic precursors such as hexa-*peri*-hexabenzocoronene[109] and hexaphenylbenzene[110] or catalyzing its growth directly on substrates.[111]

References

(1) Conner, A. H. Size Exclusion Chromatography of Cellulose and Cellulose. *Handb. size*

exclusion Chromatogr. **1995**, 331–352.
(2) Klemm, D.; Heublein, B.; Fink, H. P.; Bohn, A. Cellulose: Fascinating Biopolymer and Sustainable Raw Material. *Angew. Chemie - Int. Ed.* **2005**, *44* (22), 3358–3393. https://doi.org/10.1002/anie.200460587.
(3) Nishiyama, Y.; Langan, P.; Chanzy, H. Crystal Structure and Hydrogen-Bonding System in Cellulose Iβ from Synchrotron X-Ray and Neutron Fiber Diffraction. *J. Am. Chem. Soc.* **2002**, *124* (31), 9074–9082. https://doi.org/10.1021/ja0257319.
(4) McCormick, C. L.; Callais, P. A.; Hutchinson, B. H. J. Solution Studies of Cellulose in Lithium Chloride and N,N-Dimethylacetamide. *Macromolecules1* **1985**, *18* (12), 2394–2401.
(5) Araki, J.; Wada, M.; Kuga, S.; Okano, T. Influence of Surface Charge on Viscosity Behavior of Cellulose Microcrystal Suspension. *J. Wood Sci.* **1999**, *45* (3), 258–261. https://doi.org/10.1007/BF01177736.
(6) Sirvio, J.; Hyvakko, U.; Liimatainen, H.; Niinimaki, J.; Hormi, O. Periodate Oxidation of Cellulose at Elevated Temperatures Using Metal Salts as Cellulose Activators. *Carbohydr. Polym.* **2011**, *83* (3), 1293–1297. https://doi.org/10.1016/j.carbpol.2010.09.036.
(7) Okita, Y.; Saito, T.; Isogai, A. Entire Surface Oxidation of Various Cellulose Microfibrils by TEMPO-Mediated Oxidation. *Biomacromolecules* **2010**, *11* (6), 1696–1700. https://doi.org/10.1021/bm100214b.
(8) Shet, R. T.; Raj R. Wallajapet, P. Sulfonated Cellulose Having Improved Absorbent Properties. US5703225A, 1995.
(9) Hou, Q. X.; Liu, W.; Liu, Z. H.; Bai, L. L. Characteristics of Wood Cellulose Fibers Treated with Periodate and Bisulfite. *Ind. Eng. Chem. Res.* **2007**, *46* (23), 7830–7837. https://doi.org/10.1021/ie0704750.
(10) Nikiforova, T. E.; Kozlov, V. A. Study of the Effect of Oxidative-Bisulfite Modification of the Cotton Cellulose on Its Ion Exchange Properties. *Russ. J. Gen. Chem.* **2011**, *81* (10), 2136–2141. https://doi.org/10.1134/S1070363211100173.
(11) Qin, Z.; Ji, L.; Yin, X.; Zhu, L.; Lin, Q.; Qin, J. Synthesis and Characterization of Bacterial Cellulose Sulfates Using a SO 3 /Pyridine Complex in DMAc/LiCl. *Carbohydr. Polym.* **2014**, *101* (1), 947–953. https://doi.org/10.1016/j.carbpol.2013.09.068.
(12) Zhang, K.; Brendler, E.; Gebauer, K.; Gruner, M.; Fischer, S. Synthesis and Characterization of Low Sulfoethylated Cellulose. *Carbohydr. Polym.* **2011**, *83* (2), 616–622. https://doi.org/10.1016/j.carbpol.2010.08.030.
(13) Sirviö, J. A.; Ukkola, J.; Liimatainen, H. Direct Sulfation of Cellulose Fibers Using a Reactive Deep Eutectic Solvent to Produce Highly Charged Cellulose Nanofibers. *Cellulose*. 2019, pp 2303–2316. https://doi.org/10.1007/s10570-019-02257-8.
(14) Cremlyn, R. J. *Chlorosulfonic Acid*; Royal Society of Chemistry: Cambridge, 2007. https://doi.org/10.1039/9781847550507.
(15) Lin, N.; Dufresne, A. Surface Chemistry, Morphological Analysis and Properties of Cellulose Nanocrystals with Gradiented Sulfation Degrees. *Nanoscale* **2014**, *6* (10), 5384–5393. https://doi.org/10.1039/c3nr06761k.
(16) Luo, J.; Semenikhin, N.; Chang, H.; Moon, R. J.; Kumar, S. Post-Sulfonation of Cellulose Nanofibrils with a One-Step Reaction to Improve Dispersibility. *Carbohydr. Polym.* **2018**, *181*, 247–255. https://doi.org/10.1016/j.carbpol.2017.10.077.

(17) Zhang, K.; Brendler, E.; Geissler, A.; Fischer, S. Synthesis and Spectroscopic Analysis of Cellulose Sulfates with Regulable Total Degrees of Substitution and Sulfation Patterns via 13C NMR and FT Raman Spectroscopy. *Polymer (Guildf).* **2011**, *52* (1), 26–32. https://doi.org/10.1016/j.polymer.2010.11.017.
(18) Beck, S.; Bouchard, J. Auto-Catalyzed Acidic Desulfation of Cellulose Nanocrystals. *Nord. Pulp Pap. Res. J.* **2014**, *29* (1), 6–14. https://doi.org/10.3183/npprj-2014-29-01-p006-014.
(19) Nishino, T.; Takano, K.; Nakamae, K. Elastic Modulus of the Crystalline Regions of Cellulose Polymorphs. *J. Polym. Sci. Part B Polym. Phys.* **1995**, *33* (11), 1647–1651. https://doi.org/10.1002/polb.1995.090331110.
(20) Abitbol, T.; Rivkin, A.; Cao, Y.; Nevo, Y.; Abraham, E.; Ben-Shalom, T.; Lapidot, S.; Shoseyov, O. Nanocellulose, a Tiny Fiber with Huge Applications. *Curr. Opin. Biotechnol.* **2016**, *39*, 76–88. https://doi.org/10.1016/j.copbio.2016.01.002.
(21) Habibi, Y.; Lucia, L. A.; Rojas, O. J. Cellulose Nanocrystals: Chemistry, Self-Assembly, and Applications. *Chem. Rev.* **2010**, *110* (6), 3479–3500. https://doi.org/10.1021/cr900339w.
(22) Camarero Espinosa, S.; Kuhnt, T.; Foster, E. J.; Weder, C. Isolation of Thermally Stable Cellulose Nanocrystals by Phosphoric Acid Hydrolysis. *Biomacromolecules* **2013**, *14* (4), 1223–1230. https://doi.org/10.1021/bm400219u.
(23) Šturcová, A.; Davies, G. R.; Eichhorn, S. J. Elastic Modulus and Stress-Transfer Properties of Tunicate Cellulose Whiskers. *Biomacromolecules* **2005**, *6* (2), 1055–1061. https://doi.org/10.1021/bm049291k.
(24) Elazzouzi-Hafraoui, S.; Nishiyama, Y.; Putaux, J.-L.; Heux, L.; Dubreuil, F.; Rochas, C. The Shape and Size Distribution of Crystalline Nanoparticles Prepared by Acid Hydrolysis of Native Cellulose. *Biomacromolecules* **2008**, *9* (1), 57–65. https://doi.org/10.1021/bm700769p.
(25) Beck-Candanedo, S.; Roman, M.; Gray, D. G. Effect of Reaction Conditions on the Properties and Behavior of Wood Cellulose Nanocrystal Suspensions. *Biomacromolecules* **2005**, *6* (2), 1048–1054. https://doi.org/10.1021/bm049300p.
(26) Araki, J.; Wada, M.; Kuga, S.; Okano, T. Flow Properties of Microcrystalline Cellulose Suspension Prepared by Acid Treatment of Native Cellulose. *Colloids Surfaces A Physicochem. Eng. Asp.* **1998**, *142* (1), 75–82. https://doi.org/10.1016/S0927-7757(98)00404-X.
(27) Revol, J. F.; Bradford, H.; Giasson, J.; Marchessault, R. H.; Gray, D. G. Helicoidal Self-Ordering of Cellulose Microfibrils in Aqueous Suspension. *Int. J. Biol. Macromol.* **1992**, *14* (3), 170–172. https://doi.org/10.1016/S0141-8130(05)80008-X.
(28) Heux, L.; Chauve, G.; Bonini, C. Nonflocculating and Chiral-Nematic Self-Ordering of Cellulose Microcrystals Suspensions in Nonpolar Solvents. *Langmuir* **2000**, *16* (21), 8210–8212. https://doi.org/10.1021/la9913957.
(29) Araki, J.; Wada, M.; Kuga, S. Steric Stabilization of a Cellulose Microcrystal Suspension by Poly(Ethylene Glycol) Grafting. *Langmuir* **2001**, *17* (1), 21–27. https://doi.org/10.1021/la001070m.
(30) Araki, J.; Kuga, S. Effect of Trace Electrolyte on Liquid Crystal Type of Cellulose Microcrystals. *Langmuir* **2001**, *17* (15), 4493–4496. https://doi.org/10.1021/la0102455.
(31) Dong, X. M.; Kimura, T.; Revol, J.-F.; Gray, D. G. Effects of Ionic Strength on the Isotropic−Chiral Nematic Phase Transition of Suspensions of Cellulose Crystallites.

Langmuir **2002**, *12* (8), 2076–2082. https://doi.org/10.1021/la950133b.
(32) De Souza Lima, M. M.; Wong, J. T.; Paillet, M.; Borsali, R.; Pecora, R. Translational and Rotational Dynamics of Rodlike Cellulose Whiskers. *Langmuir* **2003**, *19* (1), 24–29. https://doi.org/10.1021/la020475z.
(33) Miler, A. F.; Donald, A. M. Imaging of Anisotropic Cellulose Suspensions Using Environmental Scanning Electron Microscopy. *Biomacromolecules* **2003**, *4* (3), 510–517. https://doi.org/10.1021/bm0200837.
(34) Roman, M.; Gray, D. G. Parabolic Focal Conics in Self-Assembled Solid Films of Cellulose Nanocrystals. *Langmuir* **2005**, *21* (12), 5555–5561. https://doi.org/10.1021/la046797f.
(35) Kimura, F.; Kimura, T.; Tamura, M.; Hirai, A.; Ikuno, M.; Horii, F. Magnetic Alignment of the Chiral Nematic Phase of a Cellulose Microfibril Suspension. *Langmuir* **2005**, *21* (5), 2034–2037. https://doi.org/10.1021/la0475728.
(36) Usov, I.; Nyström, G.; Adamcik, J.; Handschin, S.; Schütz, C.; Fall, A.; Bergström, L.; Mezzenga, R. Understanding Nanocellulose Chirality and Structure-Properties Relationship at the Single Fibril Level. *Nat. Commun.* **2015**, *6*. https://doi.org/10.1038/ncomms8564.
(37) Kim, J.; Peretti, J.; Lahlil, K.; Boilot, J. P.; Gacoin, T. Optically Anisotropic Thin Films by Shear-Oriented Assembly of Colloidal Nanorods. *Adv. Mater.* **2013**, *25* (24), 3295–3300. https://doi.org/10.1002/adma.201300594.
(38) Matos Ruiz, M.; Cavaillé, J. Y.; Dufresne, A.; Gèrard, J. F.; Graillat, C. Processing and Characterization of New Thermoset Nanocomposites Based on Cellulose Whiskers. *Compos. Interfaces* **2000**, *7* (2), 117–131. https://doi.org/10.1163/156855400300184271.
(39) Anglès, M. N.; Dufresne, A. Plasticized Starch/Tunicin Whiskers Nanocomposites. 1. Structural Analysis. *Macromolecules* **2002**, *33* (22), 8344–8353. https://doi.org/10.1021/ma0008701.
(40) Moon, R. J.; Martini, A.; Nairn, J.; Simonsen, J.; Youngblood, J. Cellulose Nanomaterials Review: Structure, Properties and Nanocomposites. *Chem. Soc. Rev.* **2011**, *40* (7), 3941–3994. https://doi.org/10.1039/c0cs00108b.
(41) Jiang, F.; Kondo, T.; Hsieh, Y. Lo. Rice Straw Cellulose Nanofibrils via Aqueous Counter Collision and Differential Centrifugation and Their Self-Assembled Structures. *ACS Sustain. Chem. Eng.* **2016**, *4* (3), 1697–1706. https://doi.org/10.1021/acssuschemeng.5b01653.
(42) Isogai, A.; Saito, T.; Fukuzumi, H. TEMPO-Oxidized Cellulose Nanofibers. *Nanoscale* **2011**, *3* (1), 71–85. https://doi.org/10.1039/c0nr00583e.
(43) Lucio Anelli, P.; Biffi, C.; Montanari, F.; Quici, S. Fast and Selective Oxidation of Primary Alcohols to Aldehydes or to Carboxylic Acids and of Secondary Alcohols to Ketones Mediated by Oxoammonium. *J. Am. Chem. Soc* **1987**, *52* (5), 4492.
(44) Jiang, F.; Han, S.; Hsieh, Y. Lo. Controlled Defibrillation of Rice Straw Cellulose and Self-Assembly of Cellulose Nanofibrils into Highly Crystalline Fibrous Materials. *RSC Adv.* **2013**, *3* (30), 12366–12375. https://doi.org/10.1039/c3ra41646a.
(45) Fall, A. B.; Lindström, S. B.; Sundman, O.; Ödberg, L.; Wågberg, L. Colloidal Stability of Aqueous Nanofibrillated Cellulose Dispersions. *Langmuir* **2011**, *27* (18), 11332–11338. https://doi.org/10.1021/la201947x.
(46) Božič, M.; Liu, P.; Mathew, A. P.; Kokol, V. Enzymatic Phosphorylation of Cellulose

Nanofibers to New Highly-Ions Adsorbing, Flame-Retardant and Hydroxyapatite-Growth Induced Natural Nanoparticles. *Cellulose* **2014**, *21* (4), 2713–2726. https://doi.org/10.1007/s10570-014-0281-8.
(47) Liimatainen, H.; Visanko, M.; Sirviö, J.; Hormi, O.; Niinimäki, J. Sulfonated Cellulose Nanofibrils Obtained from Wood Pulp through Regioselective Oxidative Bisulfite Pre-Treatment. *Cellulose* **2013**, *20* (2), 741–749. https://doi.org/10.1007/s10570-013-9865-y.
(48) Clemons, C. Nanocellulose in Spun Continuous Fibers: A Review and Future Outlook. *J. Renew. Mater.* **2016**, *4* (5), 327–339. https://doi.org/10.7569/JRM.2016.634112.
(49) Shen, Y.; Orelma, H.; Sneck, A.; Kataja, K.; Salmela, J.; Qvintus, P.; Suurnäkki, A.; Harlin, A. High Velocity Dry Spinning of Nanofibrillated Cellulose (CNF) Filaments on an Adhesion Controlled Surface with Low Friction. *Cellulose* **2016**, *23* (6), 3393–3398. https://doi.org/10.1007/s10570-016-1044-5.
(50) Walther, A.; Timonen, J. V. I.; Díez, I.; Laukkanen, A.; Ikkala, O. Multifunctional High-Performance Biofibers Based on Wet-Extrusion of Renewable Native Cellulose Nanofibrils. *Adv. Mater.* **2011**, *23* (26), 2924–2928. https://doi.org/10.1002/adma.201100580.
(51) Iwamoto, S.; Isogai, A.; Iwata, T. Structure and Mechanical Properties of Wet-Spun Fibers Made from Natural Cellulose Nanofibers. *Biomacromolecules* **2011**, *12* (3), 831–836. https://doi.org/10.1021/bm101510r.
(52) Kim, H. C.; Kim, D.; Lee, J. Y.; Zhai, L.; Kim, J. Effect of Wet Spinning and Stretching to Enhance Mechanical Properties of Cellulose Nanofiber Filament. *Int. J. Precis. Eng. Manuf. - Green Technol.* **2019**, *6* (3), 567–575. https://doi.org/10.1007/s40684-019-00070-z.
(53) Cunha, A. G.; Lundahl, M. J.; Ansari, M. F.; Johansson, L.-S.; Campbell, J. M.; Rojas, O. J. Surface Structuring and Water Interactions of Nanocellulose Filaments Modified with Organosilanes toward Wearable Materials. *ACS Appl. Nano Mater.* **2018**, acsanm.8b01268. https://doi.org/10.1021/acsanm.8b01268.
(54) Atkin, P.; Paula, J. *Physical Chemistry*; 2006. https://doi.org/10.1039/C1CS15191F.
(55) Elschner, A.; Kirchmeyer, S.; Lovenich, W.; Merker, U.; Reuter, K. *PEDOT: Principles and Applications of an Intrinsically Conductive Polymer*; CRC Press, 2010.
(56) Brédas, J. L.; Streets, G. B. Polarons, Bipolaron, and Solitons in Conducting Polymers. *Acc. Chem. Res* **1985**, *18*, 309–315.
(57) Shirakawa, H.; Louis, E. J.; MacDiarmid, A. G.; Chiang, C. K.; Heeger, A. J. *Synthesis of Electrically Conducting Organic Polymers*; 1977; Vol. 36. https://doi.org/10.1039/C39770000578.
(58) Friedrich, J.; Heywang, G.; Werner, S.; Heinze, J.; Michael, D. Polythiophenes, Process for Their Preparation and Their Use. EP 0339340 A2, 1989.
(59) Heywang, B. G.; Jonas, F. New , Very Stable Conducting Polymers. *Adv. Mater.* **1992**, *4* (2), 116–118.
(60) Moon, G. H.; Foulger, S. H. Preparation of Poly(3,4-Ethylemedioxythiophene) (PEDOT) Coated Silica Core-Shell Particles and PEDOT Hollow Particles. *Chem. Commun.* **2004**, *10* (19), 2154–2155. https://doi.org/10.1039/b409396h.
(61) Ravit, R.; Abdullah, J.; Ahmad, I.; Sulaiman, Y. Electrochemical Performance of Poly(3, 4-Ethylenedioxythipohene)/Nanocrystalline Cellulose (PEDOT/NCC) Film for

Supercapacitor. *Carbohydr. Polym.* **2018**, *203* (June 2018), 128–138. https://doi.org/10.1016/j.carbpol.2018.09.043.
(62) Winther-Jensen, B.; Breiby, D. W.; West, K. Base Inhibited Oxidative Polymerization of 3,4-Ethylenedioxythiophene with Iron(III)Tosylate. In *Synthetic Metals*; 2005; Vol. 152, pp 1–4. https://doi.org/10.1016/j.synthmet.2005.07.085.
(63) Anipsitakis, G. P.; Dionysiou, D. D. Radical Generation by the Interaction of Transition Metals with Common Oxidants. *Environ. Sci. Technol.* **2004**, *38* (13), 3705–3712. https://doi.org/10.1021/es035121o.
(64) Kim, D.; Zozoulenko, I. Why Is Pristine PEDOT Oxidized to 33%? A Density Functional Theory Study of Oxidative Polymerization Mechanism. *J. Phys. Chem. B* **2019**, *123* (24), 5160–5167. https://doi.org/10.1021/acs.jpcb.9b01745.
(65) Cho, B.; Park, K. S.; Baek, J.; Oh, H. S.; Koo Lee, Y. E.; Sung, M. M. Single-Crystal Poly(3,4-Ethylenedioxythiophene) Nanowires with Ultrahigh Conductivity. *Nano Lett.* **2014**, *14* (6), 3321–3327. https://doi.org/10.1021/nl500748y.
(66) Kudoh, Y.; Akami, K.; Matsuya, Y. Solid Electrolytic Capacitor with Highly Stable Conducting Polymer as a Counter Electrode. *Synth. Met.* **1999**, *102* (1–3), 973–974. https://doi.org/10.1016/S0379-6779(98)01012-1.
(67) Kirchmeyer, S.; Jonas, F. Transparant Layers of Polythiophene Having High Conductivity. EP 1 338 617, 2002.
(68) Levermore, P. A.; Chen, L.; Wang, X.; Das, R.; Bradley, D. D. C. Highly Conductive Poly(3,4-Ethylenedioxythiophene) Films by Vapor Phase Polymerization for Application in Efficient Organic Light-Emitting Diodes. *Adv. Mater.* **2007**, *19* (17), 2379–2385. https://doi.org/10.1002/adma.200700614.
(69) Kim, Y.; Na, J.; Park, C.; Shin, H.; Kim, E. PEDOT as a Flexible Organic Electrode for a Thin Film Acoustic Energy Harvester. *ACS Appl. Mater. Interfaces* **2015**, *7* (30), 16279–16286. https://doi.org/10.1021/acsami.5b02762.
(70) Wei, Q.; Mukaida, M.; Kirihara, K.; Naitoh, Y.; Ishida, T. Recent Progress on PEDOT-Based Thermoelectric Materials. *Materials*. 2015, pp 732–750. https://doi.org/10.3390/ma8020732.
(71) Lock, J. P.; Im, S. G.; Gleason, K. K. Oxidative Chemical Vapor Deposition of Electrically Conducting Poly(3,4-Ethylenedioxythiophene) Films. *Macromolecules* **2006**, *39* (16), 5326–5329. https://doi.org/10.1021/ma060113o.
(72) Jonas, F.; Krafft, W. New Polythiophene Dispersions, Their Preparation and Their Use. EP 440957, 1990.
(73) Hofmann, A. I.; Katsigiannopoulos, D.; Mumtaz, M.; Petsagkourakis, I.; Pecastaings, G.; Fleury, G.; Schatz, C.; Pavlopoulou, E.; Brochon, C.; Hadziioannou, G.; Cloutet, E. How to Choose Polyelectrolytes for Aqueous Dispersions of Conducting PEDOT Complexes. *Macromolecules* **2017**, *50* (5), 1959–1969. https://doi.org/10.1021/acs.macromol.6b02504.
(74) Dai, C. A.; Chang, C. J.; Chi, H. Y.; Chien, H. T.; Su, W. F.; Chiu, W. Y. Emulsion Synthesis of Nanoparticles Containing PEDOT Using Conducting Polymeric Surfactant: Synergy for Colloid Stability and Intercalation Doping. *J. Polym. Sci. Part A Polym. Chem.* **2008**, *46* (7), 2536–2548. https://doi.org/10.1002/pola.22585.
(75) Horikawa, M.; Fujiki, T.; Shirosaki, T.; Ryu, N.; Sakurai, H.; Nagaoka, S.; Ihara, H. The

Development of a Highly Conductive PEDOT System by Doping with Partially Crystalline Sulfated Cellulose and Its Electric Conductivity. *J. Mater. Chem. C* **2015**, *3* (34), 8881–8887. https://doi.org/10.1039/c5tc02074c.

(76) Lounis, F. M.; Chamieh, J.; Gonzalez, P.; Cottet, H.; Leclercq, L. Prediction of Polyelectrolyte Complex Stoichiometry for Highly Hydrophilic Polyelectrolytes. *Macromolecules* **2016**, *49* (10), 3881–3888. https://doi.org/10.1021/acs.macromol.6b00463.

(77) MacDiarmid, A. G.; Epstein, A. J. The Concept of Secondary Doping as Applied to Polyaniline. *Synth. Met.* **1994**, *65* (2–3), 103–116. https://doi.org/10.1016/0379-6779(94)90171-6.

(78) Kim, N.; Lee, B. H.; Choi, D.; Kim, G.; Kim, H.; Kim, J. R.; Lee, J.; Kahng, Y. H.; Lee, K. Role of Interchain Coupling in the Metallic State of Conducting Polymers. *Phys. Rev. Lett.* **2012**, *109* (10). https://doi.org/10.1103/PhysRevLett.109.106405.

(79) Ouyang, J.; Chu, C. W.; Chen, F. C.; Xu, Q.; Yang, Y. High-Conductivity Poly(3,4-Ethylenedioxythiophene):Poly(Styrene Sulfonate) Film and Its Application in Polymer Optoelectronic Devices. *Adv. Funct. Mater.* **2005**, *15* (2), 203–208. https://doi.org/10.1002/adfm.200400016.

(80) Kim, J. Y.; Jung, J. H.; Lee, D. E.; Joo, J. Enhancement of Electrical Conductivity of Poly(3,4-Ethylenedioxythiophene)/Poly(4-Styrenesulfonate) by a Change of Solvents. *Synth. Met.* **2002**, *126* (2–3), 311–316. https://doi.org/10.1016/S0379-6779(01)00576-8.

(81) Jönsson, S. K. M.; Birgerson, J.; Crispin, X.; Greczynski, G.; Osikowicz, W.; Denier van der Gon, A. W.; Salaneck, W. R.; Fahlman, M. The Effects of Solvents on the Morphology and Sheet Resistance in Poly(3,4-Ethylenedioxythiophene)-Polystyrenesulfonic Acid (PEDOT-PSS) Films. *Synth. Met.* **2003**, *139* (1), 1–10. https://doi.org/10.1016/S0379-6779(02)01259-6.

(82) Louwet, F.; Groenendaal, L.; Dhaen, J.; Manca, J.; Van Luppen, J.; Verdonck, E.; Leenders, L. PEDOT/PSS: Synthesis, Characterization, Properties and Applications. *Synth. Met.* **2003**, *135–136*, 115–117. https://doi.org/10.1016/S0379-6779(02)00518-0.

(83) Crispin, X.; Jakobsson, F. L. E.; Crispin, A.; Grim, P. C. M.; Andersson, P.; Volodin, A.; Haesendonck, C. Van; Auweraer, M. Van Der; Salaneck, W. R.; Berggren, M. The Origin of the High Conductivity of (PEDOT − PSS) Plastic Electrodes The Origin of the High Conductivity Of. *Chem. Mater.* **2006**, *18* (July), 4354–4360. https://doi.org/10.1021/cm061032.

(84) Ghosh, S.; Inganäs, O. Nano-Structured Conducting Polymer Network Based on PEDOT-PSS. *Synth. Met.* **2001**, *121* (1–3), 1321–1322. https://doi.org/10.1016/S0379-6779(00)01523-X.

(85) Timpanaro, S.; Kemerink, M.; Touwslager, F. J.; De Kok, M. M.; Schrader, S. Morphology and Conductivity of PEDOT/PSS Films Studied by Scanning-Tunneling Microscopy. *Chem. Phys. Lett.* **2004**, *394* (4–6), 339–343. https://doi.org/10.1016/j.cplett.2004.07.035.

(86) Döbbelin, M.; Marcilla, R.; Salsamendi, M.; Pozo-Gonzalo, C.; Carrasco, P. M.; Pomposo, J. A.; Mecerreyes, D. Influence of Ionic Liquids on the Electrical Conductivity and Morphology of PEDOT:PSS Films. *Chem. Mater.* **2007**, *19* (9), 2147–2149. https://doi.org/10.1021/cm070398z.

(87) De Izarra, A.; Park, S.; Lee, J.; Lansac, Y.; Jang, Y. H. Ionic Liquid Designed for PEDOT:PSS

Conductivity Enhancement. *J. Am. Chem. Soc.* **2018**, *140* (16), 5375–5384. https://doi.org/10.1021/jacs.7b10306.
(88) Xia, Y.; Ouyang, J. Salt-Induced Charge Screening and Significant Conductivity Enhancement of Conducting Poly(3,4-Ethylenedioxythiophene): Poly(Styrenesulfonate). *Macromolecules* **2009**, *42* (12), 4141–4147. https://doi.org/10.1021/ma900327d.
(89) Fan, B.; Mei, X.; Ouyang, J. Significant Conductivity Enhancement of Conductive Poly(3,4-Ethylenedioxythiophene): Poly(Styrenesulfonate) Films by Adding Anionic Surfactants into Polymer Solution. *Macromolecules* **2008**, *41* (16), 5971–5973. https://doi.org/10.1021/ma8012459.
(90) Xia, Y.; Ouyang, J. Significant Conductivity Enhancement of Conductive Poly(3,4-Ethylenedioxythiophene): Poly(Styrenesulfonate) Films through a Treatment with Organic Carboxylic Acids and Inorganic Acids. *ACS Appl. Mater. Interfaces* **2010**, *2* (2), 474–483. https://doi.org/10.1021/am900708x.
(91) Sakunpongpitiporn, P.; Phasuksom, K.; Sirivat, A. Tuning of PEDOT:PSS Synthesis via Multiple Doping for Enhanced Electrical Conductivity. *Polym. Int.* **2021**, *70* (10), 1534–1543. https://doi.org/10.1002/pi.6234.
(92) Nardes, A. M.; Janssen, R. A. J.; Kemerink, M. A Morphological Model for the Solvent-Enhanced Conductivity of PEDOT:PSS Thin Films. *Adv. Funct. Mater.* **2008**, *18* (6), 865–871. https://doi.org/10.1002/adfm.200700796.
(93) Zhou, J.; Hsieh, Y.-L. Conductive Polymer Protonated Nanocellulose Aerogels for Tunable and Linearly Responsive Strain Sensors. *ACS Appl. Mater. Interfaces* **2018**, *10* (33), 27902–27910. https://doi.org/10.1021/acsami.8b10239.
(94) Belaineh, D.; Andreasen, J. W.; Palisaitis, J.; Malti, A.; Håkansson, K.; Wågberg, L.; Crispin, X.; Engquist, I.; Berggren, M. Controlling the Organization of PEDOT:PSS on Cellulose Structures. *ACS Appl. Polym. Mater.* **2019**, *1* (9), 2342–2351. https://doi.org/10.1021/acsapm.9b00444.
(95) Edberg, J.; Malti, A.; Granberg, H.; Hamedi, M. M.; Crispin, X.; Engquist, I.; Berggren, M. Electrochemical Circuits from “cut and Stick” PEDOT:PSS Nanocellulose Composite. *Flex. Print. Electron.* **2017**, *2* (4). https://doi.org/10.1088/2058-8585/aa8027.
(96) Ko, Y.; Kim, J.; Kim, D.; Kwon, G.; Yamauchi, Y.; You, J. Fabrication of Highly Conductive Porous Cellulose/PEDOT: PSS Nanocomposite Paper via Post-Treatment. *Nanomaterials* **2019**, *9* (4). https://doi.org/10.3390/nano9040612.
(97) Zhou, S.; Qiu, Z.; Strømme, M.; Wang, Z. Highly Crystalline PEDOT Nanofiber Templated by Highly Crystalline Nanocellulose. *Adv. Funct. Mater.* **2020**, *30* (49), 1–9. https://doi.org/10.1002/adfm.202005757.
(98) Chen, C.; Zhang, T.; Zhang, Q.; Feng, Z.; Zhu, C.; Yu, Y.; Li, K.; Zhao, M.; Yang, J.; Liu, J.; Sun, D. Three-Dimensional BC/PEDOT Composite Nanofibers with High Performance for Electrode-Cell Interface. *ACS Appl. Mater. Interfaces* **2015**, *7* (51), 28244–28253. https://doi.org/10.1021/acsami.5b07273.
(99) Müller, D.; Cercená, R.; Gutiérrez Aguayo, A. J.; Porto, L. M.; Rambo, C. R.; Barra, G. M. O. Flexible PEDOT-Nanocellulose Composites Produced by in Situ Oxidative Polymerization for Passive Components in Frequency Filters. *J. Mater. Sci. Mater. Electron.* **2016**, *27* (8), 8062–8067. https://doi.org/10.1007/s10854-016-4804-y.
(100) Chen, C.; Yu, Y.; Li, K.; Zhao, M.; Liu, L.; Yang, J.; Liu, J.; Sun, D. Facile Approach to the

Fabrication of 3D Electroconductive Nanofibers with Controlled Size and Conductivity Templated by Bacterial Cellulose. *Cellulose* **2015**, *22* (6), 3929–3939. https://doi.org/10.1007/s10570-015-0770-4.

(101) Fan, J.; Shao, W.; Xu, G.; Cui, X. T.; Luo, X. Preparation and Electrochemical Catalytic Application of Nanocrystalline Cellulose Doped Poly(3,4-Ethylenedioxythiophene) Conducting Polymer Nanocomposites. *RSC Adv.* **2014**, *4* (46), 24328–24333. https://doi.org/10.1039/c4ra02796e.

(102) Feng, X.; Wang, X.; Wang, M.; Zhou, S.; Dang, C.; Zhang, C.; Chen, Y.; Qi, H. Novel PEDOT Dispersion by In-Situ Polymerization Based on Sulfated Nanocellulose. *Chem. Eng. J.* **2021**, *418*, 129533. https://doi.org/10.1016/j.cej.2021.129533.

(103) Allen, M. J.; Tung, V. C.; Kaner, R. B. Honeycomb Carbon: A Review of Graphene. *Chem. Rev.* **2010**, *110* (1), 132–145. https://doi.org/10.1021/cr900070d.

(104) Stankovich, S.; Piner, R. D.; Chen, X.; Wu, N.; Nguyen, S. T.; Ruoff, R. S. Stable Aqueous Dispersions of Graphitic Nanoplatelets via the Reduction of Exfoliated Graphite Oxide in the Presence of Poly(Sodium 4-Styrenesulfonate). *J. Mater. Chem.* **2006**, *16* (2), 155–158. https://doi.org/10.1039/b512799h.

(105) Coleman, J. N. Liquid Exfoliation of Defect-Free Graphene. *Acc. Chem. Res.* **2013**, *46* (1), 14–22. https://doi.org/10.1021/ar300009f.

(106) Furtado, C. A.; Kim, U. J.; Gutierrez, H. R.; Pan, L.; Dickey, E. C.; Eklund, P. C. Debundling and Dissolution of Single-Walled Carbon Nanotubes in Amide Solvents. *J. Am. Chem. Soc.* **2004**, *126* (19), 6095–6105. https://doi.org/10.1021/ja039588a.

(107) Paton, K. R.; Varrla, E.; Backes, C.; Smith, R. J.; Khan, U.; O'Neill, A.; Boland, C.; Lotya, M.; Istrate, O. M.; King, P.; Higgins, T.; Barwich, S.; May, P.; Puczkarski, P.; Ahmed, I.; Moebius, M.; Pettersson, H.; Long, E.; Coelho, J.; O'Brien, S. E.; McGuire, E. K.; Sanchez, B. M.; Duesberg, G. S.; McEvoy, N.; Pennycook, T. J.; Downing, C.; Crossley, A.; Nicolosi, V.; Coleman, J. N. Scalable Production of Large Quantities of Defect-Free Few-Layer Graphene by Shear Exfoliation in Liquids. *Nat. Mater.* **2014**, *13* (6), 624–630. https://doi.org/10.1038/nmat3944.

(108) Zhang, L.; Zaric, S.; Tu, X.; Wang, X.; Zhao, W.; Dai, H. Assessment of Chemically Separated Carbon Nanotubes for Nanoelectronics. *J. Am. Chem. Soc.* **2008**, *130* (8), 2686–2691. https://doi.org/10.1021/ja7106492.

(109) Wu, J.; Pisula, W.; Müllen, K. Graphenes as Potential Material for Electronics. *Chem. Rev.* **2007**, *107* (3), 718–747. https://doi.org/10.1021/cr068010r.

(110) Yang, X.; Dou, X.; Rouhanipour, A.; Zhi, L.; Ra, H. J.; Mu, K. Two-Dimensional Graphene Nanoribbons. **2008**, *5*, 4216–4217.

(111) Jouault, B.; Camara, N.; Jabakhanji, B.; Caboni, A.; Consejo, C.; Godignon, P.; Maude, D. K.; Camassel, J. Quantum Hall Effect in Bottom-Gated Epitaxial Graphene Grown on the C-Face of SiC. *Appl. Phys. Lett.* **2012**, *100* (5). https://doi.org/10.1063/1.3680564.

CHAPTER 2. Sulfated Cellulose Nanofibrils from Chlorosulfonic Acid Treatment and Their Wet-Spinning into High-Strength Fibers

INTRODUCTION

With growing concerns about the impact of human behavior on the environment, global interest in improving the sustainability of engineering materials and manufacturing practices has intensified. From a polymer standpoint, much of this interest has focused on eschewing synthetic, petroleum derived materials in favor of biopolymers. Cellulose—the most abundant biopolymer on the planet[1]—has been widely utilized in its native form in textiles and paper for millennia. For over a century, additional commercial uses have involved dissolution and derivatization of cellulose that fundamentally change the crystalline structure from the native cellulose I to the regenerated cellulose II polymorph, accompanied by a loss in mechanical strength.[2] In the last two decades, there has been significant interest in the development of 1D cellulose nanomaterials or nanocelluloses that retain many of the remarkable mechanical properties of cellulose I, especially desirable for high-strength applications.

Nanocelluloses represent an alternative approach to processing in which macroscopic cellulose is separated into nanoscale fragments while retaining some or most of its crystalline structure, often relying on some form of chemical pretreatment or modification. Nanocelluloses can fall into several subcategories, with the first being cellulose nanocrystals (CNC) produced by acid hydrolysis of cellulose, most commonly using concentrated sulfuric acid. Hydrolysis breaks the β(1,4) glycosidic links in cellulose to remove the easily accessible chains in the less ordered amorphous regions, leaving rod-like CNC with 3-50 nm widths and several hundred nm lengths, depending on the source and hydrolysis conditions.[1] The pristine and highly crystalline CNC are

predicted to have a tensile strength and Young's modulus as high as 7.5 GPa and ~150 GPa, respectively.[3] The second major category of nanocelluloses are the thinner and longer semicrystalline cellulose nanofibrils (CNF) with much higher length-to-width aspect ratios. CNF can be produced by subjecting cellulose to shear force processes, chemical treatments, or a combination thereof to improve quality and productivity. For instance, carboxylation of cellulose mediated by the aminoxyl radical 2,2,6,6-tetramethylpiperidin-1-oxyl (TEMPO) breaks hydrogen bonding in the less ordered domains and introduces anionic carboxylate groups to facilitate subsequent mechanical defibrillation while deterring aggregation of the dispersed nanofibrils through electrostatic double-layer repulsion. While non-hydrolytic approaches have been explored for CNC generation, large scale production still relies on hydrolysis and is accompanied by significant loss of mass. The much higher yields of CNF—particularly TEMPO oxidized CNF (TCNF)—make them more commercially attractive, and they have reviewed extensively[4–7] for applications including gas membranes, packaging materials, composites, aerogels, superabsorbent materials, biomedical scaffolds, printed electronics, and energy storage devices.

As is the case for any nanomaterials, translating the ultra-high mechanical strength of CNF on the nano-scale into macroscopic structures remains a significant engineering challenge. Alignment of CNF during processing is critical for allowing bulk materials to inherit the longitudinal strength of the nanofibrils. An effective method of alignment is wet-spinning, which has been demonstrated for both TCNF[8–15] and unmodified[16,17] CNF; several reviews explore the topic.[18–20] During the wet-spinning of a polymer solution, the dissolved polymer is extruded into a coagulation bath containing an antisolvent, which causes the polymer to fall out of solution and solidify into a continuous filament. In CNF wet-spinning, the most reported coagulants have

included acetone[8–11,16,21], ethanol[11,14,17], THF[14,15], and dioxane.[14] Aqueous calcium chloride solutions have also been utilized as coagulants for TCNF[11–13], with multivalent Ca^{2+} ions screening electrostatic repulsion among the carboxylated nanofibrils to induce aggregation and ionic crosslinking.

To advance CNF into fibers, scalable reactions and engineering processes must be considered, and the high cost of reagents like TEMPO is called into question. Other routes to CNF can also diversify the range of nanofibril chemistries available and may offer cost-effective solutions beyond the benchtop. Sulfation, while well-established for regenerated cellulose, is a less-explored alternative to produce anionic CNF. A variety of sulfating agents have been applied to cellulose. Chlorosulfonic acid, which reacts readily with alcohols to give the corresponding alkyl sulfates, has been used to produce water-soluble cellulose sulfates.[22,23] It has also been performed under milder conditions to add additional sulfate functionality to CNC produced from sulfuric acid hydrolysis[24] and CNF produced by homogenization[25], yielding respective charges of 0.4 mmol/g and 0.56-1.79 mmol/g. Sulfonated CNF has been produced by a two-step reaction involving the periodate cleavage of cellulose's 2,3 vicinal diol to produce 2,3-dialdehyde cellulose, followed by reaction with bisulfite and homogenization to a 91 % yield with 0.51 mmol/g of hydroxy sulfonate groups.[26] Using a deep eutectic solvent of sulfamic acid and urea at 150 °C in conjunction with microfluidization has also produced 4.4 nm wide sulfated CNF with 1.44-3.00 mmol/g sulfate contents.[27] However, a possible carbamation side reaction may complicate this process by generating additional functional groups. Regardless of the reactions and processes involved, sulfated cellulose or nanocellulose variants have typically been lauded for their aqueous solubility/dispersibility and superior absorbent properties imparted by the introduction

of hygroscopic sulfate groups.[22,28,29] None have been exploited for more diverse functional applications, including those building upon the unique intrinsic strength and anisotropy of CNF.

This study aimed at a direct approach of functionalizing cellulose followed by mechanical disintegration to generate functional nanocelluloses, specifically sulfated cellulose nanofibrils (SCNF), in the same manner as TEMPO CNF. The premise is that chlorosulfonic acid, acting as a robust sulfating agent, is able to simultaneously pretreat and functionalize cellulose for the purpose of maximizing sulfation in the amorphous regions without destroying the crystalline domains. In doing so, sufficient charge is generated to facilitate disintegration of sulfated cellulose into SCNF that remain stably dispersed in aqueous media while avoiding dissolution. Cellulose was heterogeneously sulfated with chlorosulfonic acid in anhydrous N,N-dimethylformamide and defibrillated into SCNF through high-speed blending. The degree of sulfation was controlled by varying the stoichiometric ratio of chlorosulfonic acid per anhydroglucose unit (AGU) and the length of reaction at ambient temperature. SCNF charge determined by conductometric titration and nanofibrillar structure and dimensions assessed using atomic force and transmission electron microscopy were evaluated to determine the relationship between necessary sulfation levels and the range of SCNF products. The assembly of SCNF into fibers was investigated by wet-spinning aqueous SNF dispersions into varied coagulants of acetone, isopropanol, and mixtures of calcium chloride and isopropanol.

EXPERIMENTAL

Materials

Sodium hydroxide (NaOH, 97.0%), toluene (99.9%), hydrochloric acid (HCl, 1.0 M), and Dowex Marathon C (H-form) acidic ion exchange resin beads were purchased from Fisher Scientific. Reagent grade ethanol, calcium chloride ($CaCl_2$, 99%), potassium bromide (KBr, 99%), and anhydrous N,N-dimethylformamide (DMF) were purchased from Sigma Aldrich. Chlorosulfonic acid (HSO_3Cl, 99%), toluene (99.5%) and sodium chlorite ($NaClO_2$, 80% purity) were purchased from Alfa Aesar. Potassium hydroxide (KOH, 85%) was purchased from Acros. Reagent grade isopropanol (IPA) and acetone were purchased from Spectrum Chemical. Purified water was obtained from a Milli-q Advantage A10 water purification system. All dialysis steps were performed using regenerated cellulose dialysis tubing with a nominal molecular weight cutoff of 12-14 kDa purchased from Fisher Scientific. All chemicals were used as received without further purification. Cellulose was isolated from Calrose variety rice straw using a previously reported procedure[30]; dewaxing by Soxhlet extraction with a 2:1 v/v mixture of refluxing toluene/ethanol, delignification with 1.4 wt% acidified NaClO, and hemicellulose removal with 5 wt% KOH.

Sulfation of cellulose via chlorosulfonic acid

Cellulose and all glassware used were oven dried prior to use to eliminate moisture. For a typical sulfation run, 0.5 g of cellulose was placed in a stoppered 50 mL Erlenmeyer flask to which 22 mL of anhydrous DMF were added. The mixture was allowed to stir for a period of approximately 10 min. Chlorosulfonic acid in varied quantities of 0.10-0.31 mL, or 0.5 to 1.5 HSO_3Cl per anhydroglucose unit (AGU) molar ratios, was added dropwise to 3 mL of anhydrous DMF chilled in an ice bath. This HSO_3Cl/DMF mixture was then added to cellulose/DMF to begin

the reaction. All reactions were performed at ambient temperature for 30 to 60 min. Termination was carried out by the addition of 10 mL purified water. The sulfated cellulose was centrifuged and washed with purified water. Remaining acid and DMF were removed through dialysis against purified water for approximately seven days, until no change in the conductivity of the water was observed.

Defibrillation into SCNF

Following dialysis, the sulfated cellulose was dispersed at a concentration of 0.2 wt% in 250 mL of purified water and blended at 37,000 rpm in a high-speed blender (Vitamix 5200) for a total of 30 min in 5-minute increments to avoid overheating. The aqueous suspension was then centrifuged (Eppendorf 5804R, 5,000 rpm, 15 min) to separate out large fragments that did not defibrillate. A known volume of supernatant and the precipitate were oven dried in tared vessels to determine their mass and concentration, respectively. The wt% of the product that remained dispersed in the supernatant relative to the original sulfated cellulose was reported as the SCNF yield.

SCNF Characterization

The height and length of SCNF were determined through atomic force microscopy (AFM) (Asylum Research MFP-3D AFM) with OMCL-AC160TS standard silicon probes (nominal tip radius of 7 nm, spring constant of 26 N/m). Several drops of diluted SCNF dispersion (ca. 0.0001 wt%) were deposited on freshly cleaved mica discs and allowed to dry. Images were collected in tapping mode under ambient conditions and processed using the open-source software Gwyddion and ImageJ to derive the fibril heights and lengths, respectively.

SCNF widths were determined using transmission electron microscopy (TEM) (JEOL JSM-1230). Samples were prepared by placing a drop of diluted SCNF dispersion (ca. 0.0001 wt%) on a glow discharged carbon grid and blotting away the excess after 10 min. Samples were negatively stained with 2 wt% uranyl acetate to enhance contrast. Micrographs were taken with a LaB_6 electron source using an accelerating voltage of 100 kV. Analysis was performed using ImageJ.

The surface charges of SCNF samples were determined by conductometric titration. To obtain pristine CNF for titration, aliquots of SCNF were dialyzed again against purified water for several days to remove small-molecule contaminants. They were then run through an ion exchange column packed with an acidic ion exchange resin (Dowex marathon C, H-form) that exchanges metallic cations for protons to ensure the sulfate half-ester groups on the SCNF were in their acid forms. The SCNF samples (50 mL, diluted to ca. 0.05 wt%) were titrated with 0.01 M sodium hydroxide while measuring the conductivity using a pH meter (Oakton pH/CON 510). The surface tension of SCNF dispersions was measured on a Kruss K100 tensiometer using the Wilhelmy plate method.

Fourier transform infrared spectroscopy (FTIR) was performed using a Thermo-Nicolet 6700 infrared spectrometer. Aqueous SCNF samples were freeze-dried and then mixed with ground potassium bromide and pressed into pellets. Spectra were collected in transmittance mode from an accumulation of 64 scans 2 cm^{-1} resolution over the range of 4000-400 cm^{-1}.

Rheological Measurements

The rheology of aqueous SCNF dispersions was measured using a Brookfield DV3T rheometer with a concentric cylinder geometry. Samples of SCNF with charges of 1.3, 1.8, and

2.2 mmol/g were degassed for several seconds in a bath sonicator (Branson 2510) prior to analysis. Viscosity measurements were taken at 25 °C in a water bath, at concentrations from 0.3-0.6 wt% and shear rates from 0.1-100 s^{-1}.

Wet-spinning of SCNF

Aqueous dispersions of 1.3 and 1.8 mmol/g SCNF were concentrated to 0.65 wt% using a rotary evaporator. Aqueous SCNF spin dope was dispensed via a syringe pump fitted with a 27-gauge needle with 210 μm inner diameter (ID) and its tip submerged in a 60 cm long horizontal channel filled with a coagulant of either acetone, IPA, or IPA with 0.1 wt% $CaCl_2$. The extrusion rate, controlled via syringe pump, was approximately 144 cm/min. After moving through the coagulation bath, fibers were pulled through an air gap to dry before being wound onto a cylindrical collector driven by a DC motor at a rate of approximately 170 cm/min.

The diameter, tensile strength, and Young's modulus of wet-spun fibers were determined using a Zellweger-Uster Mantis single fiber tensile tester designed for testing cotton fibers.[31] Fibers were conditioned at 21 °C and 65% relative humidity for at least 24 hours prior to tensile tests. SEM images of wet-spun fibers were taken on a Thermo Fisher Quattro S Environmental SEM. Fibers were sputtered with circa 1.5 nm of gold prior to imaging. Optical microscopy images of fibers were taken under crossed polars at a 45° angle with respect to the polarization plane.

RESULTS & DISCUSSION

Functionalization and Defibrillation of SCNF

Sulfation of cellulose with chlorosulfonic acid is a typical S_N2 reaction and exhibits stereoselectivity for primary C6 hydroxyls over secondary C2 and C3 hydroxyls; this has been previously confirmed by NMR.[32] The repulsive charge induced by sulfation helps facilitate the

disintegration of sulfated cellulose into sulfated cellulose nanofibrils (SCNF), allowing the SCNFs to be stably dispersed (**Scheme 2.1**). Due to the complete solubility of cellulose sulfates at higher degrees of substitution, success of the scheme pivots on identifying reaction conditions that minimize dissolution while providing sufficient sulfation to disintegrate macroscale sulfated cellulose into sulfated nanocelluloses.

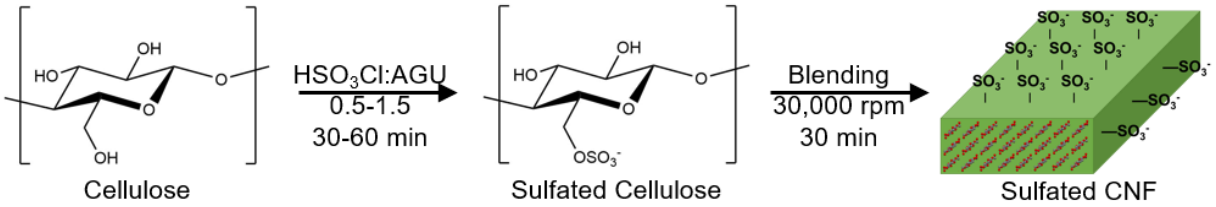

Scheme 2.1 Sulfation of cellulose through combined pretreatment and functionalization with chlorosulfonic acid followed by high-speed blending (37k rpm, 30 min) of aqueous dispersion into sulfated cellulose nanofibrils (SCNF).

By varying the HSO_3Cl/AGU molar ratio from 0.5 to 1.5 for 30 to 60 min, sulfated cellulose with charges ranging from 0.45 ± 0.10 to 2.20 ± 0.10 mmol/g were produced (**Figure 2.1a**). The HSO_3Cl/AGU ratio was found to be the most significant determiner of charge, with the effect of reaction time being smaller over the ranges studied. The skew in the 30- and 60-minute trendlines in **Figure 2.1a** indicates a two-factor interaction between time and HSO_3Cl/AGU ratio, wherein longer reaction times magnify the effect of acid ratio.

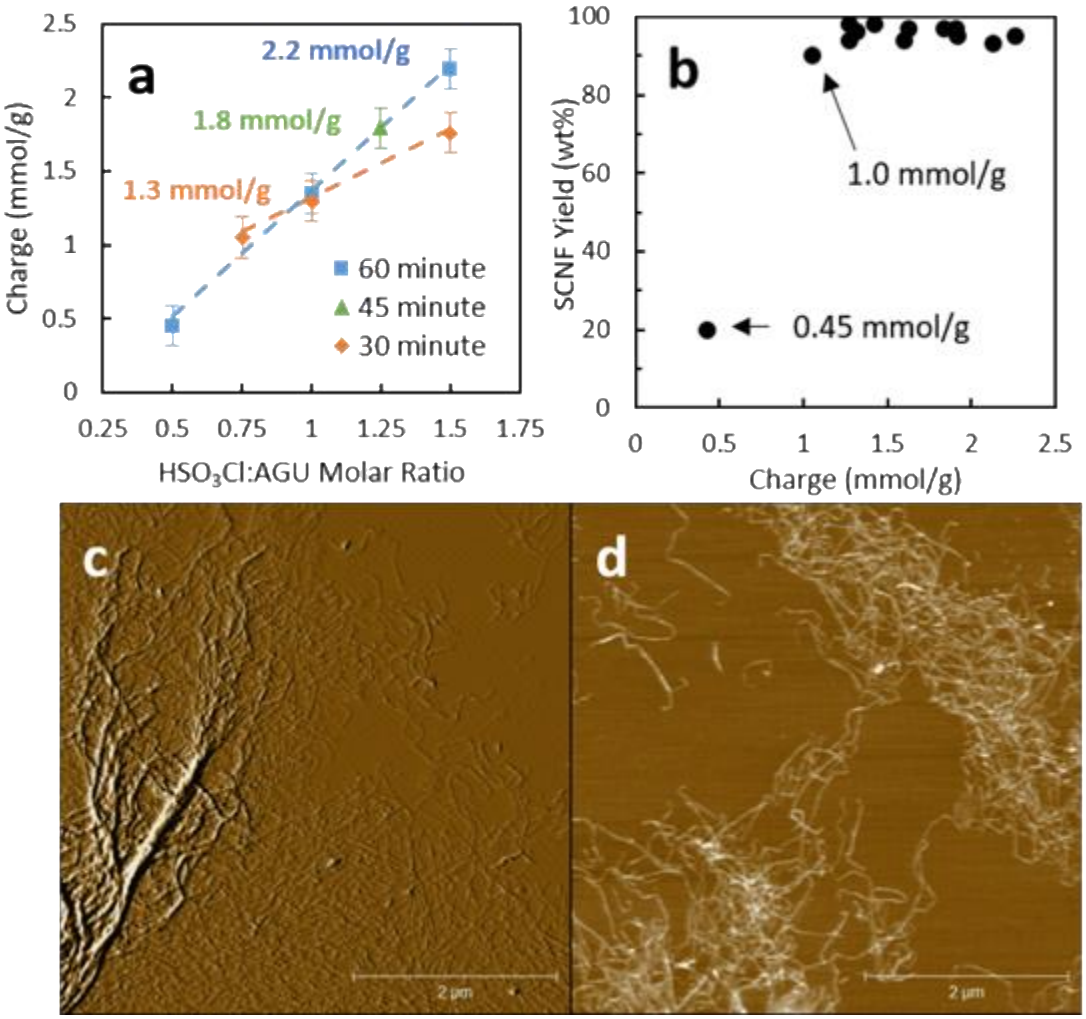

Figure 2.1 Effect of sulfation reaction conditions followed by high speed blending (30k rpm, 30 min): (a) surface charge as a function of HSO_3Cl/AGU molar ratio and reaction time; (b) SCNF yield as a function of surface charge (30 min blending); (c-d) SCNF with a charge of 1.0 mmol/g, showing branching fibrils.

The reaction performed at the lowest 0.5 HSO_3Cl/AGU ratio, for an extended 60 min, produced a charge of 0.45 mmol/g that proved insufficient for effective defibrillation, yielding only 20% nanofibrils (**Figure 2.1b**). Sulfated cellulose produced under all other reaction conditions could be effectively disintegrated to disperse at least 90% in the supernatants. AFM on the supernatant of 1.0 mmol/g SCNF (1.25 HSO_3Cl/AGU, 45 min) showed some highly branched fibrillated and entangled fibrillar structures (**Figures 2.1c, d**) which were not found in any other sample. This observation, along with the second-lowest yield of 90%, was taken as an

indication that 1.0 mmol/g is just below the sulfation threshold required to permit full disintegration of macroscale sulfated cellulose into SCNF. SCNF produced under the harshest conditions (1.5 HSO_3Cl/AGU, 60 min) maintained a 94% yield, indicating that dissolution of the cellulose had been largely avoided for all reactions.

Morphology and Properties of SCNF

Three SCNF representing three different levels of charges and from different reaction conditions—1.3 mmol/g (1.0 HSO_3Cl/AGU, 30 min), 1.8 mmol/g (1.25 HSO_3Cl/AGU, 45 min), and 2.2 mmol/g (1.5 HSO_3Cl/AGU, 60 min)—were chosen for more in-depth analyses. The average SCNF length (L) decreased with increasing levels of sulfation, from 1.24 µm at a 1.3 mmol/g to 1.08 µm at 1.8 mmol/g and 0.75 µm at 2.2 mmol/g (**Figure 2.2a-c**). A progressive reduction in fibril width (W) from 5.9 nm to 4.2 nm and 3.9 nm was also observed with increasing sulfation. The height (H) values of all SCNFs varied little from 1.23 to1.32 nm. Progressive sulfation not only decreased SCNF width and length, but also lowered their anisotropy. With increasing extents of sulfation, the W/H ratio decreased from 4.7 to 3.3 and 3.0 and the L/H ratio lowered from 984 to 843 and 568. AFM is known to underestimate the height of nanoscale features; this is sometimes attributed to sample deformation by the tip[33] or the presence of salts or other deposits on the substrate surface.[34] Heights can also be compromised when the lateral dimensions of the features being measured are smaller than the effective interaction area of the tip on the surface,[35] as is the case in the present study. Nevertheless, the SCNF cross sections were more anisotropic and rectangular compared to TCNF produced from the same cellulose (1.4 W/H, with width and height of 2.09 and 1.52 nm, respectively).[36] It is evident that sulfation even under the harshest condition produced wider SCNF than TEMPO oxidation. However, yields for the two

schemes were similar (i.e. 90-97% for SCNF and 96.8% TCNF), affirming that the sulfation of cellulose by chlorosulfonic acid is robust and highly effective at producing SCNF over a wide range of charges.

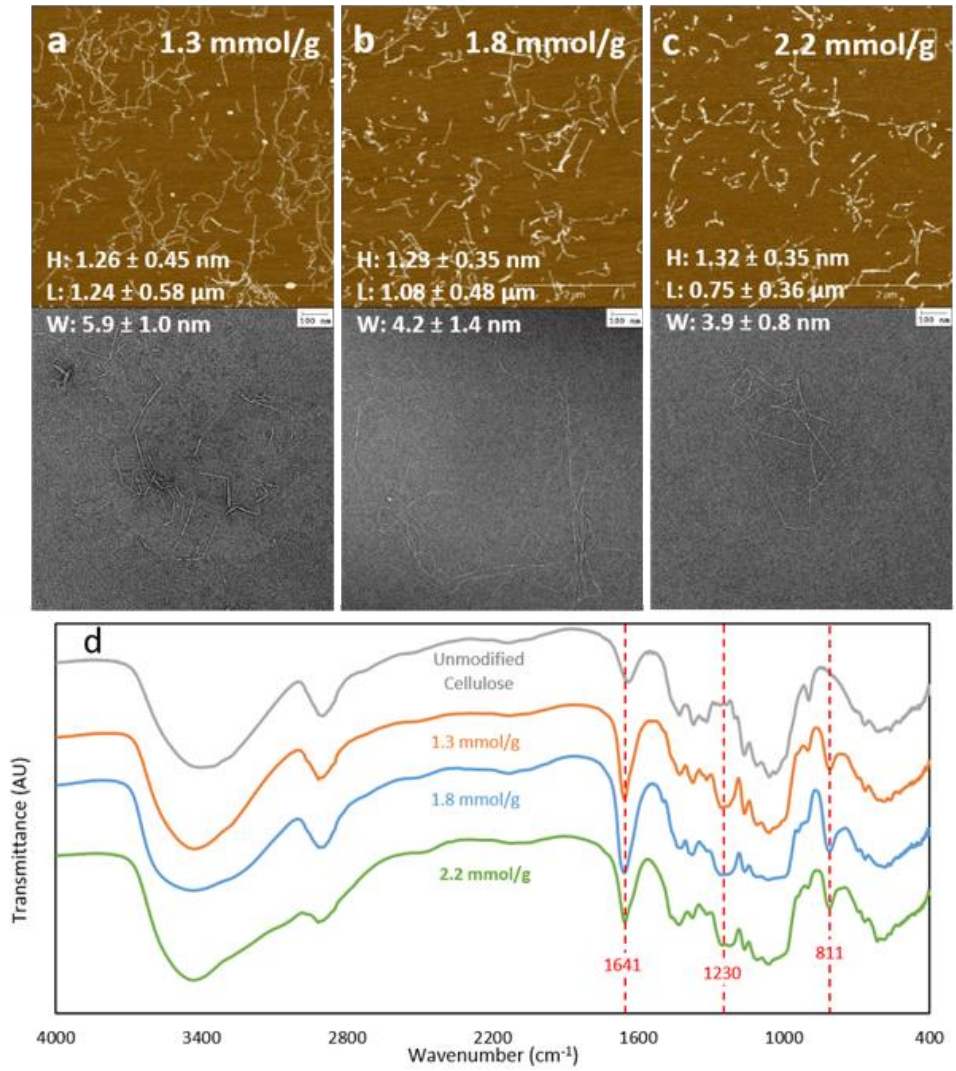

Figure 2.2 Characterization of SCNF: (a-c) AFM (top) and TEM (bottom) micrographs of SCNF with 1.3, 1.8, and 2.2 mmol/g charges; (d) FTIR spectra.

FTIR transmittance spectra of SCNF samples show all major peaks characteristic of cellulose; broad OH stretching around 3500 cm^{-1}, CH_2 stretching at 2900 cm^{-1}, and C-O-C stretching of the β-1,4 glycosidic linkage at 898 cm^{-1} (**Figure 2.2d**). In addition, two new peaks characteristic of sulfate half-ester groups appeared at 811 cm^{-1} and 1230 cm^{-1} that can be

attributed to the S-O and S=O stretching vibrations, respectively. While the intensity of these two sulfate ester peaks showed no clear trend with the levels of sulfation, the water scissoring peak at 1641 cm^{-1} intensified in all three SCNF. This intensification could be attributed to an increase in hygroscopicity brought about by sulfation and has been observed previously for cellulose sulfates.[23] The most charged 2.2 mmol/g SCNF also showed sharpened OH stretching peak and a decrease in the prominence of the CH_2 stretching peak compared to the less sulfated SCNF. Both of these traits are more characteristic of amorphous celluloses,[37] indicating possible reduction in crystallinity brought about by the harsh reaction conditions.

All SCNF dispersions exhibited thixotropy, as is typical for TCNF.[36,38] To account for this, viscosity measurements were taken after steady state was established for a particular shear rate. SCNF dispersions exhibited shear thinning behavior between shear rates of 0.1 and 100 s^{-1} that fit well to power law kinetics, also similar to TCNF.[38] Harsher reaction conditions generated SCNF that exhibited lower effective viscosities (**Figure 2.3a**). The decrease in viscosity may be attributed to both a decrease in nanofibril lengths as well as the higher charges, leading to increased electrostatic repulsion between fibrils and decreased propensity for entanglement. The viscosity of the most highly charged 2.2 mmol/g SCNF was significantly lower than the others, being approximately an order of magnitude below the 1.3 and 1.8 mmol/g SCNF at most shear rates tested. At 0.5 wt%, The viscosities obtained for 1.3 mmol/g SCNF dispersions are similar to those reported for SCNF produced from softwood pulp using sulfamic acid and urea,[27] indicating similarity in nanofibrillar characteristics between the two reaction schemes. Aqeuous SCNF also showed amphiphilicity, reducing the surface tension of water with increasing concentrations (**Figure 2.3c**). This reduction was more pronounced for 1.3 mmol/g SCNF as compared to the

higher charged 1.8 mmol/g SCNF, which only showed a reduction at higher concentrations of 0.6-0.7%. This behavior is, once again, similar to TCNF, which exhibited a similar reduction in surface tension with 1.29 mmol/g charge at ca. 0.3%.[39]

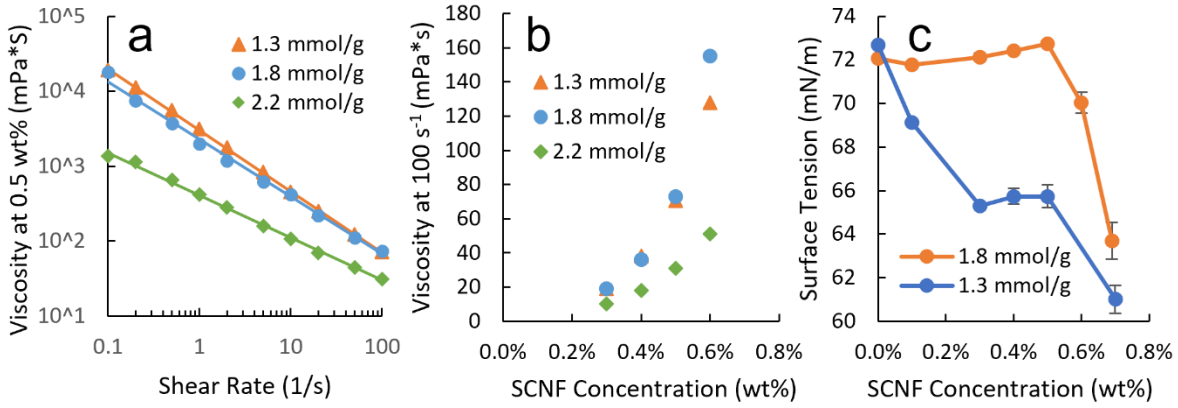

Figure 2.3 Aqueous SCH properties: (a) effective viscosities as a function of shear rate; (b) viscosities as a function of concentration; (c) surface tension as a function of concentration.

SCNF Cross Section and Surface Functionalization

Due to their semicrystalline and insoluble nature, many of the cellulose chains that constitute CNF are buried within crystalline domains and not accessible to chemical modification. Representing the degree of substitution on a basis of total anhydroglucose units is therefore of limited use. Instead, it is meaningful to look at the fraction of accessible hydroxyl groups that have been functionalized. A model can be developed based on AFM and TEM data about cross-sectional dimensions and under several assumptions. The idealized model assumed the exposed CNF surfaces to consist of the hydrophilic (110) and $(1\bar{1}0)$ planes and the treats nanofibrils as crystals considering of the cellulose 1β crystalline polymorph (**Figure 2.4**). The lattice parameters used for cellulose 1β are α = β = 90°, γ = 96.5 °, a = 7.78 Å, b = 8.20 Å, c = 10.38 Å.[40] The relevant d-spacings calculated from these parameters are $d_{110} = d_{1\bar{1}0} = 5.65\text{Å}$. It is also assumed that chlorosulfonic acid targets the hydroxyl groups exposed on those planes.

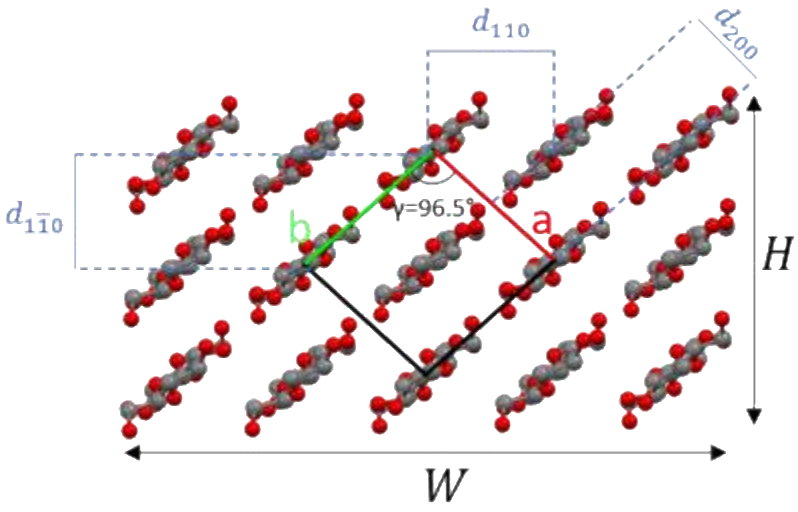

Figure 2.4 Cross-sectional model of SCNF with cellulose 1b unit cell and d-spacings indicated.

Treating cellulose chains as points on a lattice, the number of chains in the width and height directions can be represented by $H/d_{1\bar{1}0} + 1$ and $W/d_{110} + 1$, where H and W are the fibril height and width as determined from AFM and TEM, respectively. The total number of cellulose chains in the cross section, *N*, is given by

$$N = \left(\frac{H}{d_{1\bar{1}0}} + 1\right)\left(\frac{W}{d_{110}} + 1\right). \quad (1)$$

The number of cellulose chains on the fibril surface along the (110) and (1$\bar{1}$0) planes, N_S, is expressed as

$$N_s = 2 * \left[\left(\frac{H}{d_{1\bar{1}0}} + 1\right) + \left(\frac{W}{d_{110}} + 1\right)\right] - 2 = 2\left(\frac{W + H}{5.65\text{Å}} + 1\right) \quad (2)$$

where the -2 is necessary to avoid double counting the corner chains and $d_{110} = d_{1\bar{1}0} = 5.65\text{Å}$. The number of surface hydroxyls or OHs per AGU (φ) can be expressed as

$$\varphi = \frac{1.5 * N_s}{N} = \frac{3\left(\frac{W+H}{d_{110}} + 1\right)}{\left(\frac{W}{d_{110}} + 1\right)\left(\frac{H}{d_{110}} + 1\right)} \quad (3)$$

by dividing N_s by N to get the ratio of surface cellulose chains to total chains and multiplying by 1.5 (3 OH groups facing either the either the 110 or $1\bar{1}0$ plane surfaces per 2 AGU in each cellobiose).

Finally, the percentage of exposed hydroxyls that are sulfated is expressed by dividing the charge of each sample by the moles of AGU multiplied φ as follows:

$$\%\ Exposed\ OH\ Sulfated = \frac{Moles\ of\ Sulfate\ Groups}{Moles\ of\ Total\ AGU * \varphi} \quad (4)$$

This fraction is shown alongside overall degree of substitution (DS, the average number of sulfate groups per total anhydroglucose unit) for SCNF samples in **Table 2.1**.

Table 2.1 Functionalization of SCNF Surface Hydroxyls.

SCNF Charge (mmol/g)	DS (AGU basis)	Fraction of Sulfated Surface OH Groups
1.3	0.24	19%
1.8	0.34	24%
2.2	0.43	31%

While it is expected that the exposed surfaces are covered in an even split of C2, C3, and C6 cellulose hydroxyls, it may be assumed that C6 substitution is dominant. Previous work found no measurable substitution of the secondary hydroxyls when chlorosulfonic acid was applied to cellulose dissolved in N,N-dimethylacetamide and lithium chloride at 2 mol of acid per AGU for 5 hours.[32] As the reaction conditions explored in the present study are milder, being both heterogeneous and utilizing lower times and acid quantities, a similar result is expected. With

assumed C6 stereoselectivity, complete sulfation of exposed C6 hydroxyls would be 33% surface sulfation; the 2.2 mmol/g SCNF approaches this value at 31%. The selectivity of chlorosulfonic acid reaction under relatively mild conditions is particularly compelling in the context of competing with carboxylated TEMPO CNF, which is lauded for its specificity for C6 carboxylation. It may also lend a degree of surface regularity to SCNF produced via chlorosulfonic acid as opposed to other sulfation schemes such as periodate/bisulfite (which is stereospecific but cleaves the C2-C3 vicinal diol open, creating an irregular surface).

Wet-spinning of SCNF

SCNF was wet-spun from 0.65 wt% aq. SCNF with 1.3 mmol/g or 1.8 mmol/g charge through 210 μm ID needle at 140 cm/min extrusion rate and 170 cm/min take-up rate. Several different coagulants were used, including acetone and IPA as organic coagulants and a mixed ionic/organic coagulant consisting of 0.1 wt% $CaCl_2$ in IPA. The removal of water from the coagulated fiber in systems with aqueous $CaCl_2$ as the coagulant was very time consuming, requiring long drying times and temperature controls that were complicated to implement in a continuous spinning process and at the laboratory scale. The mixed ionic/organic system was chosen to alleviate this problem; the high vapor pressure of IPA facilitates faster drying.

SCNF spinnability was found to vary with respect to charge. The 1.3 mmol/g SCNF could be successfully spun into fibers in all coagulants tested. Continuous spinning of the higher charged 1.8 mmol/g SCNF into organic coagulants of either pure IPA or acetone was impossible; the extruded dope did not coagulate into a coherent fiber under the same spinning conditions but instead fragmented and was too delicate to be handled or collected. This slower coagulation behavior may be attributed to several factors. The higher charge of the SCNF leads to increased

inter-fibrillar electrostatic double-layer repulsion, hampering their association during coagulation. The higher quantities of hygroscopic sulfate groups in the 1.8 mmol/g SCNF may also correspond to an increase in bound water molecules that further hinders interfibrillar association and slows coagulation. In contrast, this 1.8 mmol/g SCNF could be easily spun into IPA with 0.1 wt% $CaCl_2$. With calcium ions screening electrostatic repulsion and higher charge facilitating ionic cross-linking, this system is well suited for spinning fibers from highly substituted SCNF.

Microscopy on wet-spun fibers showed indications of nanofibrillar alignment during wet-spinning, a necessary step for achieving strong fibers. Striations along the fibrillar axis were observed in lateral SEM images (**Figure 2.5a-d**). The optical microscopy of fibers viewed under crossed polars showed bright birefringence in all cases (**Figure 2.5a-d**, insets), further confirming the alignment of SCNF. SEM of a tensile fractured end of a fiber coagulated in $CaCl_2$/IPA showed lamellar structures aligned along the fibrillar axis (**Figure 2.5e-f**). While these oriented fibrillar structures showed clear SCNF alignment or assembly at the nanofibril level, there are visible inter-fibrillar spacings. Combined with the larger diameter of the fiber coagulated in $CaCl_2$/IPA, ionic coagulation of the more highly charged SCNF produced fibers with a greater degree of porosity than coagulation in pristine organic solvents.

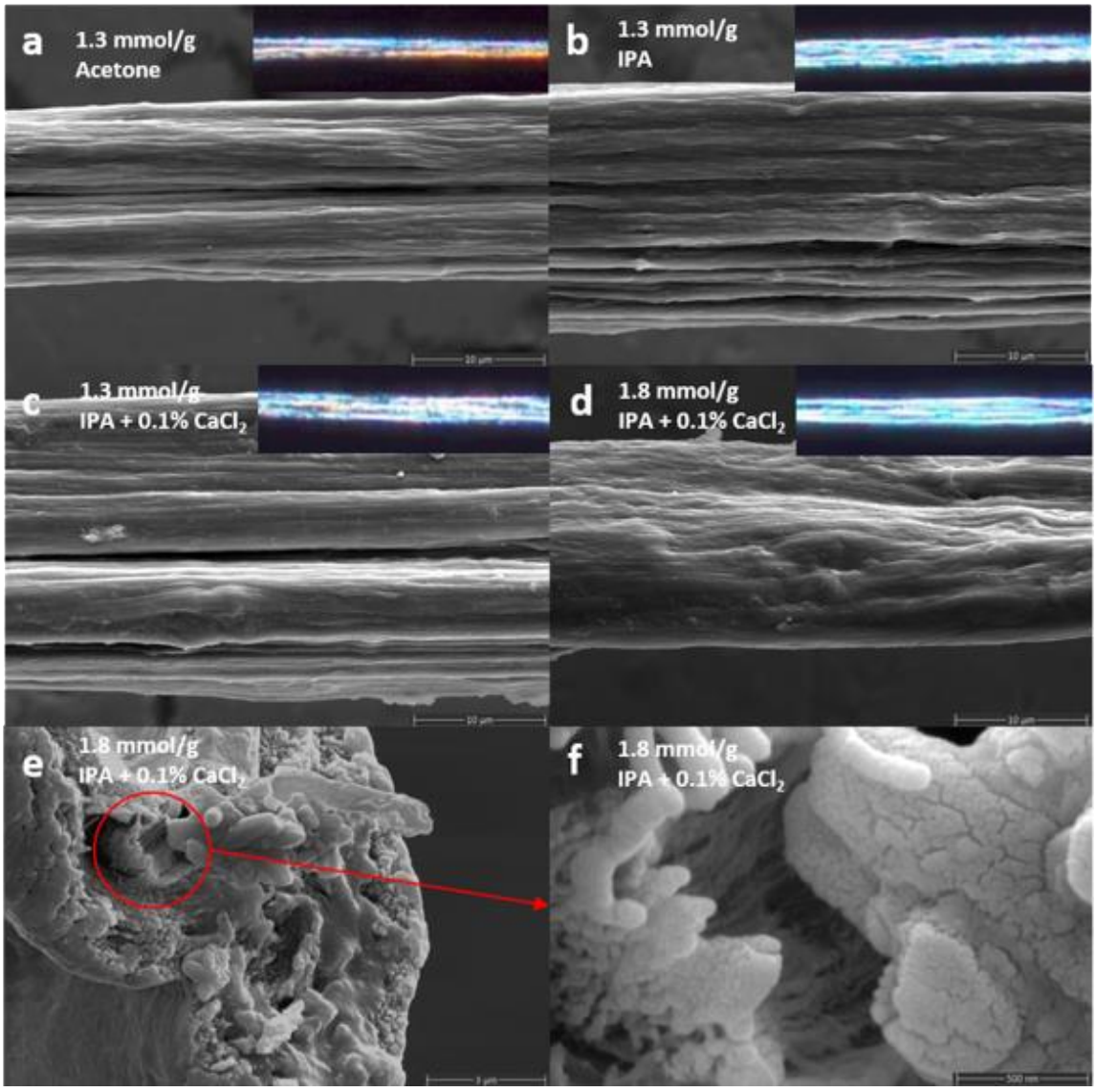

Figure 2.5 SEM of wet-spun SCNF fibers: (a-d) longitudinal images with charges and coagulants indicated; (e-f) fractured surface of SCNF in d. Insets in a-d: optical microscopy under crossed polars.

The tensile properties and fiber sizes of the wet-spun SCNF fibers also showed strong dependence on the coagulant (**Figure 2.6a**). With 1.3 mmol/g SCNF, the highest Young's modulus of 26.0 ±4.8 GPa and tensile strength of 675 ± 120 MPa were achieved in fibers coagulated in acetone, followed by those coagulated in IPA and IPA/$CaCl_2$ with respective mean tensile modulus of 16.1 and 8.5 GPa and tensile strength of 422 and 188 MPa. (**Table 2.2**). The fibers coagulated in IPA and IPA + $CaCl_2$ also showed increased porosity as compared to those

coagulated in acetone, as evidenced by the larger fiber diameter for equal spinning/take-up rates.

The mechanical performance of wet-spun SCNF fibers was found to correlate with the relative speeds at which each solvent system is expected to coagulate. Coagulation in acetone is visibly faster than in IPA, possibly due to the absence of acetone interaction with SCNF in comparison to the hydrogen bonding ability of IPA with SCNF. The IPA/$CaCl_2$ system coagulates even more slowly, as the ionic cross-linking and coagulating of the fiber's surface forming a skin that hampers ion diffusion to and from the core and water diffusion out of the fiber. This may also contribute to the increased porosity observed in fibers coagulated from the IPA/$CaCl_2$ system. The fibers spun from 1.8 mmol/g SCNF were same in diameter and similar in tensile strength and modulus (ca. 200 MPa and 9 GPa, respectively) as those from 1.3 mmol/g SCNF, both spun into IPA/$CaCl_2$. However, the toughness was significantly lower, driven by the lower strain at break.

When compared to fibers wet-spun from a variety of CNF—both TEMPO[8–16,20] and unmodified[16,17,20]—in the literature (**Figure 2.6b**), all four fibers from SCNF showed higher tensile strength at corresponding modulus, with the acetone coagulated fiber having the highest tensile strength and modulus only lower than two others. The other fibers used for comparison were mostly spun under similar conditions to the SCNF fibers in the present study; coagulated predominantly in acetone or aqueous $CaCl_2$ with no polymeric additives. Overall, SCNF fibers wet-spun in acetone are among the strongest CNF fibers made through traditional wet spinning—even without additional drawing steps or treatments—highlighting the potential of SCNF as a structural material.

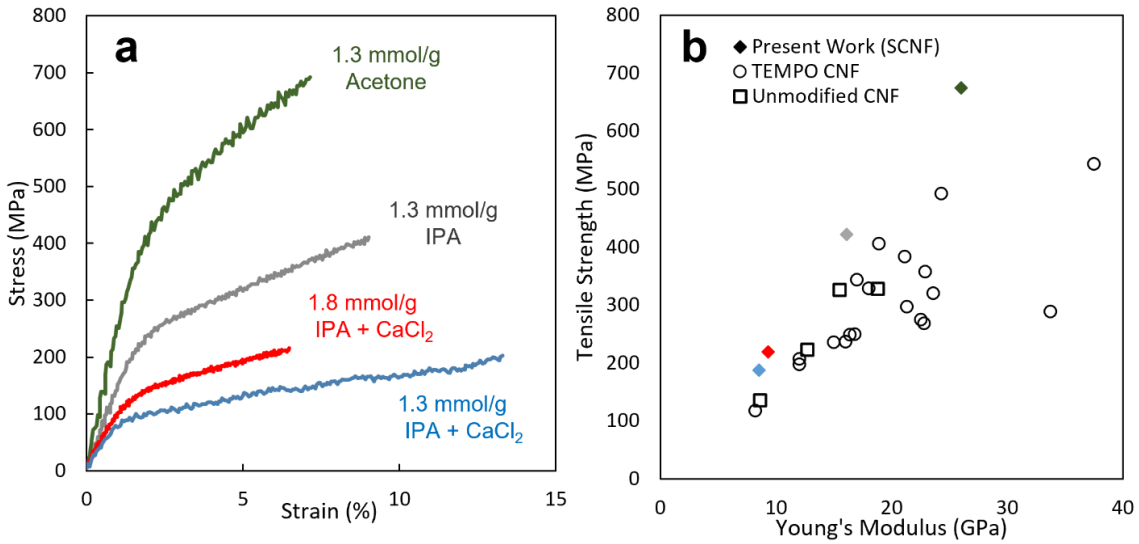

Figure 2.6 Tensile strength of wet-spun SCNF fibers: (a) representative stress strain curves; (b) comparison of with other wet-spun CNF fibers in the literature.

Table 2. Properties of wet-spun SCNF fibers. All fibers were spun at 0.05 mL/min from a g27 needle (ID=210 µm) with a 0.65 wt% spinning dope.

SCNF Charge (mmol/g)	Coagulant	Fiber Diameter (µm)	Strain at break (%)	Tensile Strength (MPa)	Young's Modulus (GPa)
1.3	Acetone	10.1 ± 1.2	6.6 ± 1.2	675 ± 120	26.0 ± 4.8
1.3	IPA	15.2 ± 3.0	8.4 ± 1.1	422 ± 160	16.1 ± 6.1
1.3	IPA + 0.1% CaCl2	16.3 ± 2.4	12.6 ± 1.6	188 ± 53	8.5 ± 2.5
1.8	IPA + 0.1% CaCl2	16.4 ± 3.6	7.0 ± 2.5	219 ± 60	9.3 ± 2.3

CONCLUSIONS

The production of sulfated CNF was achieved through simultaneous functionalization and pretreatment of cellulose with chlorosulfonic acid. By varying molar ratio of chlorosulfonic acid per AGU from 1.0-1.5 and reaction time from 30-60 min, SCNF could be produced with variable sulfation levels ranging between 1.0 and 2.2 mmol/g while maintaining yields in excess of 90%. Nanofibrils exhibited a ribbon-like shape, with widths that were several times larger than observed heights, and having average lengths of 0.75-1.24 µm, decreasing with harsher

treatment. SCNF was both thixotropic and shear thinning, with a two order of magnitude reduction in viscosity between shear rates of 0.1 and 100 s^{-1}. Additionally, it was demonstrated that SCNF with a charge of 1.3 mmol/g could be wet-spun into fibers bearing comparable or greater strength to those produced from other CNFs, without extensive drawing or additional treatments.

By making use of sulfation chemistry that is established in industry for the preparation of alkyl sulfates, this scheme provides a scalable alternative to TEMPO oxidation, without the need for costly oxoammonium catalysts. The conclusions drawn in this work about the generation and properties of SCNF from chlorosulfonic acid may also prove generalizable to other prominent sulfation methods such as SO_3/amine complexes, which proceed by way of a similar bimolecular substitution mechanism to that of chlorosulfonic acid. These advances further the goal of bringing nanocellulose beyond the benchtop and into the commercial sector.

REFERENCES

(1) Habibi, Y.; Lucia, L. A.; Rojas, O. J. Cellulose Nanocrystals: Chemistry, Self-Assembly, and Applications. *Chem. Rev.* **2010**, *110* (6), 3479–3500. https://doi.org/10.1021/cr900339w.

(2) Nishino, T.; Takano, K.; Nakamae, K. Elastic Modulus of the Crystalline Regions of Cellulose Polymorphs. *J. Polym. Sci. Part B Polym. Phys.* **1995**, *33* (11), 1647–1651. https://doi.org/10.1002/polb.1995.090331110.

(3) Moon, R. J.; Martini, A.; Nairn, J.; Simonsen, J.; Youngblood, J. Cellulose Nanomaterials Review: Structure, Properties and Nanocomposites. *Chem. Soc. Rev. Chem. Soc. Rev* **2011**, *40*, 3941–3994. https://doi.org/10.1039/c0cs00108b.

(4) Stark, N. M. Opportunities for Cellulose Nanomaterials in Packaging Films: A Review and Future Trends. *Journal of Renewable Materials*. Scrivener Publishing LLC October 1, 2016, pp 313–326. https://doi.org/10.7569/JRM.2016.634115.

(5) Wang, Q.; Yao, Q.; Liu, J.; Sun, J.; Zhu, Q.; Chen, H. *Processing Nanocellulose to Bulk Materials: A Review*; Springer Netherlands, 2019; Vol. 26. https://doi.org/10.1007/s10570-019-02642-3.

(6) Thomas, B.; Raj, M. C.; Athira, B. K.; Rubiyah, H. M.; Joy, J.; Moores, A.; Drisko, G. L.; Sanchez, C. Nanocellulose, a Versatile Green Platform: From Biosources to Materials and Their Applications. *Chemical Reviews*. 2018, pp 11575–11625. https://doi.org/10.1021/acs.chemrev.7b00627.

(7) Abitbol, T.; Rivkin, A.; Cao, Y. F.; Nevo, Y.; Abraham, E.; Ben-Shalom, T.; Lapidot, S.; Shoseyov, O. Nanocellulose, a Tiny Fiber with Huge Applications. *Curr. Opin. Biotechnol.* **2016**, *39*, 76–88. https://doi.org/10.1016/j.copbio.2016.01.002.

(8) Iwamoto, S.; Isogai, A.; Iwata, T. Structure and Mechanical Properties of Wet-Spun Fibers Made from Natural Cellulose Nanofibers. *Biomacromolecules* **2011**, *12* (3), 831–836. https://doi.org/10.1021/bm101510r.

(9) Geng, L.; Chen, B.; Peng, X.; Kuang, T. Strength and Modulus Improvement of Wet-Spun Cellulose I Filaments by Sequential Physical and Chemical Cross-Linking. *Mater. Des.* **2017**, *136*, 45–53. https://doi.org/10.1016/j.matdes.2017.09.054.

(10) Yao, J.; Chen, S.; Chen, Y.; Wang, B.; Pei, Q.; Wang, H. Macrofibers with High Mechanical Performance Based on Aligned Bacterial Cellulose Nanofibers. *ACS Appl. Mater. Interfaces* **2017**, *9* (24), 20330–20339. https://doi.org/10.1021/acsami.6b14650.

(11) Wang, L.; Lundahl, M. J.; Greca, L. G.; Papageorgiou, A. C.; Borghei, M.; Rojas, O. J. Effects of Non-Solvents and Electrolytes on the Formation and Properties of Cellulose I Filaments. *Sci. Rep.* **2019**, *9* (1), 1–11. https://doi.org/10.1038/s41598-019-53215-0.

(12) Kim, H. C.; Kim, D.; Lee, J. Y.; Zhai, L.; Kim, J. Effect of Wet Spinning and Stretching to Enhance Mechanical Properties of Cellulose Nanofiber Filament. *Int. J. Precis. Eng. Manuf. - Green Technol.* **2019**, *6* (3), 567–575. https://doi.org/10.1007/s40684-019-00070-z.

(13) Kafy, A.; Kim, H. C.; Zhai, L.; Kim, J. W.; Hai, L. Van; Kang, T. J.; Kim, J. Cellulose Long Fibers Fabricated from Cellulose Nanofibers and Its Strong and Tough Characteristics. *Sci. Rep.* **2017**, *7* (1), 1–8. https://doi.org/10.1038/s41598-017-17713-3.

(14) Walther, A.; Timonen, J. V. I.; Díez, I.; Laukkanen, A.; Ikkala, O. Multifunctional High-Performance Biofibers Based on Wet-Extrusion of Renewable Native Cellulose Nanofibrils. *Adv. Mater.* **2011**, *23* (26), 2924–2928. https://doi.org/10.1002/adma.201100580.

(15) Torres-rendon, J. G.; Schacher, F. H.; Ifuku, S.; Walther, A.; Jena, D.-. Mechanical Performance of Macro Fibers of Cellulose and Chitin Nano Fibrils Aligned by Wet-Stretching: A Critical Comparison. *Biomacromolecules* **2014**.

(16) Lundahl, M. J.; Cunha, A. G.; Rojo, E.; Papageorgiou, A. C.; Rautkari, L.; Arboleda, J. C.; Rojas, O. J. Strength and Water Interactions of Cellulose i Filaments Wet-Spun from Cellulose Nanofibril Hydrogels. *Sci. Rep.* **2016**, *6* (July), 1–13. https://doi.org/10.1038/srep30695.

(17) Mohammadi, P.; Toivonen, M. S.; Ikkala, O.; Wagermaier, W.; Linder, M. B. Aligning Cellulose Nanofibril Dispersions for Tougher Fibers. *Sci. Rep.* **2017**, *7* (1), 1–10. https://doi.org/10.1038/s41598-017-12107-x.

(18) Lundahl, M. J.; Klar, V.; Wang, L.; Ago, M.; Rojas, O. J. Spinning of Cellulose Nanofibrils into Filaments: A Review. *Ind. Eng. Chem. Res.* **2017**, *56* (1), 8–19. https://doi.org/10.1021/acs.iecr.6b04010.

(19) Clemons, C. Nanocellulose in Spun Continuous Fibers: A Review and Future Outlook. *J. Renew. Mater.* **2016**, *4* (5), 327–339. https://doi.org/10.7569/jrm.2016.634112.

(20) Rosén, T.; Hsiao, B. S.; Söderberg, L. D. Elucidating the Opportunities and Challenges for Nanocellulose Spinning. *Adv. Mater.* **2020**. https://doi.org/10.1002/adma.202001238.

(21) Vuoriluoto, M.; Orelma, H.; Lundahl, M.; Borghei, M.; Rojas, O. J. Filaments with Affinity Binding and Wet Strength Can Be Achieved by Spinning Bifunctional Cellulose Nanofibrils. *Biomacromolecules* **2017**, *18* (6), 1803–1813.

https://doi.org/10.1021/acs.biomac.7b00256.
(22) Shet, R. T.; Raj R. Wallajapet, P. Sulfonated Cellulose Having Improved Absorbent Properties. US5703225A, 1995.
(23) Horikawa, M.; Fujiki, T.; Shirosaki, T.; Ryu, N.; Sakurai, H.; Nagaoka, S.; Ihara, H. The Development of a Highly Conductive PEDOT System by Doping with Partially Crystalline Sulfated Cellulose and Its Electric Conductivity. *J. Mater. Chem. C* **2015**, *3* (34), 8881–8887. https://doi.org/10.1039/C5TC02074C.
(24) Lin, N.; Dufresne, A. Surface Chemistry, Morphological Analysis and Properties of Cellulose Nanocrystals with Gradiented Sulfation Degrees. *Nanoscale* **2014**, *6* (10), 5384–5393. https://doi.org/10.1039/c3nr06761k.
(25) Luo, J.; Semenikhin, N.; Chang, H.; Moon, R. J.; Kumar, S. Post-Sulfonation of Cellulose Nanofibrils with a One-Step Reaction to Improve Dispersibility. *Carbohydr. Polym.* **2018**, *181*, 247–255. https://doi.org/10.1016/j.carbpol.2017.10.077.
(26) Liimatainen, H.; Visanko, M.; Sirviö, J.; Hormi, O.; Niinimäki, J. Sulfonated Cellulose Nanofibrils Obtained from Wood Pulp through Regioselective Oxidative Bisulfite Pre-Treatment. *Cellulose* **2013**, *20* (2), 741–749. https://doi.org/10.1007/s10570-013-9865-y.
(27) Sirviö, J. A.; Ukkola, J.; Liimatainen, H. Direct Sulfation of Cellulose Fibers Using a Reactive Deep Eutectic Solvent to Produce Highly Charged Cellulose Nanofibers. *Cellulose*. 2019. https://doi.org/10.1007/s10570-019-02257-8.
(28) Zhang, J.; Jiang, N.; Dang, Z.; Elder, T. J.; Ragauskas, A. J. Oxidation and Sulfonation of Cellulosics. *Cellulose* **2008**, *15* (3), 489–496. https://doi.org/10.1007/s10570-007-9193-1.
(29) Hou, Q. X.; Liu, W.; Liu, Z. H.; Bai, L. L. Characteristics of Wood Cellulose Fibers Treated with Periodate and Bisulfite. *Ind. Eng. Chem. Res.* **2007**, *46* (23), 7830–7837. https://doi.org/10.1021/ie0704750.
(30) Lu, P.; Hsieh, Y.-L. Preparation and Characterization of Cellulose Nanocrystals from Rice Straw. *Carbohydr. Polym.* **2012**, *87* (1), 564–573. https://doi.org/https://doi.org/10.1016/j.carbpol.2011.08.022.
(31) Hsieh, Y.-L.; Hu, X.-P.; Wang, A. Single Fiber Strength Variations of Developing Cotton Fibers—Strength and Structure of G. Hirsutum and G. Barbedense. *Text. Res. J.* **2000**, *70* (8), 682–690. https://doi.org/10.1177/004051750007000805.
(32) Zhang, K.; Brendler, E.; Geissler, A.; Fischer, S. Synthesis and Spectroscopic Analysis of Cellulose Sulfates with Regulable Total Degrees of Substitution and Sulfation Patterns via 13C NMR and FT Raman Spectroscopy. *Polymer (Guildf).* **2011**, *52* (1), 26–32. https://doi.org/10.1016/j.polymer.2010.11.017.
(33) García, R.; Pérez, R. Dynamic Atomic Force Microscopy Methods. *Surface Science Reports*. Elsevier September 1, 2002, pp 197–301. https://doi.org/10.1016/s0167-5729(02)00077-8.
(34) Moreno-Herrero, F.; Colchero, J.; Baró, A. M. DNA Height in Scanning Force Microscopy. *Ultramicroscopy* **2003**, *96* (2), 167–174. https://doi.org/10.1016/S0304-3991(03)00004-4.
(35) Santos, S.; Barcons, V.; Christenson, H. K.; Font, J.; Thomson, N. H. The Intrinsic Resolution Limit in the Atomic Force Microscope: Implications for Heights of Nano-Scale Features. *PLoS One* **2011**, *6* (8). https://doi.org/10.1371/journal.pone.0023821.
(36) Jiang, F.; Han, S.; Hsieh, Y.-L. Controlled Defibrillation of Rice Straw Cellulose and Self-Assembly of Cellulose Nanofibrils into Highly Crystalline Fibrous Materials. *Rsc Adv.* **2013**,

3 (30), 12366–12375. https://doi.org/10.1039/c3ra41646a.
(37) Ciolacu, D.; Ciolacu, F.; Popa, V. I. Amorphous Cellulose—Structure and Characterization. *Cellul. Chem. Technol.* **2011**, *45* (1).
(38) Lasseuguette, E.; Roux, D.; Nishiyama, Y. Rheological Properties of Microfibrillar Suspension of TEMPO-Oxidized Pulp. *Cellulose* **2008**, *15* (3), 425–433. https://doi.org/10.1007/s10570-007-9184-2.
(39) Xu, X.; Hsieh, Y. Lo. Aqueous Exfoliated Graphene by Amphiphilic Nanocellulose and Its Application in Moisture-Responsive Foldable Actuators. *Nanoscale* **2019**, *11* (24), 11719–11729. https://doi.org/10.1039/c9nr01602c.
(40) Nishiyama, Y.; Langan, P.; Chanzy, H. Crystal Structure and Hydrogen-Bonding System in Cellulose Iβ from Synchrotron X-Ray and Neutron Fiber Diffraction. *J. Am. Chem. Soc.* **2002**, *124* (31), 9074–9082. https://doi.org/10.1021/ja0257319.

CHAPTER 3. Hybrid Polyelectrolyte Complexes of PEDOT with PSS and Sulfated Cellulose Nanofibrils Through in-situ Polymerization

INTRODUCTION

Poly(3,4-ethylene dioxythiophene) (PEDOT) is a 3,4-disubstituted polythiophene conducting polymer. Since its initial discovery by Bayer AG in 1988,[1] PEDOT has attracted intensive attention for research from both academia and industry and has gained a significant degree of commercial success. A number of factors differentiate PEDOT from other intrinsically conducting polymers. While polyacetylene boasts significantly higher conductivity than PEDOT—on the order of 10^5 S/cm^2—the inherent instability of polyacetylene hampers its commercial utility. PEDOT itself has higher conductivity than poly(p-phenylene vinylene) and other polyphenylenes, exceeding the latter by approximately an order of magnitude.[2] The EDOT monomer is less toxic and volatile than pyrrole—the precursor to polypyrrole—facilitating safer manufacturing.[3] PEDOT exhibits stable conductivity up to temperatures of 280 °C, significantly higher than the stable range for polypyrrole and polyaniline and above the temperatures needed when using lead free solder.[3] This allows PEDOT to be incorporated into components such as electrolytic capacitors without risking thermal degradation due to soldering.[4]

Another major advantage of PEDOT is its ability to form stable polyelectrolyte complexes to be aqueous dispersible, which facilitates processing. PEDOT on its own is insoluble in any known solvent, thus cannot be directly processed into films unless either chemically or electrochemically polymerized onto a surface to form a PEDOT layer. With the discovery that PEDOT can be polymerized in the presence of a host polyelectrolyte, typically poly(styrene sulfonate) (PSS), to form stable aqueous dispersions, this issue was circumvented. In these

PEDOT:PSS polyelectrolyte complexes, positive charges formed during oxidation of the PEDOT chain—analogous to *p*-type doping in traditional semiconductors—are electrostatically bound to the PSS anionic sulfonate groups.[3] These dispersions are attractive from an engineering point of view because they allow PEDOT be processed using a myriad of well-established solution-based techniques, including spin coating,[5] doctor blading,[6] dip coating,[7] drop casting,[8] ink-jetting,[9] and wet spinning.[10] However, the quantity of PSS included is significant, with dispersions typically having a 2.5:1 PSS:PEDOT mass ratio. This represents 71 wt% of insulating PSS that has a profound effect on the resulting conductivity.

Various strategies have been implemented to improve both the conductivity and dispersibility of PEDOT:PSS. The most prolific is the use of so-called *secondary dopants*[11] or *conductivity enhancement agents*.[3] These are chemicals—commonly high boiling point solvents, such as dimethyl sulfoxide (DMSO) or ethylene glycol (EG)—which are added to PEDOT:PSS dispersions prior to processing and are often (but not always[12,13]) removed from the final product during curing.[14] In truth, the term *secondary dopant*, while widely used, is somewhat of a misnomer. In traditional semiconductors, doping refers to the inclusion of foreign atoms into a lattice to bring about a change in electrical structure. In conducting polymers, doping generally refers to redox reactions that bring about positive or negative charges along the polymeric chain.[3] The species created in these redox reactions—predominantly bipolarons in the case of PEDOT—lead to additional valid energy levels in the band gap of the polymer that dramatically increase conductivity.[15] In PEDOT:PSS, secondary dopants bring about no oxidative nor electronic change and, in many cases, aren't even present in the final material; it is therefore somewhat misleading to refer to the process as *doping*. Despite this fact, the application of so-called secondary dopants

is known to bring about drastic increases in conductivity, as large as 2-3 order of magnitude.[14] The exact mechanism of this enhancement has been a topic of great debate. One proposed explanation is that the enhancement results from of small amounts of the secondary dopant remaining in the film and screening interactions between PEDOT and PSS with their polar moieties.[16] Another postulated that the additives acted as plasticizers, facilitating the reorganization of PEDOT chains and their phase-separation from PSS in a manner that leads to larger PEDOT-rich domains with reduced resistance and, in turn, higher conductivity.[17] Other explanations include the washing away of the non-conductive PSS during secondary doping[18] or the conformational change in PEDOT from a benzoid to a planar quinoid structure whose conjugated backbone is favored for higher conductivity.[19]

Another method that has been examined for improving the conductivity of PEDOT dispersions is by manipulating the morphology of PEDOT:PSS materials through templating. PEDOT:PSS complexes are inherently heterogeneous materials whose conductivity depends as much on ordering and supramolecular structure of both PEDOT and PSS as it does on factors like degree of polymerization or doping level. It has been shown that the inclusion of cellulose nanofibrils (CNF), 1D nanomaterials formed by breaking down cellulose through a combination of chemical and mechanical treatments[20], into a PEDOT:PSS matrix can lead to enhanced p-stacking of PEDOT along the nanofibrils and increased conductivity.[21] This effect has been shown to lead to a 2-fold increase in bulk conductivity, despite the fact that the insulating CNF dilutes the overall fraction of conducting PEDOT present.[22] While these works proceeded by mixing commercial PEDOT:PSS (Clevios PH1000) dispersions with CNF, the fact that many CNF are functionalized with anionic moieties leads to a second option: the in-situ polymerization of

PEDOT in the direct presence of an anionic CNF to form dispersible complexes, cutting PSS out of the system entirely. It has been demonstrated that stable aqueous dispersions can be formed by polymerizing PEDOT in the presence of sulfated cellulose nanofibrils (SCNF).[23] This work utilized pretreatment with sulfamic acid in N,N-dimethylformamide (DMF) followed by homogenization to produce nanofibrils from pine pulp with diameters of 2-5 nm, lengths of 100-600 nm, and a degree of substitution of 0.497. Notably, these PEDOT:SCNF dispersions remained stable even at relatively high concentrations of PEDOT up to 50 wt%. This was attributed to the unfunctionalized hydroxyl groups of cellulose aiding in dispersion. Despite these preliminary successes, work in this area is still limited, with many questions persisting about the behavior and properties of systems in which PEDOT is complexed with nanocelluloses. One factor that can confound the literature involving CNF, including the works utilizing CNF in conjunction with PEDOT, is that most groups synthesize their nanofibrils in-house with different starting materials, reagents, and synthesis procedures, leading to variability in nanofibril dimensions, crystallinity, and functionalization. It is therefore imperative that work involving CNF includes adequate dimensional and chemical characterization.

The present study aims to further explore the use of SCNF as host polyelectrolytes in PEDOT dispersions and examine its effect when used in conjunction with secondary dopants. Sulfated cellulose nanofibrils (SCNF) were produced from dissolving pulp by a previously established method through the use of chlorosulfonic acid treatment in N,N-dimethylformamide (DMF) followed by mechanical blending.[24] EDOT was polymerized into PEDOT in the presence of SCNF and PSS in varying ratios. Dispersion stability, morphology, and conductivity are examined as functions of dispersion anion composition. The effect of secondary doping with EG and DMSO

on PEDOT:SCNF and hybrid PEDOT:PSS/SCNF systems is examined with the goal of maximizing dispersion conductivity. Fibers were wet spun from PEDOT:PSS/SCNF in order to induce shear-mediated alignment of polymer chains and nanofibrils, leading to dramatically increased conductivity.

EXPERIMENTAL

Materials

Anhydrous N,N-dimethylformamide (DMF), sodium persulfate, iron(III) sulfate monohydrate, and poly(styrene sulfonic acid) (75 kDa, aqueous, 18 wt%) were purchased from Sigma-Aldrich. 3,4-ethylenedioxythiophene (99%) was purchased from Acros. Sodium hydroxide (1.00 N solution) was purchased from Spectrum Chemical. Chlorosulfonic acid (99%) was purchased from Alfa Aesar. Ethylene glycol (EG), dimethyl sulfoxide (DMSO), and acetone were purchased from Fischer Scientific. Sheets of softwood dissolving pulp cellulose were received from the US Forest Product Laboratory of the US Forest Service in Madison, WI. Ultra-pure water was acquired from a Milli-Q Advantage A10 water purification system. Regenerated cellulose dialysis tubing (3 kDa molecular weight cutoff) was purchased from Spectrum Laboratories. Silver conductive epoxy was purchased form MG Chemicals. Unless otherwise specified, all chemicals were utilized as-is.

Synthesis and characterization of SCNF

SCNF was produced from dissolving pulp cellulose through a previously reported procedure.[24] Cellulose pulp sheets (1.0 g) were torn into squares with sides of 1 cm or smaller and placed in a 50 mL round-bottom flask. Anhydrous DMF (45 mL) was added to the flask and the cellulose pulp was allowed to disperse under vigorous stirring for 2 hours. Chlorosulfonic acid

(1.25 moles per mole of anhydroglucose, AGU) was added dropwise to 5 mL of anhydrous DMF chilled in an ice bath to prevent excessive heating. This acid/DMF mixture was added to the dispersed pulp and the reaction was allowed to proceed for 45 minutes. Termination was carried out through the addition of 10 mL of purified water, after which the cellulose sulfate product was washed with more water by repeated centrifugation and decanting. Residual DMF and acid was removed through dialysis against purified water changed daily for a period of approximately one week, until the conductivity of the dialyzing water plateaued below 1 µS/cm. Sulfated cellulose was disintegrated by 10 minutes of high-speed blending (Vitamix 5200, 37,000 RPM) at a concentration of 0.2 wt%. Blending was performed in 5-minute increments with cooldown periods between to avoid excessive heating. SCNF was concentrated as needed using a rotary evaporator.

The height and length of SCNF were assessed using atomic force microscopy (AFM) (Asylum Research MFP-3D) using OMCL-AC160TS standard silicon probes with a nominal tip radius of 7 nm and spring constant of 26 N/m. Several drops of SCNF diluted to 0.00003 wt% were deposited on freshly cleaved mica disks and dried under ambient conditions. AFM surface profiles were collected in AC mode and processed using the open-source programs Gwyddion and ImageJ to determine fibril dimensions. The width of SCNF was additionally assessed using transmission electron microscopy (TEM). Aqueous SCNF was diluted to 0.01 wt% and deposited on a glow discharged TEM grid (carbon/formvar over 300 mesh copper). After 10 minutes the excess was blotted off and the samples was repeatedly stained with 2 wt% uranyl acetate. Micrographs were taken at 50,000x magnification on a JEOL JEM 2100F-AC TEM. Micrographs were analyzed with

the program imageJ, with SCNF widths being determined by finding the full width at half maximum (FWHM) of the intensity profiles across fibrils.

SCNF charge was determined through conductometric titration. SCNF was dialyzed again against purified water for several days to remove small-molecule contaminants, after which it was run through an ion exchange column loaded with a strong acid exchange resin (DOWEX Marathon C) to ensure that the sulfate half-ester groups were in their acid form. Titration was carried out with 0.01 M NaOH, and the equivalence point was determined by finding the minima in the conductivity curve where all acidic sulfate groups were neutralized.

The crystallinity of the dissolving pulp cellulose and all nanocellulose samples was determined through X-ray diffraction (XRD). Films of SCNF approximately 10 μm thick were made by depositing 10 mL of SCNF at a concentration of 0.2 wt% in a glass dish and allowing it to dry at 50 °C. The dissolving pulp was ground and deposited as a powder on an XRD sample stage using a very small amount of high-vacuum grease. Scans were collected of the films/powder on a Bruker D8 Advance Eco diffractometer with a Cu Kα radiation source. Samples were scanned at 2θ values ranging from 5° to 40° with an angular increment of 0.03° and a scan time of 2.5 s per increment. Crystallinity was estimated from XRD via a peak deconvolution with four crystalline peaks and the fitting software Fityk,[25] with each peak being modeled using a Voigt function.

Syntheses of PEDOT:PSS:SCNF Complexes

All PEDOT complexes were synthesized through the chemical polymerization of EDOT in the presence of either SCNF, PSS, or some mixture thereof. The amount of EDOT in each reaction was kept constant to maintain an aqueous concentration of 0.2 wt%, near its aqueous solubility limit. The amount of either SCNF or PSS polyanion or total SCNF/PSS polyanions were varied to

achieve 2.5:1, 1.5:1, or 1:1 polyanion:PEDOT w/w ratios. The composition of the polyanion was also varied, consisting of 0, 10, 30, 50, 70, 90, or 100 wt% SCNF, with any remainder being PSS.

For a typical reaction, the polyanion or polyanions (0.1–0.25 g) were added to a 50 mL round bottom flask and purified water was added to reach a total volume of 50 mL. EDOT (0.1 g) was added and allowed to dissolve for two hours under magnetic stirring. The mixture was degassed via 10 minutes of sonication (Branson 2510 bath sonicator) and the reaction was initiated by adding sodium persulfate (0.234 g) as an oxidizing agent and a small amount of ferric sulfate catalyst (10.5 mg). Reactions were allowed to proceed for a period of 24 hours, at which point the PEDOT complexes were adjusted to neutral pH with 1 M NaOH and purified via dialysis against ultra-pure water using regenerated cellulose dialysis tubing. Once the conductivity of the dialyzing water plateaued, the complexes were concentrated using a rotary evaporator to 0.8 wt%.

Characterization of PEDOT complexes

PEDOT:SCNF and PEDOT:PSS:SCNF were imaged by AFM with a procedure similar to the one detailed for SCNF. PEDOT complexes were diluted to 0.00008 wt%, deposited on mica, and scanned using an Asylum Research MFP-3D atomic force microscope. TEM micrographs were collected and analyzed for PEDOT:PSS and PEDOT:PSS:SCNF dispersions utilizing a procedure analogous to that outlined previously for the analysis of SCNF.

The viscosity of aqueous PEDOT dispersions was measured using a Brookfield DV3T rheometer with a concentric circle geometry. PEDOT dispersions were concentrated to 0.8 wt% via rotary evaporation. Viscosity measurements were taken at 25 °C at shear rates of 0.1 to 200 s^{-1}.

Films of PEDOT complexes were cast on glass substrates. Glass squares 2.5 cm on each side were first cleaned through sonication in acetone, followed by a rinse in isopropanol. Substrates were then soaked in 30% nitric acid for a period of at least 24 hours to increase surface hydrophilicity. Films of PEDOT dispersions were deposited through drop casting 250 µL of dispersion at a concentration of 0.8 wt%. Each dispersion was cast both as-is and with the addition of 5 wt% EG or DMSO to act as conductivity enhancers. Films were allowed to dry in air and then cured at 120 °C for 60 minutes.

The resistivity of films was measured using the four-point probe method with colinear probes. One film was tested for each experimental condition, and at least 3 resistivity measurements were taken for each film and averaged. Film thickness was measured by using AFM as a stylus profilometer, measuring the height difference between the bulk of the film and the substrate surface in several locations along a scored groove. Two height measurements were taken for each film in different locations and averaged. Conductivity was calculated from thickness and resistivity measurements according to the equation $\sigma = 1/(R \cdot t)$, where σ is conductivity, R is the sheet resistance of the film, and t is the film thickness.[22]

The thermal decomposition of PEDOT:PSS/SCNF complexes was assessed using thermogravimetric analysis (TGA). Dispersions at 0.8 wt% were oven dried overnight at 50 °C. Between 3 and 5 mg of these dispersions were placed in a platinum pan and analyzed using a Shimadzu TGA-50 in a nitrogen environment with a heating rate of 10 °C/min and a maximum temperature of 500 °C.

Wet spinning of PEDOT:PSS/SCNF dispersions

A PEDOT:PSS/SCNF dispersion with 30 wt% PSS in the polyanion and a 2.5:1 w/w polyanion:PEDOT ratio was concentrated to 1.38 wt% via rotary evaporation. The dispersion was run through a syringe filter with 5 μm pores to remove small particulates and degassed using a bath sonicator for 5 minutes. Wet spinning was carried out by extruding the dispersion through a g27 needle (ID = 210 μm) and into a 1L beaker filled with acetone at a rate of 0.03 mL/min controlled by a syringe pump. The coagulated fiber was wound onto a cylindrical collector using a DC electric motor. Fibers were oven dried overnight at 50 °C. A portion of the dried fibers were treated with EG vapor by placing them in a glass jar with an open dish of EG at 50 °C for 24 hours. Both the EG treated and untreated fibers were cured at 120 °C for 60 minutes.

The diameter of the fibers was measured using optical microscopy. The conductivity of the fibers was measured using the two-point probe method by first mounting the fibers using conductive epoxy with a distance of 1 cm between epoxy electrodes and measuring the resistance between points using a multimeter. Resistance (R) measurements were converted to conductivity (σ) with the equation $\sigma = L/(R \cdot A)$, where A is the cross-sectional area of the fiber. Multiple measurements were taken in different locations along each fiber and averaged.

RESULTS & DISCUSSION

SCNF Properties

Sulfated cellulose nanofibrils (SCNFs) were robustly produced by sulfation of dissolving pulp using chlorosulfonic acid (1.25 moles per AGU, 45 min) and disintegration via high-speed blending (37,000 RPM, 10 min) in 99 % yield. These SCNFs were 1.7 ± 0.7 nm high (H) and 880 ± 320 nm long (L), measured by AFM, and 3.6 ± 0.9 nm wide (W), measured by TEM (**Figure 3.1**). SCNFs

were anisotropic in cross-section with a 2.1 W/H ratio and high aspect ratios of 244 L/W or 518 L/H. The degree of surface modification by sulfate half-ester groups ($R\text{-}OSO_3^-$) was 1.81 ± 0.09 mmol per gram of SCNF. The nanofibrils had a crystallinity index of 0.58, down from 0.78 of the starting dissolving pulp cellulose due to the effects of chlorosulfonic acid treatment. Prepared by identical procedure and with the same charge, pulp SCNF are slightly less anisotropic than rice straw SCNF that had a 2.9 W/H ratio, 257 L/W or 878 L/H ratio and similarly reduced CrI from 0.76 to 0.60.[24]

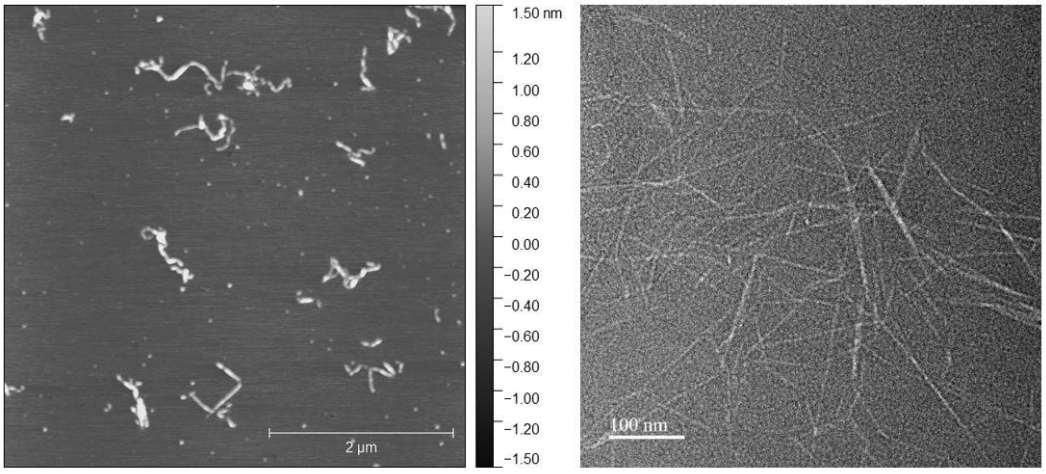

Length (nm)	Width (nm)	Height (nm)	Charge (mmol/g)	Crystallinity
880 ± 320	3.6 ± 0.9	1.7 ± 0.7	1.81 ± 0.09	58%

Figure 3.1 AFM (left) and TEM (right) of SCNF with SCNF dimensions and properties (bottom)

Applying a previously documented[24] model for determining the degree to with nanofibril surfaces are functionalized by looking at fibril cross-sectional dimensions and predicting what fraction of hydroxyl groups are internal or surface-facing estimates that ~28% of exposed surface hydroxyl groups are sulfated. As sulfation via chlorosulfonic acid is known to occur preferentially at the C6 position,[26] it can be estimated that 84% of exposed C6 hydroxyls are sulfated. Adjacent

C6 hydroxyls on a nanofibril's outward facing surface are located every other anhydroglucose unit 10.38 Å apart (**Figure 3.2**). Factoring in unfunctionalized sites by dividing this spacing by the estimated percentage of C6 surface sulfation, an average charge spacing for the SCNF used can be estimated as 12.3 Å. This charge spacing has ramifications for how SCNF forms polyelectrolyte complexes with PEDOT. Two molecular arrangements for polyelectrolyte complexes are typically discussed: the ladder type, where polycation and polyanion chains are paired more parallel to each other and "scrambled egg" type based on more random pairing between multiple polycation and polyanion chains.[3] While most polyelectrolyte complexes exist somewhere between these two extremes, similar charge spacing between the polycation and polyanion and a large discrepancy between the molecular weights of the two polymers have shown to favor the more organized ladder-like structure.[27] Doped PEDOT is found to carry approximately one positive charge per three thiophene rings[3] and has a repeating unit length of 3.963 Å,[28] leading to an expected charge spacing of 11.89 Å; reasonably similar to the spacings of SCNF. SCNF and PEDOT possess a vast difference in molecular weights, as SCNF are hundreds of nanometers long while PEDOT typically has very low molecular weights, on the order of several kDa, which corresponds to only a few dozen monomeric units.[3] Both of these factors favor the formation of more ordered ladder-like complexes.

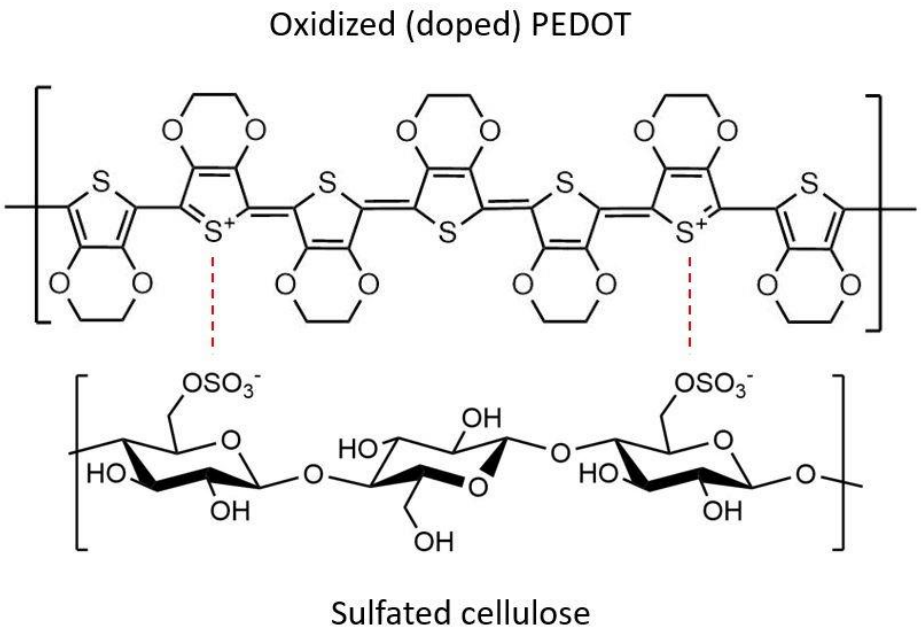

Figure 3.2 Complex between doped PEDOT (top) and sulfated cellulose (bottom)

PEDOT:PSS/SCNF dispersions

PEDOT were synthesized by polymerization of EDOT (0.2 wt%) in the presence of various SCNF/PSS polyanion ratios to produce PEDOT/PSS/SCNF complexes in 2.5:1, 1.5:1, or 1:1 polyanion:PEDOT mass ratios. The aqueous dispersion stability of these PEDOT/PSS/SCNF complexes was assessed as a function of two experimental factors. First, the total PSS/SCNF polyanions to PEDOT mass ratios, i.e., 2.5:1, 1.5:1, and 1:1 w/w, that correspond to 29%, 40%, and 50% PEDOT wt% in the final dispersions of PEDOT/PSS/SCNF**.** Second, the amount of SCNF in the polyanion was varied between 0%, 30%, and 100%, with the remainder in each case being PSS. These dispersions were left in glass vials for 21 days at a concentration of 0.2 wt% and then inverted for observation (**Figure 3.3**).

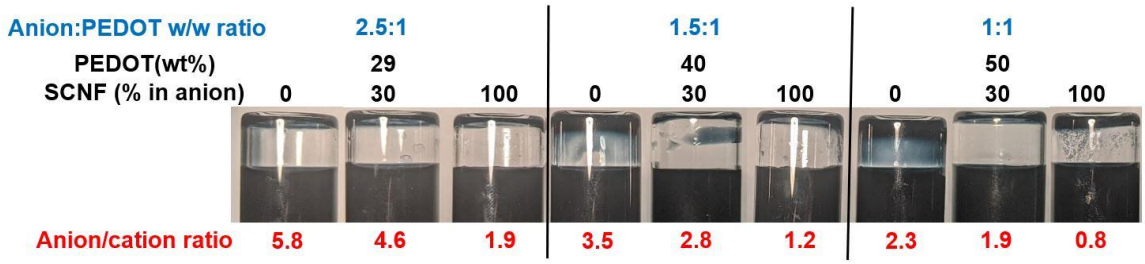

Figure 3.3 PEDOT:PSS/SCNF complexes in varied SCNF/PSS anion and PEDOT

At a 2.5:1 polyanion/PEDOT w/w ratio, the PEDOT:PSS complex containing 0% SCNF showed very little sedimentation. This is to be expected, as this is the most commonly reported PEDOT:PSS composition and has the total anion/cation ratio is 5.8. As the polyanion/PEDOT ratio lowered to 1.5:1 and 1:1, still with 0% SCNF in the polyanion, significant amounts of sediment were observed, more so than any other conditions tested, despite the fact that both of these compositions still contained a significant excess of anionic charge with 3.5 and 2.3 respective anion/cation charge ratios. With 30% SCNF in the polyanion, very little sediment was observed across all three polyanion/PEDOT ratios, even for the dispersions with 1.5:1 or 1:1 polyanion/PEDOT ratios, despite the fact that these samples contained a smaller excess of cations (4.6, 2.8, and 1.9 anion/cation charge ratios) compared to the corresponding dispersions with only PSS (5.8, 3.5, and 2.3 anion/cation charge ratios). Similarly, the dispersions with 100% SCNF and no PSS in the polyanion showed little sedimentation at polyanion/PEDOT w/w ratios of 2.5:1 and 1.5:1. However, the most PEDOT-rich sample at a 1:1 w/w polyanion/PEDOT ratio exhibited a thick layer of grainy sediment. Notably, this is the only composition in which the anion/cation charge ratio was below unity, being 0.77; poor dispersion stability is the expected result. The fact that many of the PEDOT:PSS/SCNF dispersions showed reduced settling compared to analogous PEDOT:PSS, despite the lower excess of anions, is attributed to the polar unfunctionalized

hydroxyl groups remained on the SCNF surfaces that aid the dispersion of PEDOT:PSS/SCNF complexes.

Properties of PEDOT:PSS/SCNF complexes

Further characterization was carried out on PEDOT:PSS/SCNF dispersions all synthesized at 2.5:1 w/w polyanion/PEDOT ratios and with 0, 10, 30, 50, 70, 90, or 100% SCNF in the polyanion. As expected, the rheology of 0.8 wt% PEDOT:PSS/SCNF dispersions was found to display more characteristics typical of CNF as the nanofibril loading was increased. Specifically, higher SCNF fractions led to an increase in overall viscosity coupled with stronger shear thinning behavior (**Figure 3.4a**). Part of this shear thinning behavior can be attributed to the strong tendency of SCNF to align themselves parallel to the direction of shearing. Certain processing techniques that rely on or induce large amounts of shearing, such as doctor blading or wet spinning, could leverage this tendency to intentionally induce anisotropy in fabricated materials. In the case of PEDOT:PSS/SCNF dispersions, alignment of chains along an axis is expected to significantly increase conductivity along that axis.

The thermal decomposition of PEDOT:PSS/SCNF complexes are shown in **Figure 3.4b**. As the amount of nanofibrils increased, significant decomposition develops that can be attributed to SCNF. One documented downside of sulfation processes is that sulfating nanocellulose is reported to compromise their thermal stability.[29] At 70% and above SCNF loading in the polyanion, significant loss of mass is observed at around 250 °C, below the maximum temperatures at which PEDOT is resistance stable (ca. 280°C),[3] reducing the viable operating temperature range of these SCNF rich dispersions. With up to 50 % SCNF, the TGA curves of

PEDOT:PSS/SCNF complexes were comparable to pure PEDOT:PSS with mass losses beginning closer to 280-300 °C.

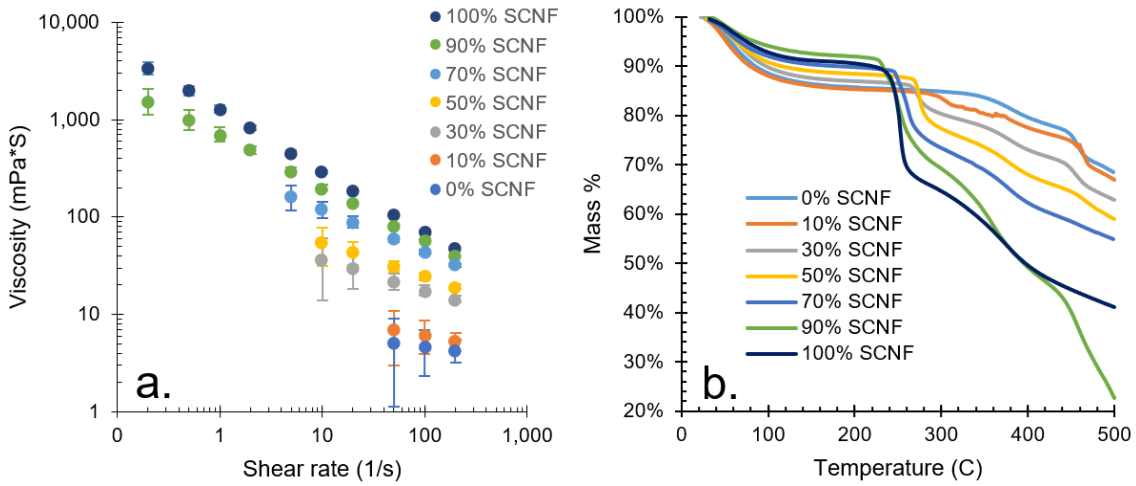

Figure 3.4 Characteristics of PEDOT:PSS/SCNF complexes with 2.5:1 polyanion ratio: (a) Viscosity vs shear rate of 0.8 wt% dispersions; (b) TGA curves.

Morphology of PEDOT:PSS/SCNF complexes

The PEDOT:PSS/SCNF complexes observed under AFM and TEM showed stark differences in behavior depending on whether PSS is included in the dispersion. With PEDOT synthesized with SCNF as the sole polyanion in the system, the PEDOT/SCNF complex exhibited a string-of-beads like morphology, with large aggregates that are presumed to be PEDOT-rich regions interspersed and seemingly attached to individual SCNF (**Figure 3.5a,d**). With as little as 10 % PSS in the SCNF/PSS polyanions, TEM and AFM both showed only nanofibrillar structures without PEDOT aggregates interspersed (**Figure 3.5b,e**). In this case it stands to reason that PEDOT is well dispersed among SCNF/PSS and likely located on the SCNF surfaces. Even increasing PSS to 70% of the polyanion, similar fibrillar structures without aggregates are still observed (**Figure 3.5c,f**). TEM contrast for this sample was significantly poorer, possibly due to the presence of significant amounts of PSS interfering with the uranyl acetate staining of SCNF. However, AFM reveals

thicker nanofibrils covered in small spherical beads, presumably PEDOT and PSS sticking to the SCNF surfaces. This same ordering of PEDOT/PSS along fibrils has also been observed in previous work on mixing PEDOT:PSS with 33 wt% of carboxymethylated CNF, even when mixing was carried out using commercial PEDOT dispersions that were already polymerized, indicating that this morphology is constant regardless of whether nanofibrils are introduced before or after polymerization.[21]

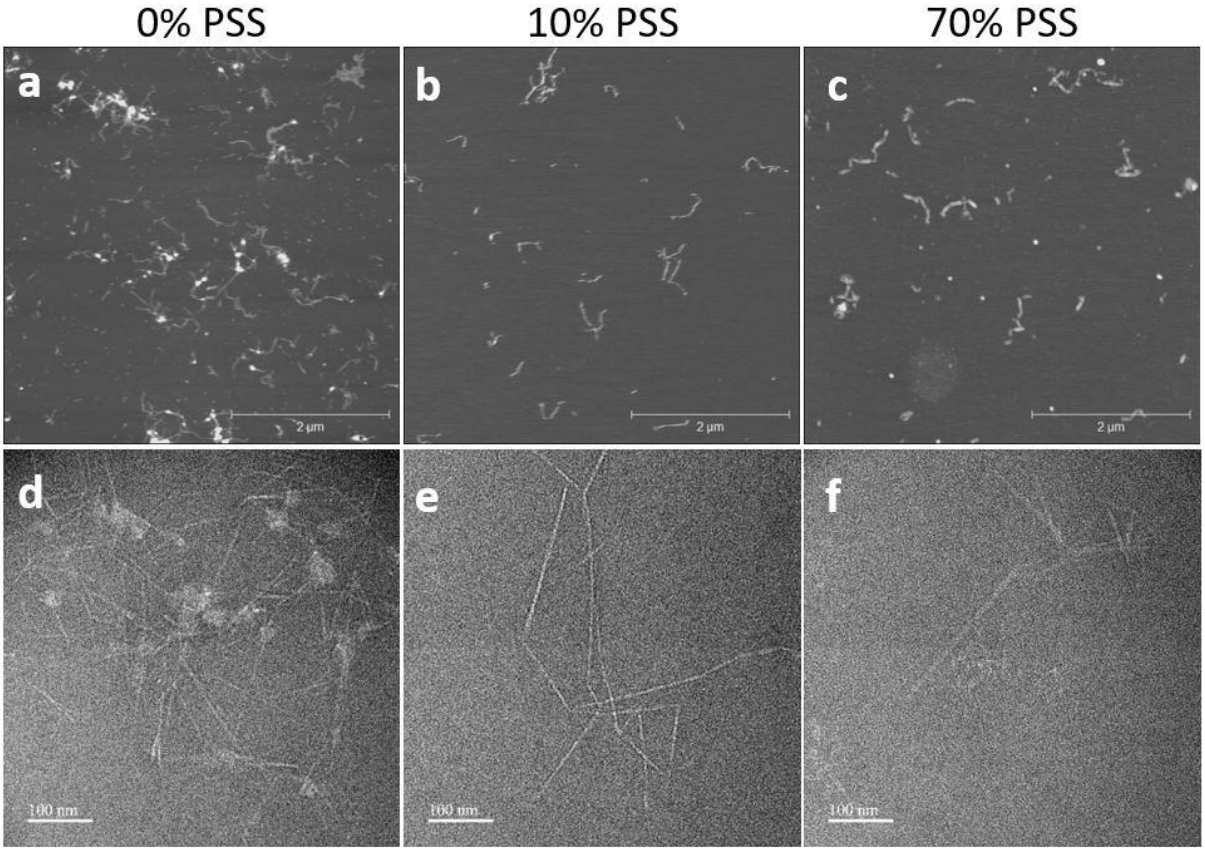

Figure 3.5 AFM (a-c) and TEM (d-f) of PEDOT:PSS/SCNF complexes with varying amounts of SCNF in the anion, all at a 2.5:1 polyanion ratio.

Conductivity of PEDOT:PSS/SCNF Complexes

Films cast from PEDOT:PSS with a 2.5:1 PSS/PEDOT w/w ratio exhibited a conductivity of 0.048 S/cm without any secondary doping. This conductivity remained unchanged when SCNF

replaced 10 wt% of the polyanion. The conductivity increased at higher polyanion replacements of 30 through 100 % SCNF (**Figure 3.6a**). The highest conductivity of 0.140 S/cm was observed at 30% SCNF replacement; a nearly 3-fold increase over the pure PEDOT:PSS. This could be attributed to the PEDOT and PSS sticking to the fibrils surface and creating a longer, more cohesive conductive pathway, as was observed by AFM (**Figure 3.5c**). When secondary dopants were included—either EG or DMSO in this case—a different picture emerges. Adding 5 wt% of either compound to PEDOT:PSS dispersions increased conductivity by more than two orders of magnitude (**Figure 3.6b)**, to 23.8 S/cm and 10.0 S/cm for EG and DMSO, respectively. This falls in line with the enhancement factors that have been reported for CLEVIOS PH 1000 previously.[14] EG was found to give slightly higher conductivities than DMSO in many cases, although the difference was small. Notably, PEDOT:PSS/SCNF with 10% SCNF loading was found to give a higher conductivity than PEDOT:PSS—37.5 S/cm for the EG treated film, the highest conductivity of all compositions tested in this work and 58% higher in conductivity than EG treated PEDOT:PSS. As SCNF loading was increased to 30% and above, the conductivity of EG and DMSO treated films steadily decreased, falling below the levels of EG treated PEDOT:PSS at loadings of 50-100% SCNF in the polyanion. In particular, neither EG nor DMSO enhanced conductivity of PEDOT:PSS/SCNF with 90-100% SCNF in the polyanion, evident by their enhancement factors that were, within the bounds of uncertainty, unity. These observations support that the mechanism behind secondary doping acts on the PSS in the system, rather than having a direct effect on the PEDOT. Of the previously suggested explanations, this observation is most in line with the idea that secondary dopants act as plasticizers, allowing PSS chains to flow and phase separate from PEDOT during curing.[17] Because the inclusion of significant amounts (i.e. 30 wt% or more) of SCNF in the

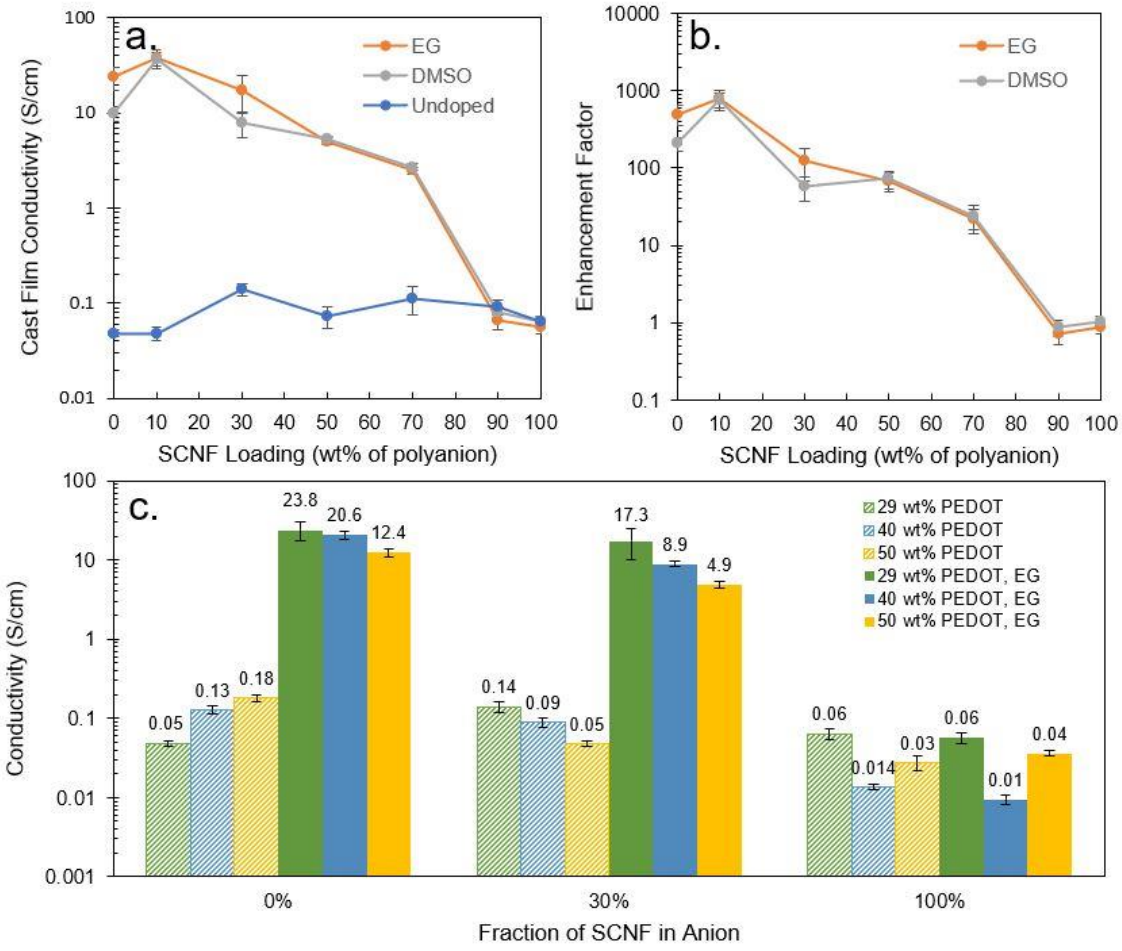

Figure 3.6. Conductivity of PEDOT complexes with PSS, SCNF, or a combination thereof as the host polyelectrolyte: (a) Conductivity of cast films with varying anion composition and secondary doping; (b) Enhancement factor of secondary dopants; (c) Effect of increased PEDOT fraction on cast film conductivity with and without secondary doping.

polyanion, and the resulting reduction in PSS, quenches the effect secondary doping, the two effects must be balanced in order to maximize conductivity. Only small quantities of SCNF should be used in conjunction with secondary dopants to improve the conductivity of hybrid PEDOT:PSS/SCNF complexes. It can be postulated that this same principle applies to some of the other works published that utilize similar strategies of including nanofibrils in commercial PEDOT dispersions, though often the use of secondary dopants or their effect in relation to undoped dispersions is not reported, so a broad generalization is difficult to make.

The conductivity of PEDOT:PSS/SCNF films at varying polyanion/PEDOT w/w ratios was also studied, both with and without EG treatment (**Figure 3.6c**); these are the same dispersions pictured in **Figure 3.3**. Without secondary doping nor SCNF, the PEDOT:PSS controls showed a nearly fourfold increase in conductivity as the polyanion/PEDOT w/w ratio was reduced from 2.5:1 to 1:1. The opposite trend was observed for the 30% SCNF samples, with conductivity of the 1:1 PEDOT dispersion being 2/3 lower than at 2.5:1, despite there being more PEDOT in the system. With EG, both films from PEDOT:PSS/SCNF with 0 and 30% SCNF showed diminishing conductivity with increasing amounts of PEDOT in the dispersions. The dispersions made with 100% SCNF in the polyanion showed no clear trend, with more variability between samples, particularly those with more PEDOT. This may be a result of increased heterogeneity, as these dispersions appeared somewhat grainy (**Figure 3.3**). Regardless of the amount of PEDOT, EG addition yielded no substantial changes in conductivity for the samples with no PSS. What these results further emphasize is that PEDOT:PSS, PEDOT:PSS/SCNF, and all other dispersions based off of PEDOT polyelectrolyte complexes lead to heterogeneous materials whose conductivity is complex and depends heavily on supramolecular ordering, morphology, and other factors beyond polymeric chain structure, the fraction of conducting material, and doping level.

Wet-spun PEDOT:PSS/SCNF fibers

A major advantage of 1D nanomaterials like SCNF is their ability to be oriented through the use of shear force, creating anisotropic materials. When PEDOT/PSS are complexed with SCNF, it is anticipated that orientation of the SCNF will lead to increased conductivity in along the oriented direction as PEDOT/PSS are carried along. To demonstrate this effect, fibers were wet spun from a PEDOT:PSS/SCNF dispersion with 30 wt% SCNF in the polyanion and a 2.5:1 w/w

polyanion:PEDOT ratio (**Figure 3.7**). Fibers spun in this way boasted a conductivity of 40 ± 4 S/cm without secondary doping. The fibers were too delicate (10-14 µm diameter) to withstand submersion in EG, so treatment was instead carried out by exposing them to EG vapor in an over for 24 hours. After EG vapor treatment, the fibers had a conductivity of 6150 ± 1000 S/cm, a more than 350-fold increase compared to EG treated films cast from the same dispersion (17.3 S/cm). These are among the most conductive PEDOT fibers ever reported in the literature, showcasing the efficacy of shear-mediated alignment for boosting electrical performance.

It is important to note that the rheology of the PEDOT:PSS/SCNF dispersions did introduce some challenges for the wet-spinning process. SCNF exhibit significant thixotropy,[24] a quality which they imparted to the PEDOT:PSS/SCNF dispersion. The intense shearing that occurred during filtration and degassing of the spin dope rendered it homogeneous and spinnable, yet as spinning progressed the viscosity visibly increased as the dope began to gel. This led to fibers becoming heterogeneous and breaking, making continuous wet-spinning challenging at the laboratory scale.

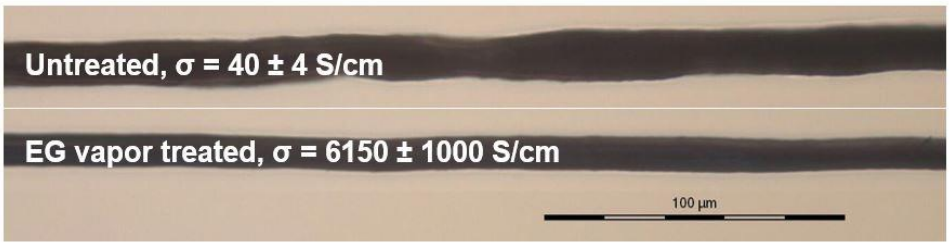

Figure 3.7 Fibers wet-spun from PEDOT:PSS/SCNF with 30 wt% SCNF in the polyanion and 2.5:1 polyanion:PEDOT w/w, shown with and without EG vapor treatment. Conductivity ± standard error shown.

CONCLUSIONS

Hybrid PEDOT polyelectrolyte complexes were synthesized by polymerizing the EDOT monomer in the presence of varying amounts of PSS and SCNF as co-polyanions. SCNF with a surface charge of 1.8 mmol/g was found to be able to stably disperse PEDOT on its own. The inclusion of SCNF into PEDOT dispersions led to increased base conductivity, up to a threefold increase with 30% SCNF in the PSS/SCNF polyanion mixture. Upon treatment with ethylene glycol, films from PEDOT synthesized with 10 % SCNF in the polyanion exhibited significantly higher conductivities of 37.5 S/cm; an increase of more than two orders of magnitude compared to untreated films and 58% higher than EG treated PEDOT:PSS synthesized without SCNF.

The application of cellulose nanofibrils as a means of increasing the conductivity of PEDOT and PEDOT dispersions has been examined several times, but the effect of secondary doping has largely been ignored. While the ability of functionalized nanofibrils to participate as the lone host polyelectrolyte in a polyelectrolyte complex is intriguing in and of itself, the fact that this scheme is unaffected by secondary doping renders PEDOT:SCNF complexes suboptimal on their own. Any attempt to maximize PEDOT dispersion conductivity must examine the wider picture and not overemphasize a singular strategy. The competing effects of secondary doping and the enhancement brought about by the inclusion of nanofibrils highlights this important fact, while also providing a route towards future development, wherein small amounts of nanofibrils can provide tangible benefits without compromising other strategies that have been employed to improve the performance of PEDOT:PSS. Judiciously employed, this technique is another tool that could help push the boundaries of what conducting polymers are capable of.

REFERENCES

(1) Friedrich, J.; Heywang, G.; Werner, S.; Heinze, J.; Michael, D. Polythiophenes, Process for Their Preparation and Their Use. EP 0339340 A2, 1989.

(2) Nezakati, T.; Seifalian, A.; Tan, A.; Seifalian, A. M. Conductive Polymers: Opportunities and Challenges in Biomedical Applications. *Chem. Rev.* **2018**, *118* (14), 6766–6843.

(3) Elschner, A.; Kirchmeyer, S.; Lovenich, W.; Merker, U.; Reuter, K. *PEDOT: Principles and Applications of an Intrinsically Conductive Polymer*; CRC Press, 2010.

(4) Kudoh, Y.; Akami, K.; Matsuya, Y. Solid Electrolytic Capacitor with Highly Stable Conducting Polymer as a Counter Electrode. *Synth. Met.* **1999**, *102* (1–3), 973–974.

(5) Nardes, A. M.; Kemerink, M.; Janssen, R. A. J.; Bastiaansen, J. A. M.; Kiggen, N. M. M.; Langeveld, B. M. W.; Van Breemen, A. J. J. M.; De Kok, M. M. Microscopic Understanding of the Anisotropic Conductivity of PEDOT:PSS Thin Films. *Adv. Mater.* **2007**, *19* (9), 1196–1200.

(6) Padinger, F.; Brabec, C. J.; Fromherz, T.; Hummelen, J. C.; Sariciftci, N. S. Fabrication of Large Area Photovoltaic Devices Containing Various Blends of Polymer and Fullerene Derivatives by Using the Doctor Blade Technique. *Opto-Electronics Rev.* **2000**, *8* (4), 280–283.

(7) Huang, L.; Hu, Z.; Zhang, K.; Chen, P.; Zhu, Y. Dip-Coating of Poly(3,4-Ethylenedioxythiophene):Poly(Styrenesulfonate) Anodes for Efficient Polymer Solar Cells. *Thin Solid Films* **2015**, *578*, 161–166.

(8) Eslamian, M.; Soltani-Kordshuli, F. Development of Multiple-Droplet Drop-Casting Method for the Fabrication of Coatings and Thin Solid Films. *J. Coatings Technol. Res.* **2018**, *15* (2), 271–280.

(9) Xiong, Z.; Liu, C. Optimization of Inkjet Printed PEDOT:PSS Thin Films through Annealing Processes. *Org. Electron.* **2012**, *13* (9), 1532–1540.

(10) Zhou, J.; Li, E. Q.; Li, R.; Xu, X.; Ventura, I. A.; Moussawi, A.; Anjum, D. H.; Hedhili, M. N.; Smilgies, D. M.; Lubineau, G.; et al. Semi-Metallic, Strong and Stretchable Wet-Spun Conjugated Polymer Microfibers. *J. Mater. Chem. C* **2015**, *3* (11), 2528–2538.

(11) MacDiarmid, A. G.; Epstein, A. J. The Concept of Secondary Doping as Applied to Polyaniline. *Synth. Met.* **1994**, *65* (2–3), 103–116.

(12) Döbbelin, M.; Marcilla, R.; Salsamendi, M.; Pozo-Gonzalo, C.; Carrasco, P. M.; Pomposo, J. A.; Mecerreyes, D. Influence of Ionic Liquids on the Electrical Conductivity and Morphology of PEDOT:PSS Films. *Chem. Mater.* **2007**, *19* (9), 2147–2149.

(13) Fan, B.; Mei, X.; Ouyang, J. Significant Conductivity Enhancement of Conductive Poly(3,4-Ethylenedioxythiophene): Poly(Styrenesulfonate) Films by Adding Anionic Surfactants into Polymer Solution. *Macromolecules* **2008**, *41* (16), 5971–5973.

(14) Ouyang, J.; Xu, Q.; Chu, C. W.; Yang, Y.; Li, G.; Shinar, J. On the Mechanism of Conductivity Enhancement in Poly(3,4- Ethylenedioxythiophene):Poly(Styrene Sulfonate) Film through Solvent Treatment. *Polymer (Guildf).* **2004**, *45* (25), 8443–8450.

(15) Brédas, J. L.; Streets, G. B. Polarons, Bipolaron, and Solitons in Conducting Polymers. *Acc. Chem. Res* **1985**, *18*, 309–315.

(16) Kim, J. Y.; Jung, J. H.; Lee, D. E.; Joo, J. Enhancement of Electrical Conductivity of Poly(3,4-Ethylenedioxythiophene)/Poly(4-Styrenesulfonate) by a Change of Solvents. *Synth. Met.*

2002, *126* (2–3), 311–316.
(17) Pettersson, L. A. .; Ghosh, S.; Inganäs, O. Optical Anisotropy in Thin Films of Poly(3,4-Ethylenedioxythiophene)–Poly(4-Styrenesulfonate). *Org. Electron.* **2002**, *3* (3–4), 143–148.
(18) Jönsson, S. K. M.; Birgerson, J.; Crispin, X.; Greczynski, G.; Osikowicz, W.; Denier van der Gon, A. W.; Salaneck, W. R.; Fahlman, M. The Effects of Solvents on the Morphology and Sheet Resistance in Poly(3,4-Ethylenedioxythiophene)-Polystyrenesulfonic Acid (PEDOT-PSS) Films. *Synth. Met.* **2003**, *139* (1), 1–10.
(19) Ouyang, J.; Chu, C. W.; Chen, F. C.; Xu, Q.; Yang, Y. High-Conductivity Poly(3,4-Ethylenedioxythiophene):Poly(Styrene Sulfonate) Film and Its Application in Polymer Optoelectronic Devices. *Adv. Funct. Mater.* **2005**, *15* (2), 203–208.
(20) Thomas, B.; Raj, M. C.; Athira, B. K.; Rubiyah, H. M.; Joy, J.; Moores, A.; Drisko, G. L.; Sanchez, C. Nanocellulose, a Versatile Green Platform: From Biosources to Materials and Their Applications. *Chemical Reviews*. 2018, pp 11575–11625.
(21) Belaineh, D.; Andreasen, J. W.; Palisaitis, J.; Malti, A.; Håkansson, K.; Wågberg, L.; Crispin, X.; Engquist, I.; Berggren, M. Controlling the Organization of PEDOT:PSS on Cellulose Structures. *ACS Appl. Polym. Mater.* **2019**, *1* (9), 2342–2351.
(22) Zhou, J.; Hsieh, Y.-L. Conductive Polymer Protonated Nanocellulose Aerogels for Tunable and Linearly Responsive Strain Sensors. *ACS Appl. Mater. Interfaces* **2018**, *10* (33), 27902–27910.
(23) Feng, X.; Wang, X.; Wang, M.; Zhou, S.; Dang, C.; Zhang, C.; Chen, Y.; Qi, H. Novel PEDOT Dispersion by In-Situ Polymerization Based on Sulfated Nanocellulose. *Chem. Eng. J.* **2021**, *418*, 129533.
(24) Pingrey, B.; Hsieh, Y.-L. Sulfated Cellulose Nanofibrils from Chlorosulfonic Acid Treatment and Their Wet Spinning into High-Strength Fibers. *Biomacromolecules* **2022**, *23* (3), 1269–1277.
(25) Park, S.; Baker, J. O.; Himmel, M. E.; Parilla, P. A.; Johnson, D. K. Cellulose Crystallinity Index: Measurement Techniques and Their Impact on Interpreting Cellulase Performance. *Biotechnol. Biofuels* **2010**, *3* (10).
(26) Zhang, K.; Brendler, E.; Geissler, A.; Fischer, S. Synthesis and Spectroscopic Analysis of Cellulose Sulfates with Regulable Total Degrees of Substitution and Sulfation Patterns via 13C NMR and FT Raman Spectroscopy. *Polymer (Guildf).* **2011**, *52* (1), 26–32.
(27) Rembaum, A. Polyelectrolyte Complexes. *J. Macromol. Sci. Part A - Chem.* **1969**, *3* (1), 87–99.
(28) Kim, E. G.; Brédas, J. L. Electronic Evolution of Poly(3,4-Ethylenedioxythiophene) (PEDOT): From the Isolated Chain to the Pristine and Heavily Doped Crystals. *J. Am. Chem. Soc.* **2008**, *130* (50), 16880–16889.
(29) Camarero Espinosa, S.; Kuhnt, T.; Foster, E. J.; Weder, C. Isolation of Thermally Stable Cellulose Nanocrystals by Phosphoric Acid Hydrolysis. *Biomacromolecules* **2013**, *14* (4), 1223–1230.

CHAPTER 4. Aqueous Exfoliation and Dispersion of Monolayer and Bilayer Graphene from Graphite using Sulfated Cellulose Nanofibrils

INTRODUCTION

Since its originally discovery in 2004, graphene has been making waves throughout scientific community. Consisting of single layers of sp^2 hybridized carbon, graphene possesses an array of impressive electrical, mechanical, and thermal properties that have led to intensive interest. It has a high electron carrier mobility of up to 200,000 $cm^2 \cdot V^{-1} \cdot s^{-1}$, giving rise to a correspondingly high in-plane electrical conductivity.[1] Its thermal conductivity is also high, on the order of 3000 $W \cdot m^{-1} \cdot K^{-1}$; nearly an order of magnitude higher than that of copper.[1] Monolayers of graphene possess a staggeringly high tensile modulus of 1 TPa, making it among the strongest materials ever measured.[2] Despite these properties, graphene has not been widely implemented throughout the industrial sector. This is largely due to an inability to produce producing high quality graphene samples reliably and in bulk.[3]

The simplest top-down method to produce graphene is to mechanically exfoliate it from graphite using cellophane tape.[1] Incidentally, this method also produces some of the highest quality graphene sheets available. However, it is neither scalable nor high-yielding and is unsuitable for any form of bulk production. Alternative top-down approaches have focused on chemical methods of exfoliating graphene in solution such as chemical modification of graphite—often to graphite oxide—followed by ultrasonication in various organic media such as N,N-dimethylformamide (DMF)[4], with subsequent reduction into graphene using hydrazine.[5] Other strategies include mechanically shearing graphite in organic liquids with surface energies close to that of graphene (ca. 70-80 mJ/m^2)[6] , including DMF[7], N-methyl-2-pyrrolidone (NMP)[8], and

1,2-dichloroethane.[9] A number of dispersants have also been utilized to suspend graphene in water, including porphyrins[10], sodium salts[11], 1-pyrenebutyrate[12], and poly(styrene sulfonate).[5] These dispersants act by building up electrical double layers on graphene, often requiring significant quantities of dispersant and leading to a dramatic reduction in the conductivity of the resulting product. As an example, 1-pyrenebutyrate was able to stabilize graphene at a concentration of 0.1 mg/mL, but yielded a conductivity of only 2 S/cm.[12]

It has been previously demonstrated that TEMPO-oxidized CNF, exhibiting amphiphilic behavior[13] due to the presence of both hydrophilic crystalline planes with abundant hydroxyl groups and hydrophobic (200) planes faced with carbon and hydrogen atoms, could act as both an aid to the aqueous exfoliation of graphene by high-speed blending and a dispersant for the resulting graphene, capable of dispersing high graphene concentrations of up to 1 mg/mL.[14] The current work expands upon this discovery by examining the use of sulfated cellulose nanofibrils (SCNF), which can possess a wider degree of charges through tuning reaction conditions. The relationship between the degree of sulfation and the exfoliation efficacy and optimizing exfoliation conditions by mechanical blending to maximize graphene production and quality. The effectiveness of SCNF at producing monolayer and bilayer graphene sheets is assessed, along with the conductivity of films formed by vacuum filtering the graphene dispersions. Additionally, it is shown that the defibrillation of sulfated cellulose into SCNF and graphene exfoliation may be carried out simultaneously.

EXPERIMENTAL

Materials

Anhydrous N,N-dimethylformamide (DMF) and graphite flakes (~50 µm thickness) were obtained from Sigma-Aldrich. Sodium hydroxide (1.00 N solution) was obtained from Spectrum chemical. Chlorosulfonic acid (99%) was obtained from Alfa Aesar. Sheets of softwood dissolving pulp cellulose were received from the US Forest Product Laboratory of the US Forest Service in Madison, WI. Ultra-pure water was acquired from a Milli-Q Advantage A10 water purification system. Regenerated cellulose dialysis tubing (12-14 kDa molecular weight cutoff) and polycarbonate filters (47 mm diameter, 0.6 µm pores) were purchased from Spectrum Laboratories. Dowex Marathon C (H-form) acidic ion exchange resin beads were purchased from Fisher Scientific. Unless otherwise noted, all materials were utilized as-is.

Synthesis of SCNF

Sulfated cellulose nanofibrils (SCNF) were synthesized from dissolving pulp cellulose following a previously reported procedure.[15] In brief, sheets of dissolving pulp cellulose (1 g) were torn into small squares circa 1 cm on each side and dispersed under vigorous stirring in anhydrous DMF (45 mL) for two hours. Chlorosulfonic acid was added dropwise to 5 mL of DMF chilled in an ice bath (1.0, 1.25, or 1.5 moles of acid per mole of anhydroglucose units in the dispersing cellulose, corresponding to volumes of approximately 0.41, 0.51, or 0.62 mL, respectively). The acid/DMF mixture was added to the dispersed cellulose and allowed to react for 30, 45, or 60 minutes. The reaction was terminated by the addition of 10 mL purified water, followed by three rounds of washing via centrifugation and resuspension. The washed sulfated cellulose (SCell) was then dialyzed against purified water using regenerated cellulose dialysis membranes for approximately one week, until the conductivity of the dialyzing water plateaued.

To defibrillate the SCell into SCNF, the dialyzed SCell was blended for 30 minutes (Vitamix 5200) in 5-minute increments with cooldown periods between to prevent excessive heating. A separate batch of the most highly substituted SCell sample (1.5 moles of acid per mole of AGU, 60-minute reaction time) was blended for a duration of only 5 minutes.

SCNF Characterization

The degree of sulfation for each reacted condition was determined through conductometric titration. SCNF was diluted to below 0.2 wt% and run through a column packed with Dowex Marathon C acidic ion exchange beads to ensure that the sulfate half-ester groups were in their protonated form. The protonated SCNF was then titrated with NaOH while measuring conductivity to determine the equivalence point.

Atomic force microscopy (AFM) was used to determine nanofibril height and length. SNF samples were diluted to ca. 0.0001 wt%, deposited on freshly cleaved mica discs, and allowed to dry. Samples were scanned using an Asylum Research MFP-3D AFM in tapping mode with OMCL-AC160TS standard silicon probes with a nominal tip radius of 7 nm and force constant of 26 N/m. The open-source software programs Gwyddion and ImageJ were utilized to determine the height and length of nanofibrils from collected scans.

Exfoliation of Graphene from Graphite using SCNF

SCNF and graphite flakes were mixed together in aqueous media in varying ratios and blended similarly to a previously reported procedure applied to carboxylated, TEMPO-oxidized CNF.[14] Based on the findings of this prior work, two variables were examined; the aqueous concentration of graphite and the weight ratio of graphite to SCNF in the feed. Graphite concentrations of 5, 10, and 15 mg/mL and graphite/SCNF feed ratios of 2.5, 5, and 7.5 were

examined. For a typical experimental run, SCNF was brought to neutral pH through the addition of NaOH. SCNF and graphite flakes were mixed together with a total volume of 100 mL. This mixture was blended (Vitamix 5200) at 37,000 RPM for 30 minutes in 10-minute increments with cooldown periods between. After blending, the mixture was allowed to cool to room temperature before being centrifuged (Eppendorf 5804R, 5,000 rpm, 15 min) to precipitate unexfoliated graphite.

Several experimental runs were carried out using SCell in place of SCNF. These trials otherwise proceeded through a procedure identical to the one detailed above, with 10 mg/mL of aqueous graphite and a graphite/SCell feed ratio of 5.

Graphene Characterization

The composition of the supernatant of the SCNF/graphene mixtures were determined through thermogravimetric analysis (TGA). Aliquots of the suspensions were dried at 50 °C and ca. 5 mg of each dried sample tested using a Shimadzu TGA-50 in a nitrogen environment with a heating rate of 10 °C/min and max temperature of 500 °C. Quantitative analysis was performed using the free software package TRIOS (TA Instruments) by taking the first derivative of the TGA scan and integrating the primary cellulose decomposition peak, occurring at approximately 250 °C. As graphene shows no appreciable decomposition at this point[14], the wt% of SCNF in each sample was estimated by dividing this integral by the integrated decomposition peak of a pure SCNF standard.

The quality of exfoliated graphene was assessed using AFM. Drops of diluted SCNF/graphene suspension (0.0005 wt%) were deposited on mica and AFM was carried out through an identical procedure to that highlighted for the analysis of SCNF. The height and lateral

dimensions of the exfoliated graphene sheets were determined using Gwyddion. In the event that a graphene sheet was rectangular or oblong the shorter lateral dimension was used.

SCNF/graphene films were made through vacuum filtration. 25 mL of 0.1 wt% aqueous SCNF/graphene were filtered for 24 hours using polycarbonate filters with a diameter of 47 mm and a 0.6 μm pore size. The film conductivity was measured using the four-point probe method with colinear probes.[16]

RESULTS & DISCUSSION

SCNF Properties

SCNF with three different charges, or levels of sulfation, were produced: 1.49 mmol/g (30 min reaction time, 1.0 acid:AGU molar ratio), 1.81 mmol/g (45 min, 1.25 acid:AGU), and 2.23 mmol/g (60 min, 1.5 acid:AGU). When blended for 30 minutes, the 1.49 and 1.81 mmol/g SCNF were found to have similar nanofibrillar dimensions, while the 2.23 mmol/g SCNF had significantly shorter nanofibrils. To compensate for this, an additional run of 2.23 mmol/g SCNF was blended for 5 minutes, leading to nanofibrils with sizes more comparable to the lower charged SCNF. The properties of the SCNF samples used are summarized in **Table 4.1**.

Table 4.1. Summary of SCNF properties

SCNF Charge (mmol/g)	Blending Time (min)	Length (nm)	Height (nm)
1.49	30	690 ± 330	1.17 ± 0.52
1.81	30	580 ± 29	1.48 ± 0.39
2.23	30	365 ± 194	1.28 ± 0.32
2.23	5	501 ± 295	1.48 ± 0.46

Graphene Exfoliation

An initial optimization of exfoliation conditions was carried out by examining two experimental factors: the aqueous concentration of graphite and the weight ratio of graphite/SCNF in the feed. A two-level full factorial with five replicate center points was carried out to assess the effect of each variable on two responses of interest. For this experiment, 1.49 mmol/g SCNF was used; adding in the SCNF charge as a third variable at three levels would have provided a more comprehensive view of the system, but the number of required experimental runs made this design infeasible.

The first response examined was the composition of the supernatant following exfoliation via blending and centrifugation, expressed as the wt% of graphene in the suspended solids, with the remainder being SCNF. This serves as a measure of how efficiently SCNF was able to exfoliate and suspend graphene, while also giving the graphene content of any materials made from the graphene/SCNF dispersions. The second response of interest is the graphene yield, expressed as the wt% of graphene which was exfoliated from the starting graphite. The main effects plots (**Figure 4.1**) for the experiment shows that as the graphite/SCNF feed ratio is increased from 2.5 to 5, the graphene content of the supernatant shows an initial increase from 13.5 to 19.5 wt% (**Figure 4.1a)**. However, a further increase to a feed ratio of 10 shows no significant change. Increasing the feed ratio from 2.5 to 5 and then 7.5 also leads to a continual decrease in the graphite to graphene conversion from 4.8% to 3.9% and 2.1%, respectively (**Figure 4.1b**). This falls within expectations, as higher feed ratios see more graphite added to the system without any increase in SCNF. The effect of aqueous graphite concentration on the composition of the supernatant closely aligns with that of the feed ratio, with an initial increase in graphene content

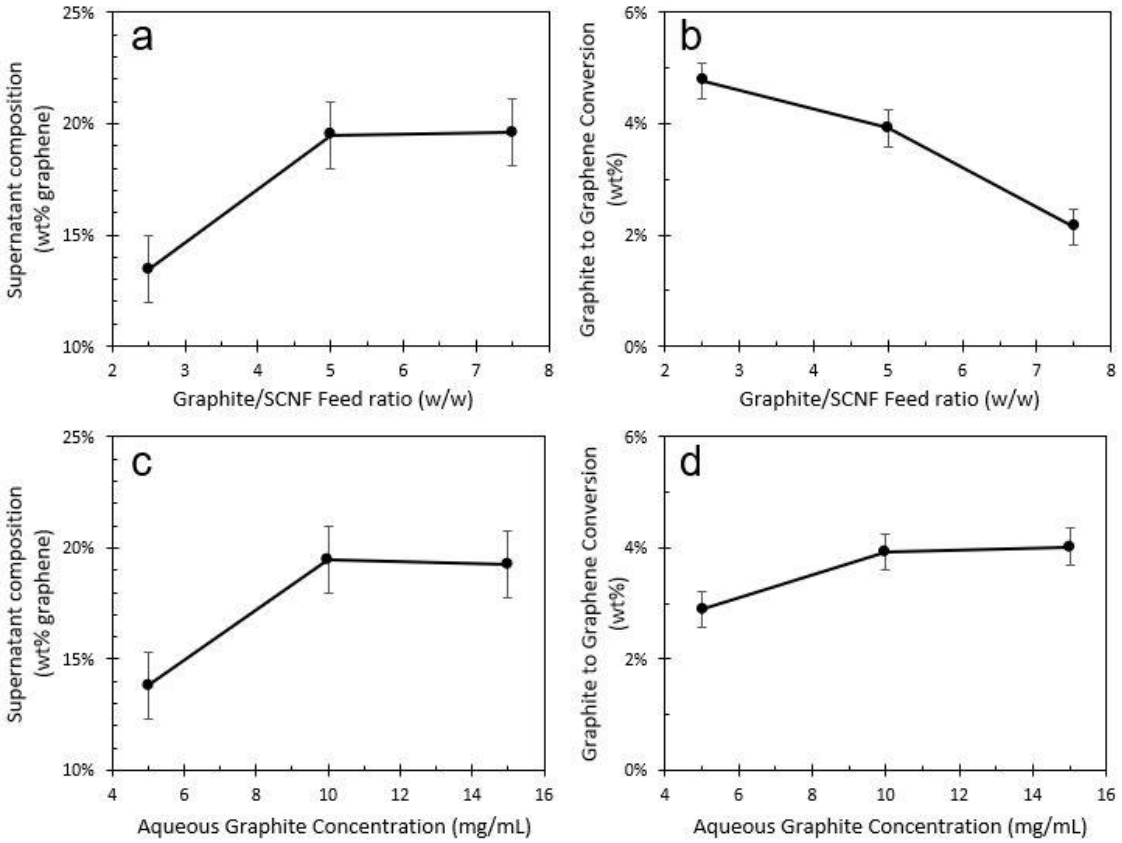

Figure 4.1 Main effects plots for the effect of Graphite/SCNF feed ratio (a, b) and aqueous graphite concentration (c, d) on supernatant composition (a, c) and graphite to graphene conversion (b, d).

observed when moving from 5 to 10 mg/mL followed by a plateau (**Figure 4.1c**). Interestingly, the conversion of graphite to graphene was improved by a small but statistically significant margin as graphite concentration as increased (**Figure 4.1d**). The interaction plots for this experiment appear parallel, indicating that no significant two-factor interaction is present (**Figure 4.2**). Based on these results, the exfoliation condition that gave the best overall performance for 1.49 mmol/g SCNF, balancing both the graphene composition in the supernatant and the graphite to graphene conversion, was with a graphite:SCNF feed ratio of 5 and an aqueous graphite

concentration of 10 mg/mL. At these conditions, graphene comprised 19.5 ± 1.5 wt% of the suspended solids and 3.9 ± 0.3 wt% of graphite was exfoliated into graphene.

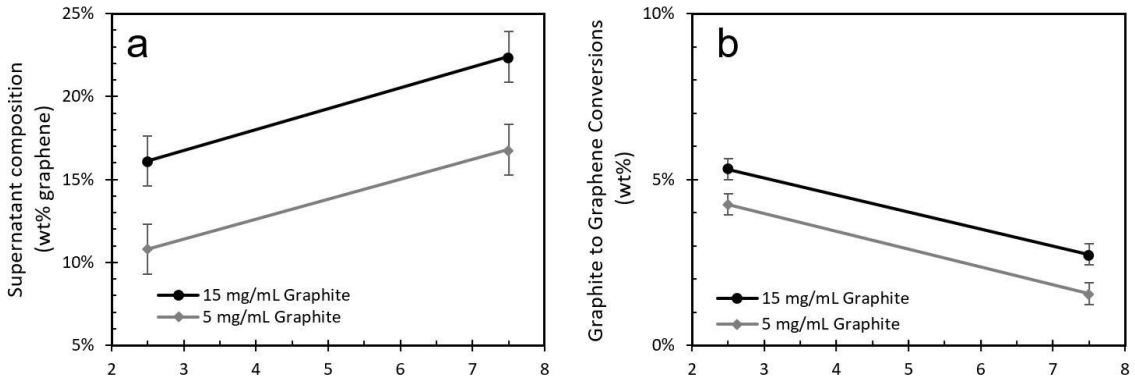

Figure 4.2 Interaction plots showing the effect of varying graphite/SCNF feed ratio at different aqueous graphite concentrations on the supernatant composition (a) and graphite to graphene conversion (b).

The effect of SCNF charge on graphene exfoliation was also examined. Batches were blended using SCNF with 1.49, 1.81, and 2.23 mmol/g of sulfate groups. For the 2.23 mmol/g sample, the 5-minute blended sample was used in order to keep the nanofibrillar dimensions as similar as possible between samples. Runs were done using 10 mg/mL of graphite and a graphite/SCNF feed ratio of 5. As the level of charge increased, less graphene was exfoliated and suspended, with the concentration of graphene in the supernatant falling from 19.5 wt% at 1.49 mmol/g to 8.9 and 8.2 wt% at 1.81 and 2.23 mmol/g, respectively (**Figure 4.3**).

Owing to the fact that both the defibrillation of SCell into SCNF and the exfoliation of graphite into graphene were carried out by blending in aqueous media, the prospect of combining the two processes was examined. Unblended SCell was substituted in for SCNF at the same conditions (10 mg/mL graphite, 5:1 feed ratio) for SCell of each charge level. In this case, the effect of charge on the amount of graphene exfoliated was the opposite of when SCNF was

utilized, with increased charge corresponding to a greater extent of exfoliation (**Figure 4.3**). In particular, the 2.23 mmol/g SCell sample led to a higher fraction of graphene in the supernatant (12.2 wt%) compared to when that same SCNF was used (8.2 wt%). This could be an indication that the presence of graphite during blending changes the way in which SCell defibrillates (e.g., the proportion of breaks along hydrophilic versus hydrophobic planes). With further experimentation and tuning of SCell charge and exfoliation conditions, it may be possible to match the exfoliation efficiency observed with SCNF while reducing the required energy expenditure by combining the two blending processes into one.

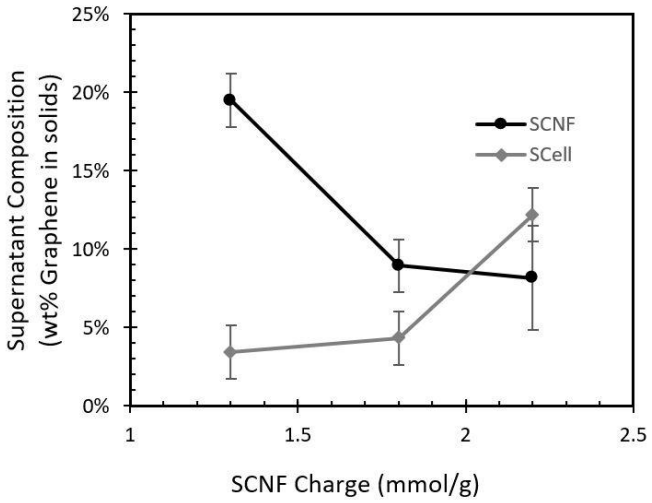

Figure 4.3 Effect of cellulose charge on graphene exfoliation efficacy.

Graphene Quality

Further tests to assess graphene quality were carried out on the graphene/SCNF dispersion that yielded the largest amount of graphene in the supernatant (19.5 wt% graphene and 80.5 wt%% SCNF, exfoliated using 1.49 mmol/g SCNF, 10 mg/mL graphite, 5:1 feed ratio). AFM of the dispersion shows visible graphene sheets amidst nanofibrils (**Figure 4.4a**), with measured heights ranging between 0.20 and 0.49 nm. Based on a monolayer thickness for graphene of 0.335 nm[17], it can be assumed that all the graphene observed consisted of either

monolayer or bilayers. The distribution of graphene sheet thicknesses (**Figure 4.4d**) does not appear obviously bimodal, so determining the relative abundance of mono- and bilayers requires setting a threshold as the cutoff point. Taking a conservative estimate that monolayers should have a thickness measured by AFM of no more than 0.335 nm yields the result that 42% of observed graphene sheets are monolayers, with the remaining 58% being bilayers.

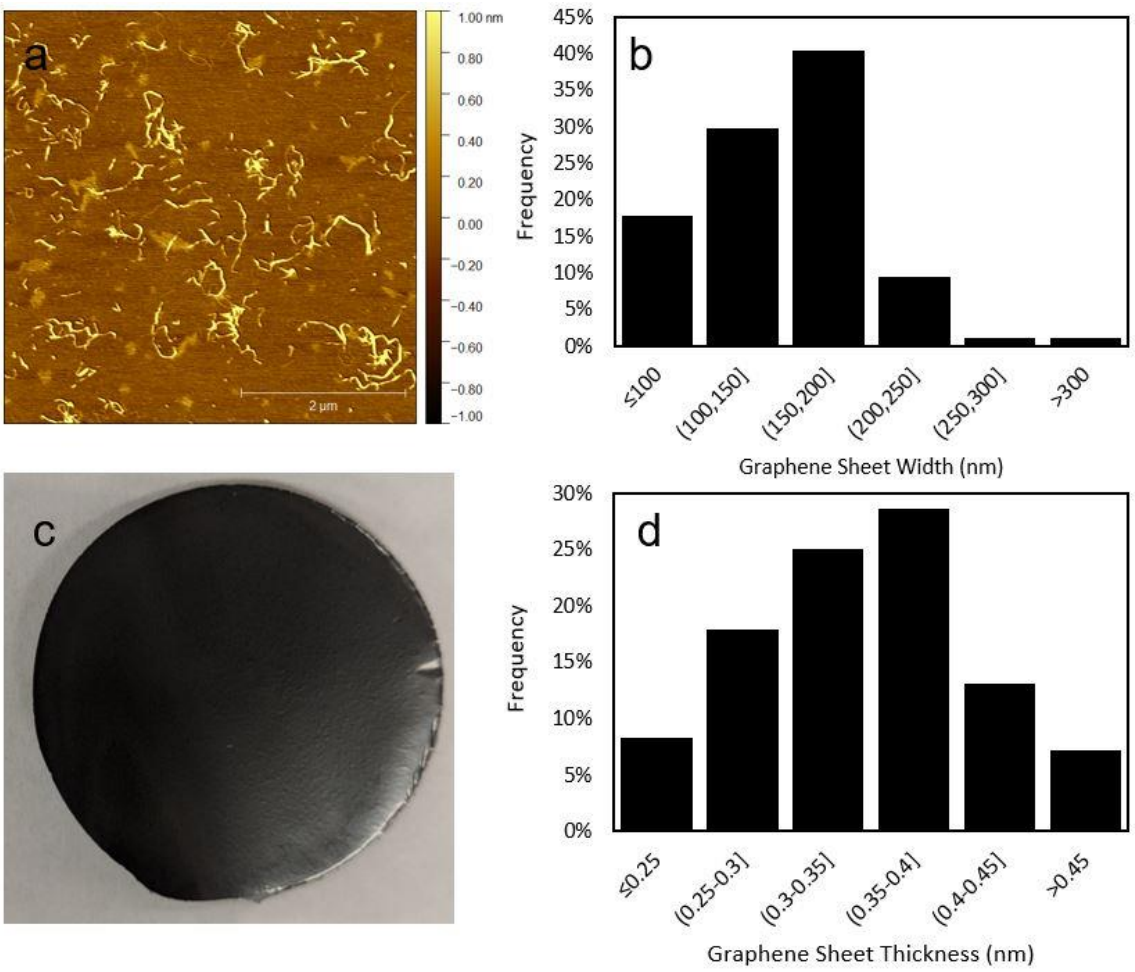

Figure 4.4 AFM height profile of graphene/SCNF dispersion (a), histograms of graphene sheet width (b) and thickness (d), vacuum filtered graphene/SCNF film (c).

This result differs significantly from the layer distribution found when using TEMPO CNF, which resulted in graphene consisting of approximately 5% monolayers, 19% bilayers, 26% triple layers, 47% with 4-9 layers, and 3% with 10+ layers.[14] A possible explanation for this phenomenon

is that the hydrophobic interactions between (200) planes on SCNF and graphite are weaker compared to TEMPO, either due to the difference in charge level (1.49 mmol/g compared to 1.33 mmol/g for TEMPO) or in the relative abundance of exposed (200) planes themselves. Weaker hydrophobic interactions could lead to a gentler exfoliation process, wherein only smaller and lighter mono- and bilayers could be removed from the bulk graphene flakes during blending. This finding is significant, as monolayer graphene is generally considered more desirable than multilayer samples. The width of graphene sheets ranged from 76 to 353 nm (**Figure 4.4b**), with the highest fraction of sheets having widths on the order of 150-200 nm. This are similar to the lateral dimensions measured for graphene exfoliated by TEMPO CNF, which had average sheet widths of 248 ± 121 nm.[14] Even the finest of the sheets measured have widths many times larger than the radius of the AFM probe tip (nominally 7 nm), which means that height measurements of graphene sheets should be unaffected by the peak broadening and height reduction that is often observed when nanoscale features (such as SCNF themselves) are measured due to finite tip sharpness.[18]

The same graphene/SCNF dispersion was formed into a free-standing film with a thickness of 18.8 ± 0.8 μm through vacuum filtration (**Figure 4.4c**). Like the prior films made from graphene/TEMPO CNF[14], the graphene/SCNF film showed sensitivity to moisture, curling when exposed to a humid environment and straightening again once in a low-humidity setting. This behavior can be explained by the absorption of water molecules causing asymmetric expansion in SCNF on the side of the film exposed to moisture, leading to bending. The conductivity of the graphene/SCNF film was 0.60 ± 0.05 S/cm, dramatically reduced from the in-plane conductivity of graphene or even graphite due to the very large amount of SCNF (ca. 80 wt%) still present in

the film. One possible solution to this issue is to add an additional step to the processing of the graphene/SCNF, wherein the thermal or chemical stability of graphene relative to SCNF is leveraged to selectively remove SCNF from the system after exfoliation. Thermally, this could be carried out pyrolysis of SCNF. Chemically through treatment with solvents like N-methylmorpholine N-oxide (NMMO) that could selectively dissolve and destroy the SCNF and/or other chemical reactions that could degrade or depolymerize cellulose and allow for its removal from the system. Ultimately, the additional cost of any other treatments would have to be weighed with the potential increases in graphene quality, but this strategy could allow for the creation of large amounts of mono- and bilayer graphene.

Conclusion

The aqueous exfoliation of graphite using SCNF and mechanical blending was demonstrated to be an effective strategy for producing graphene sheets. A 3.9% conversion of graphite to graphene was achieved, with graphene comprising 19.5 wt% of the solids in the graphene/SCNF dispersions. Compared to the previously demonstrated use of carboxylated TEMPO-CNF, SCNF produced a dramatically higher fraction of high-quality monolayer graphene (~42%), though the electrical performance of the dispersion was compromised by the high amounts of SCNF present. Upon removal of SCNF through thermal or chemical means, this scheme could allow for the creation of large amounts of graphene monolayers.

REFERENCES

(1) Allen, M. J.; Tung, V. C.; Kaner, R. B. Honeycomb Carbon: A Review of Graphene. *Chem. Rev.* **2010**, *110* (1), 132–145. https://doi.org/10.1021/cr900070d.

(2) Lee, C.; Wei, X.; Kysar, J. W.; Hone, J. Measurement of the Elastic Properties and Intrinsic Strength of Monolayer Graphene. *Science (80-.).* **2008**, *321* (July), 385–388.

(3) Ruoff, R. Calling All Chemists. *Nat. Nanotechnol.* **2008**, *3* (1), 10–11.

https://doi.org/10.1038/nnano.2007.432.
(4) Stankovich, S.; Dikin, D. A.; Dommett, G. H. B.; Kohlhaas, K. M.; Zimney, E. J.; Stach, E. A.; Piner, R. D.; Nguyen, S. B. T.; Ruoff, R. S. Graphene-Based Composite Materials. *Nature* **2006**, *442* (7100), 282–286. https://doi.org/10.1038/nature04969.
(5) Stankovich, S.; Piner, R. D.; Chen, X.; Wu, N.; Nguyen, S. T.; Ruoff, R. S. Stable Aqueous Dispersions of Graphitic Nanoplatelets via the Reduction of Exfoliated Graphite Oxide in the Presence of Poly(Sodium 4-Styrenesulfonate). *J. Mater. Chem.* **2006**, *16* (2), 155–158. https://doi.org/10.1039/b512799h.
(6) Coleman, J. N. Liquid Exfoliation of Defect-Free Graphene. *Acc. Chem. Res.* **2013**, *46* (1), 14–22. https://doi.org/10.1021/ar300009f.
(7) Furtado, C. A.; Kim, U. J.; Gutierrez, H. R.; Pan, L.; Dickey, E. C.; Eklund, P. C. Debundling and Dissolution of Single-Walled Carbon Nanotubes in Amide Solvents. *J. Am. Chem. Soc.* **2004**, *126* (19), 6095–6105. https://doi.org/10.1021/ja039588a.
(8) Paton, K. R.; Varrla, E.; Backes, C.; Smith, R. J.; Khan, U.; O'Neill, A.; Boland, C.; Lotya, M.; Istrate, O. M.; King, P.; Higgins, T.; Barwich, S.; May, P.; Puczkarski, P.; Ahmed, I.; Moebius, M.; Pettersson, H.; Long, E.; Coelho, J.; O'Brien, S. E.; McGuire, E. K.; Sanchez, B. M.; Duesberg, G. S.; McEvoy, N.; Pennycook, T. J.; Downing, C.; Crossley, A.; Nicolosi, V.; Coleman, J. N. Scalable Production of Large Quantities of Defect-Free Few-Layer Graphene by Shear Exfoliation in Liquids. *Nat. Mater.* **2014**, *13* (6), 624–630. https://doi.org/10.1038/nmat3944.
(9) Zhang, L.; Zaric, S.; Tu, X.; Wang, X.; Zhao, W.; Dai, H. Assessment of Chemically Separated Carbon Nanotubes for Nanoelectronics. *J. Am. Chem. Soc.* **2008**, *130* (8), 2686–2691. https://doi.org/10.1021/ja7106492.
(10) Geng, J.; Kong, B. S.; Yang, S. B.; Jung, H. T. Preparation of Graphene Relying on Porphyrin Exfoliation of Graphite. *Chem. Commun.* **2010**, *46* (28), 5091–5093. https://doi.org/10.1039/c001609h.
(11) Xu, X.; Zhou, J.; Colombo, V.; Xin, Y.; Tao, R.; Lubineau, G. Sodium Hypochlorite and Sodium Bromide Individualized and Stabilized Carbon Nanotubes in Water. *Langmuir* **2017**, *33* (41), 10868–10876. https://doi.org/10.1021/acs.langmuir.7b00850.
(12) Xu, Y.; Bai, H.; Lu, G.; Li, C.; Shi, G. Flexible Graphene Films via the Filtration of Water-Soluble Noncovalent Functionalized Graphene Sheets. *J. Am. Chem. Soc.* **2008**, *130* (18), 5856–5857. https://doi.org/10.1021/ja800745y.
(13) Jiang, F.; Hsieh, Y.-L. Amphiphilic Superabsorbent Cellulose Nanofibril Aerogels. *J. Mater. Chem. A* **2014**, *2* (18), 6337–6342. https://doi.org/10.1039/c4ta00743c.
(14) Xu, X.; Hsieh, Y. Lo. Aqueous Exfoliated Graphene by Amphiphilic Nanocellulose and Its Application in Moisture-Responsive Foldable Actuators. *Nanoscale* **2019**, *11* (24), 11719–11729. https://doi.org/10.1039/c9nr01602c.
(15) Pingrey, B.; Hsieh, Y.-L. Sulfated Cellulose Nanofibrils from Chlorosulfonic Acid Treatment and Their Wet Spinning into High-Strength Fibers. *Biomacromolecules* **2022**, *23* (3), 1269–1277. https://doi.org/10.1021/acs.biomac.1c01505.
(16) Miccoli, I.; Edler, F.; Pfnür, H.; Tegenkamp, C. The 100th Anniversary of the Four-Point Probe Technique: The Role of Probe Geometries in Isotropic and Anisotropic Systems. *J. Phys. Condens. Matter* **2015**, *27* (22). https://doi.org/10.1088/0953-8984/27/22/223201.
(17) Ni, Z. H.; Wang, H. M.; Kasim, J.; Fan, H. M.; Yu, T.; Wu, Y. H.; Feng, Y. P.; Shen, Z. X.

Graphene Thickness Determination Using Reflection and Contrast Spectroscopy. *Nano Lett.* **2007**, *7* (9), 2758–2763. https://doi.org/10.1021/nl071254m.

(18) Santos, S.; Barcons, V.; Christenson, H. K.; Font, J.; Thomson, N. H. The Intrinsic Resolution Limit in the Atomic Force Microscope: Implications for Heights of Nano-Scale Features. *PLoS One* **2011**, *6* (8). https://doi.org/10.1371/journal.pone.0023821.